

Editor-in-Chief >>

ISSN (Print): 1872-2121
ISSN (Online): 2212-4047

Back Journal Subscribe

LIF Neuron with Hypo-exponential Distributed Delay: Emergence of Unimodal, Bimodal, Multimodal ISI Distribution with Long Tail

Author(s): Saket K. Choudhary and Vijender K. Solanki*

Volume 14, Issue 2, 2020

Page: [148 - 160]

Pages: 13

DOI: 10.2174/1872212113666190315165139

Price: \$65



Become An Editorial Board Member Register Here

Become a Reviewer Register Here

Call for Editors Register Here

Abstract

Background: Distributed Delay Framework (DDF) has suggested a mechanism to incorporate the delay factor in the evolution of the membrane potential of a neuron model in terms of distributed delay kernel functions. Incorporation of delay in neural networks provide comparatively more efficient output. Depending on the parameter of investigation, there exist a number of choices of delay kernel function for a neuron model.

Objective: We investigate the Leaky integrate-and-fire (LIF) neuron model in DDF with hypoexponential delay kernel. LIF neuron with hypo-exponential distributed delay (LIFH) model is capable to regenerate almost all possible empirically observed spiking patterns.

Methods: In this article, we perform the detailed analytical and simulation based study of the LIFH model. We

Article Metrics PDF 25



1	Total citation
1	Recent citation
0.32	Field Citation Ratio
n/a	Relative Citation Ratio




FIND YOUR INSTITUTION

715 Views
2 CrossRef citations to date
0 Altmetric

Detection of distributed denial of service attack in cloud computing using the optimization-based deep networks

S. Velliangiri , P. Karthikeyan  & V. Vinoth Kumar

Pages 405-424 | Received 19 Aug 2019, Accepted 15 Mar 2020, Published online: 15 Apr 2020

 Cite this article  <https://doi.org/10.1080/0952813X.2020.1744196> 

 Full Article  Figures & data  References  Citations  Metrics  Reprints & Permissions 

Sample our Behavioral Sciences Journals
>> [Sign in here](#) to start your access to the latest two volumes for 14 days

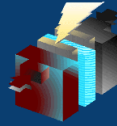
ABSTRACT

Cloud computing services provide a wide range of resource pool for maintaining a large amount of data. Cloud services are commonly used as the private or public data forum based on the demand, and the increase in usage has lead to security concerns. The information in the cloud comes under threat due to hackers, and the most common attack on the cloud data is considered as the Distributed Denial of Service (DDoS) attack. This work has concentrated on detecting the DDoS attack by developing the deep learning-based classifier. The service request from the users is collected and grouped as the log information. From the log file, some important features are selected for the classification using the Bhattacharya distance measure to reduce the training time of the classifier. Here, Taylor-Elephant Herd Optimisation based Deep Belief Network (TEHO-DBN), is developed by modifying the Elephant Herd Optimisation (EHO) with the Taylor series and the algorithm thus developed is adopted to train the Deep Belief Network (DBN) for the DDoS attack detection. From the simulation results, it can be concluded that the proposed TEHO based DBN classifier has improved performance with a maximum accuracy of 0.830.

Related research

- People also read**
 - Recommended articles**
 - Cited by 2**
- Denial of service attack detection through machine learning for the IoT >
- Naeem Firdous Syed et al.
Journal of Information and Telecommunication
Published online: 12 Jun 2020
- Defense against distributed DoS attack detection by using intelligent evolutionary algorithm >
- Shubhra Dwivedi et al.
International Journal of Computers and Applications
Published online: 30 Jan 2020

Image Creator from Designer



Mechanical Behavior and Microstructure Evolution of Al-5%Cu/TiC Metal Matrix Composite

L. Ponraj Sankar^{1,*}, R. Kamalakannan², G. Aruna¹, M.R. Meera³, V. Vijayan⁴ and S. Sivananthan⁵

¹ Department of Civil Engineering, CMR Institute of Technology, Hyderabad, India

² Department of Mechanical Engineering, M.Kumarasamy College of Engineering, Karur, India

³ Department of Physics, Sree Ayyappa College for Women, Chunkankadai, Nagercoil, Tamil Nadu 629003, India

⁴ Department of Mechanical Engineering, K.Ramakrishnan College of Technology, Samayapuram, Trichy 621112, India

⁵ Department of Mechanical Engineering, K.Ramakrishnan College of Engineering, Trichy, India

Corresponding Author Email: ponrajresearch@gmail.com

ABSTRACT

This paper aims to analyze the mechanical characteristics of Al-5%Cu/TiC metal matrix composite, like Surface Roughness, Tensile strength, wear rate of the cutting tool. Copper particles added with aluminum alloy, which can improve the machinability and also reduce wear rate. Typically the titanium materials prefer for its excellent strength during the load-carrying process. Here the TiC particles added with aluminum alloy to increase the composite hardness range. The casting samples are machined by the uncoated carbide cutting tool in CNC. The input turning parameters are speed, depth of cut, feed rate, and cutting force. The surface roughness measurement was done after the machining operation. The build-up edge and microstructure behavior of the tool and workpiece were analyzed using Scanning Electron Microscope. The result shows the more Built-up edge formed at low cutting speed and less build-up edge formed at low cutting speed. The higher cutting force indicates the lower cutting speed of 50m/min. The Build-up edges investigated at lower cutting speed and higher cutting speed. While adding TiC in Al-5%Cu, the elongation of MMC reduced, so it can able to increase the strength of the MMC specimen. Based on these results can able to predict the good mechanical and surface properties of metal matrix composite for the specific application.

Keywords: metal matrix composite, build-up edge, machinability, hardness, SEM analysis

Received: October-10-2020, Accepted: November-15-2020, <https://doi.org/10.14447/jnmes.v23i4.a05>

1. INTRODUCTION

In recent years metal matrix composite plays a vital role in the making of engine components and other mechanical applications. The metal matrix composite has preferred for its higher strength and good modulus of rigidity. This paper focused on the selection of materials for preparing the metal matrix composite, preparation ratio, and investigate the mechanical and surface properties of MMC. The types of chips formation can fix the quality of the product during the machining process [1-3]. Here this paper discussed the methodology for preparing the MMC, build-up edge formation, and analyzing the mechanical properties. Metal matrix composite is generally classified as in-situ metal matrix composite and ex-situ metal matrix composite. The in-situ metal matrix composite has good wettability and also has powerful bonding with another metal matrix [4, 5]. Ceramic reinforcement of metal matrix composite has got the poor machinability, so while adding the SiC can slightly improve the machinability. [7, 8]. The standard conventional cutting tool has provided good accuracy at no longer time due to the wear characteristics. So preferred the carbide tool in one of the solutions to wear problems [9]. The study was analyzed the build-up edge, cutting speed, and depth of cut in Al-SiC metal matrix composite, which affects the surface quality. This paper provides the information about excellent surface finish achieved by the maximum cutting speed, minimum depth of cut, and also has the less build-up edge occurred [10, 11]. The number of turning operations on Al-25%SiC and CBN, silicon nitride inserts carried out by the high-speed lathe using carbide

cutting tool. Here cubic boron nitride produces a better result than silicon nitride [14]. The Duplex alloy steel work pieces on the Computer Numerical Controlled (CNC) lathe were machined with cemented carbide tools. The Speed and Depth of cut parameters have a significant effect on MRR. The feed parameter has a big impact on surface roughness [15, 16]. The machining test was investigated with uncoated carbide cutting inserts on turning Al-4 % Cu-7.5 % SiC. They employed macro-examination and micro-examination [17]. Based on the literature study, the majority of literature prepares the aluminum alloy with Silicon and Tungsten. This study helps to analyze the various percentage of TiC and Cu mixed with aluminum, which is used to improve the strength and toughness of the MMC.

2. EXPERIMENTAL METHODOLOGY

2.1 Preparing the metal matrix composite

Metal matrix composite prepared using Al-5%Cu added with 6%, 8%, 10% of (TiC) by the in-situ method. The material compositions of MMC are shown in Table 1. Typically Ti has solid materials, so the 99.98% pure Ti melted in a furnace at 1980°C up to 40 minutes for complete melting. Then the charcoal (grain size < 60 µm) was added with pure titanium and formed the (TiC) Titanium Carbide. Pure aluminum and 5% Copper added with molten metal in the stir casting. After that, the melting metal poured into the 50mm diameter and 300mm length mould cavity. The chemical

bonding of Al-5%Cu/TiC is shown in SEM analysis Figure 1. Normally the 5%Cu consist with 0.27%Mg, 0.22%Fe, 0.10%Cr, 0.09%Ni, 0.16%Si and 0.14%Ti.

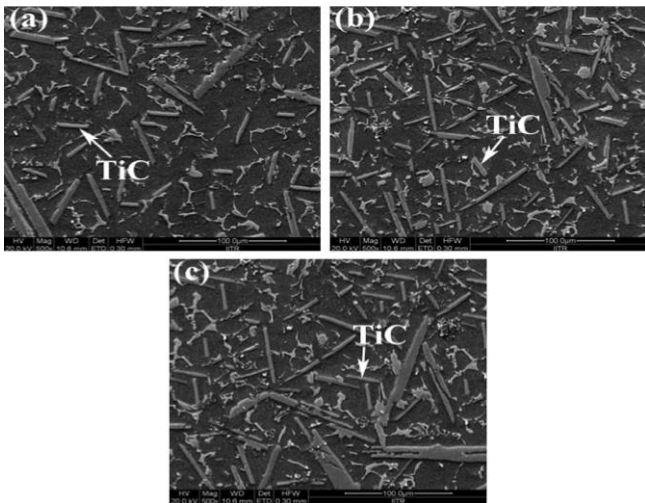


Figure 1. The SEM Analysis (a) Al-5%Cu/6%TiC (b) Al-5%Cu/8%TiC (c) Al-5%Cu/10%TiC

Table 1. Sample Preparation

Sample No	Aluminum (%)	Cu (%)	TiC (%)
1	88	5	6
2	86	5	8
3	84	5	10

2.2 Tensile test and Hardness test

The tensile workpiece machined 25mm gauge length and 5mm diameter range at the cylindrical shape, which followed the ASTM E8M-96 standard. The test was carried out at room temperature to maintain a good accuracy result, the hardness value of the three different specimens measured by the Rockwell hardness tester. The Universal Testing Machine measured the tensile strength of MMC. In a hardness test, the five measurements are taken from each sample, and the mean value of the five measurements used for further process, the experimental analysis of hardness, and tensile strength is shown in Table 2.

Table 2. Mechanical Properties of MMC

Composition	Ultimate Tensile Strength (Mpa)	Elastic Modulus (Gpa)	Rockwell Hardness (HRL)	Elongation (%)
Al-5%Cu/6%TiC	143	85.98	65.26	3.12
Al-5%Cu/8%TiC	164	93.45	72.67	2.24
Al-5%Cu/10%TiC	180	98.85	76.54	1.54

2.3 Machinability test

The cutting force analysis of Al-5%Cu/TiC composite specimen (300mm length and 50mm diameter) in

Conventional lathe by lathe tool dynamometer. The tool dynamometer is attached to the lathe for measuring the cutting force. The uncoated carbide material act as the cutting tool during the turning process in Figure 2. The experimental test were carried out by different speed rate (50m/min, 90m/min, 130 m/min), feed rate at (0.15mm/rev, 0.25mm/rev, 0.35mm/rev) and Depth of Cut (0.6mm, 0.8mm, 1.0mm). Here the cutting speed is predicted according to the spindle speed and workpiece dimension. Each test takes the surface roughness measurement by Mitutoyo conventional stylus probe, five measurements taken from each specimen, and the mean value used for the experimental reference in Table 3.



Figure 2. Experimental setup for measuring cutting force

3. RESULT AND DISCUSSION

3.1 Mechanical characteristics

A tensile testing machine did the tensile test for three different Al-5%Cu/TiC MMC. The prepared and testing samples are shown in Figure 3. Hardness test results for three different components of metal matrix composite showed in Table 2 by the in-situ method. The TiC has paly a vital role in increasing the hardness value of metal matrix composite. The specimen has contained 6% TiC, and its hardness value is 65.26. specimens 2 and 3, TiC percentage, increased while the hardness values also increased. Table 2 shows the mechanical properties of different metal matrix composite. During increases the TiC composite, which reduces the ductility of the metal matrix composite (3.12 to 1.54).



Figure 3. The specimen under the tensile test

3.2 Cutting force and surface quality

The specimen is machined by the uncoated carbide cutting tool in CNC machining. The tool dynamometer is used to measure the cutting force induced by the cutting tool. From this experiment, we observed that the Depth of Cut decreased cutting speed was increased, and also the cutting force decreased. Figure 4 shows the cutting speed in the various metal matrix composite. In this experiment, the feed rate at a constant rate of 0.24mm/rev. The cutting speed increased at the 50m/min, 90m/min, and 130 m/min. The surface quality of the specimen was analyzed by SEM in Figure 5. Figure 5 shows the surface roughness value of Al-5%Cu/TiC composite. The results project the maximum cutting speed produced the good surface roughness.

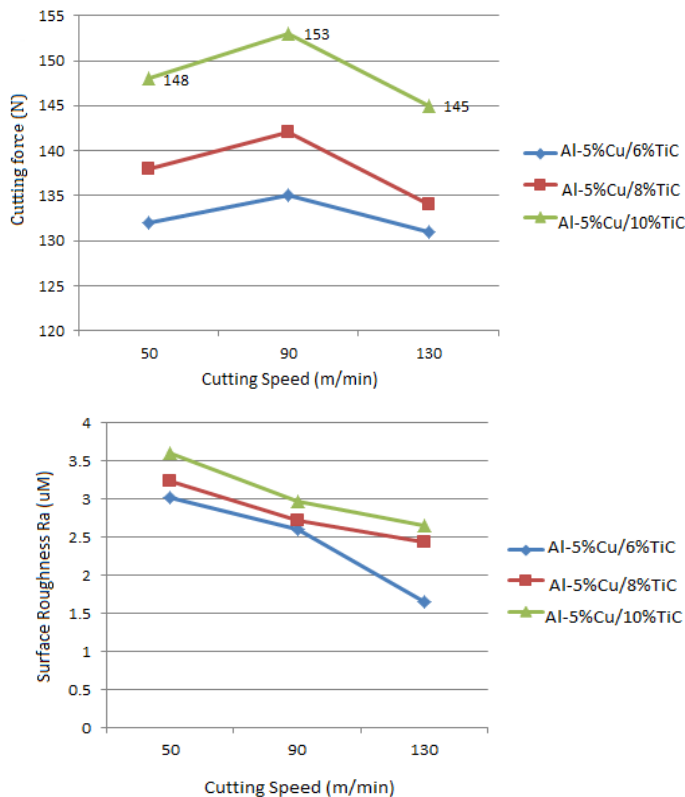
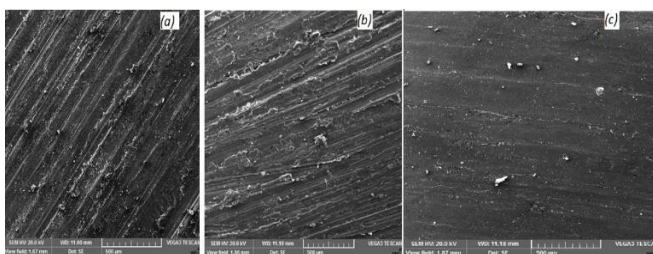


Figure 4. The Relation between cutting speed with Cutting force and surface roughness



(a) 50m/min; (b) 90m/min; (c) 130m/min

Figure 5. The SEM analysis of machined specimen surface at different cutting speed

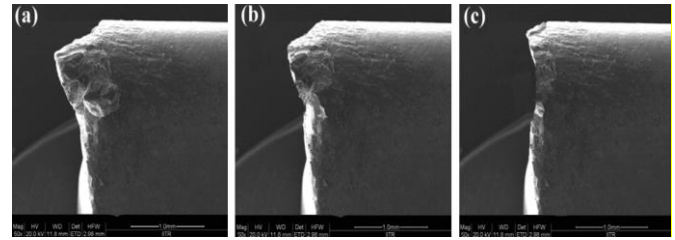


Figure 6. The SEM analysis of build-up edge in cutting tool

If the cutting force increased, the metal removal rate also increased; It raises the wear rate in the cutting tool. So the different cutting speeds carried out in metal matrix composite to predict the optimal solution for wear analysis. The cutting tool wear study investigated by SEM analysis in Figure 6.

4. CONCLUSION

Engine components need to resist high vibrational and temperature. In general, Al-Cu/TiC has excellent thermal characteristics [18]. This present study used to justify the excellent mechanical characteristics of MMC by the various testing method. Al-5%Cu metal matrix mixed with various percentages of Titanium Carbide by the in-situ method for analyzing the strength of MMC. The study used to analyze the mechanical properties, machinability characteristics of metal matrix composite, and the cutting tool analysis by various techniques. The following points concluded from this work,

- (1) Hardness and tensile strength directly proportional to the percentage of TiC, while increasing the TiC range, the hardness and tensile also increased.
- (2) The elongation range is indirectly proportional to the ductility of MMC. Table 2 results show the while increasing the TiC percentage, and it reduced the elasticity of the MMC.
- (3) Based on the above investigation, the higher cutting speed induced the lower cutting force. So the good surface roughness value was achieved by higher cutting at 130m/min.
- (4) The cutting force increased while the wear occurs on the cutting tool is higher. So the Build-Up Edge formation was increased at the lower cutting speed.

REFERENCES

- [1] Tjong, S.C., Ma, Z.Y. (2000). Microstructural and mechanical characteristics of in situ metal matrix composites. *Materials Science and Engineering: R: Reports*, 29(3-4): 49-113. [https://doi.org/10.1016/S0927-796X\(00\)00024-3](https://doi.org/10.1016/S0927-796X(00)00024-3)
- [2] Kennedy, A.R., Weston, D.P., Jones, M.I. (2001). Reaction in Al-TiC metal matrix composites. *Materials Science and Engineering: A*, 316(1-2): 32-38. [https://doi.org/10.1016/S0921-5093\(01\)01228-X](https://doi.org/10.1016/S0921-5093(01)01228-X)
- [3] Bandyopadhyay, N.R., Ghosh, S., Basumallick, A. (2007). New generation metal matrix composites. *Materials and Manufacturing Processes*, 22(6): 679-682. <https://doi.org/10.1080/10426910701384872>
- [4] Florea, R.M. (2017). Metal-Ceramic composites via “in situ” methods. In *IOP Conference Series. Materials*

- Science and Engineering, 227(1).
<https://doi.org/10.1088/1757-899X/227/1/012044>
- [5] Miracle, D.B. (2005). Metal matrix composites—from science to technological significance. *Composites science and technology*, 65(15-16): 2526-2540. <https://doi.org/10.1016/j.compscitech.2005.05.027>
- [6] Lee, K.B., Sim, H.S., Kwon, H. (2005). Reaction products of Al/TiC composites fabricated by the pressureless infiltration technique. *Metallurgical and materials transactions A*, 36(9): 2517-2527. <http://dx.doi.org/10.1007/s11661-006-0052-8>.
- [7] Mukherjee, I., Ray, P.K. (2006). A review of optimization techniques in metal cutting processes. *Computers & Industrial Engineering*, 50(1-2): 15-34. <https://doi.org/10.1016/j.cie.2005.10.001>
- [8] Ozcatalbas, Y. (2003). Investigation of the machinability behaviour of Al4C3 reinforced Al-based composite produced by mechanical alloying technique. *Composites Science and Technology*, 63(1): 53-61. [https://doi.org/10.1016/S0266-3538\(02\)00177-X](https://doi.org/10.1016/S0266-3538(02)00177-X)
- [9] Sahin, Y., Kok, M., Celik, H. (2002). Tool wear and surface roughness of Al2O3 particle-reinforced aluminium alloy composites. *Journal of Materials Processing Technology*, 128(1-3): 280-291. [https://doi.org/10.1016/S0924-0136\(02\)00467-3](https://doi.org/10.1016/S0924-0136(02)00467-3)
- [10] Manna, A., Bhattacharayya, B. (2005). Influence of machining parameters on the machinability of particulate reinforced Al/SiC–MMC. *The International Journal of Advanced Manufacturing Technology*, 25(9-10): 850-856. <https://doi.org/10.1007/s00170-003-1917-2>
- [11] Ciftci, I., Turker, M., Seker, U. (2004). Evaluation of tool wear when machining SiCp-reinforced Al-2014 alloy matrix composites. *Materials & design*, 25(3): 251-255. <https://doi.org/10.1016/j.matdes.2003.09.019>
- [12] Chambers, A.R. (1996). The machinability of light alloy MMCs. *Composites Part A: Applied Science and Manufacturing*, 27(2): 143-147.
- [13] Krishnan, B.R., Ramesh, M., (2019). Experimental evaluation of Al-Zn-Al2O3 composite on piston analysis by CAE tools. *Mechanics and Mechanical Engineering*, 23(1): 212-217. <https://doi.org/10.2478/mme-2019-0028>
- [14] Looney, L.A., Monaghan, J.M., O'Reilly, P. and Taplin, D.M.R., (1992). The turning of an Al/SiC metal-matrix composite. *Journal of materials processing technology*, 33(4): 453-468.
- [15] Dinesh, S., Antony, A.G., Karuppusamy, S., Kumar, B.S., Vijayan, V. (2016). Experimental investigation and optimization of machining parameters in CNC turning operation of duplex stainless steel. *Asian Journal of Research in Social Sciences and Humanities*, 6(10): 179-195. <https://doi.org/10.5958/2249-7315.2016.01006.6>
- [16] Dinesh, S., Antony, A.G., Rajaguru, K., Vijayan, V. (2016). Investigation and prediction of material removal rate and surface roughness in CNC turning of EN24 alloy steel. *Asian Journal of Research in Social Sciences and Humanities*, 6(8): 849-863. <https://doi.org/10.5958/2249-7315.2016.00654.7>
- [17] Tamizharasan, T., Senthilkumar, N., Selvakumar, V., Dinesh, S. (2019). Taguchi's methodology of optimizing turning parameters over chip thickness ratio in machining P/M AMMC. *SN Applied Sciences*, 1(2): 160. <https://doi.org/10.1007/s42452-019-0170-8>
- [18] Bassani, P., Gariboldi, E., Ripamonti, D. (2008). Thermal analysis of Al-Cu-Mg-Si alloy with Ag/Zr additions. *Journal of thermal analysis and calorimetry*, 91(1): 29-35. <https://doi.org/10.1007/s10973-007-8376-1>

Determination of Wear, Friction Behavior and Characterization of Carbon Fiber Reinforced Epoxy Composites for Transport Applications

S.Sudhagar^a, S.Sathees Kumar^b 

^a University College of Engineering Dindigul, Department of Mechanical Engineering, Tamil Nadu, India.

^b CMR Institute of Technology, Department of Mechanical Engineering, Hyderabad, Telangana, India.

Received: June 21, 2020; Revised: October 26, 2020; Accepted: December 10, 2020

Thermoplastics are finding the place in the current industrial sector due to its load bearing capacities. In this research, With the aid of pin on disc test set up, adhesive and abrasive wear behavior of leaf spring materials 30% short carbon fiber reinforced epoxy (SF), 30% long carbon fiber reinforced epoxy (LF) as well as Unreinforced epoxy (UF) are evaluated for automobile applications. Under multi pass abrasive wear condition, the effect of fiber reinforcement on plastic energy of deformation, matrix crystallinity and clogging behavior were investigated. The transient friction of Leaf spring materials was carried out under the load condition of 19.62N and 28.43N. During the friction test, the effect of fiber length, fiber loading condition on the co-efficient of friction and its specific wear rate of the composite materials are also investigated. The increase in load during adhesive mode for all the materials, specific wear rate and wear volume of the test materials also increased. Furthermore, the fiber- matrix interface, fractured surfaces were observed thoroughly through Scanning Electron microscopic (SEM) morphology.

Keywords: Carbon fiber, Short carbon fiber, Long carbon fiber, Transient friction, Wear, SEM.

1. Introduction

In the current scenario, thermoplastic started replacing thermoset plastic for its ecological nature and high mass production capability. discontinuous long fiber reinforced thermoplastics (LFRT) have shown significant application in replacing metals, short fiber reinforced thermoplastics, thermoset sheet molding and bulk molding composites. A leaf spring is the main component commonly used for suspension in every wheeled vehicle. Leaf springs were used in automobiles to isolate shocks and vibrations transmitted due to the uneven road conditions. Due to the superior performance of specific strain energy, damping and corrosion resistance of composite materials over steel, Composite leaf springs were being broadly used in light weight vehicles, passenger cars, heavy tank trailer suspension systems and in vibrating machineries^{1,2}. Composite leaf springs are being broadly used in light weight vehicles, passenger cars, heavy tank trailer suspension systems and in vibrating machineries^{3,5} because of the superior performance of specific strain energy, damping and corrosion resistance of composite materials over steel. The following techniques are followed for manufacturing composite leaf springs; filament winding, compression moulding, pultrusion and hand lay-up vacuum bag process. Due to utilization of continuous fibers, excellent mechanical properties are provided by filament winding process. Nevertheless, the higher degree of design flexibility is constrained by the leaf springs with varying thickness and changing contours. Various shapes and sizes of leaf springs

can be produced by compression moulding; however, the mass production capability⁶ is limited by manufacturing time involved in compression moulding. The mass production features of composite leaf springs⁷ are limited by hand lay-up vacuum bag process involves high level of skills for mixing and control of resin contents. Once, the fabrication of composite leaf spring manufactured by using epoxy, polyester and polyimide resins. For the reinforcement of leaf springs, unidirectional E-glass, S-glass and carbon fibers were used. The improved potential for commercial leaf spring applications over S-glass and carbon fibers is provided by the finest blend of cost and performance of E-glass fibers. In the matrix resins, epoxy resins based on cost and ease of processability⁸ was dominated by polyester. Lhymn et al.⁹ investigated the abrasive wear behavior of PEEK/polypropylene sulfide (PPS) blended thermoplastic polymer reinforced with short carbon and glass fiber, and stated that the wear rate was sensitive to the orientation of the fiber axis with regards to the sliding direction. Cirino et al.¹⁰ examined the abrasive wear behavior of unidirectional continuous glass fiber and focused the effect of operating variables on the polymer matrices. McGee et al.¹¹ examined the importance of fiber matrix adhesion in reducing the abrasive wear resistance in the graphite filled nylon matrix configuration. Bijwe et al.¹² stated that the abrasive wear characteristics are enhanced notably by the addition of glass, aramid and carbon fibers in polyetherimide composites and reported the influence of operating parameters on abrasive wear resistance. Barkoula and Karger-Kocsis¹³ stated that the fiber length did not affect

*e-mail: ssudhagar6@gmail.com

the erosive wear at high impact angle, through his investigation over the erosive wear of polypropylene reinforced with glass fibers with length of 2 and 10 mm and Tong et al.¹⁴ reported that the abrasive wear resistance was improved by hindering the easy deduction of fibers from high molecular weight polyethylene (HMWPE) matrix through the influence of aspect ratio on wear resistance; with the addition of wollastonite fibers with a large aspect ratio. Suresha et al.¹⁵ examined the worn out surface of carbon epoxy and glass epoxy composites by means of scanning electron microscope and envisaged the rupture of more glass fibers compared to carbon fiber because of improved interfacial adhesion between epoxy and carbon fiber. Kanagaraj et al.¹⁶ identified that the decrease in wear coefficient and wear volume when the carbon nano tubes are added in ultrahigh molecular weight polyethylene (UHMWPE) polymer and stated that wear volume increases with regards to the sliding distance. Reason for using carbon fibers in this work, carbon fibers have great specific strength, high modulus, good in fatigue resistance and dimensional stability and lower density fibers composite materials have their high strength and stiffness. If it combined with low density, when compared with bulk materials, allows for a weight reduction in the finished part.

In this research work, the wear resistance under adhesive condition is essential for leaf spring material, as the leaf spring materials such as SF, LF and UF has subjected to contact loads. The transient friction of leaf spring materials has carried out under the load condition of 19.62 N. During the friction test, the effect of fiber length, fiber loading condition on the co-efficient of friction and its specific wear rate of the composite materials are performed. However, with the assistance of Scanning Electron microscopic morphology, the adhesive wear mechanisms of selected thermoplastic composites were identified.

2. Experimental work

2.1 Fabrication Process of the composites

For the development of thermoplastic leaf springs, unreinforced epoxy (UF), 30% short carbon fiber reinforced epoxy (SF) and 30% long carbon fiber reinforced epoxy (LF) were taken into account. Leaf spring material characteristics like friction and damping were also assessed before the development of leaf spring, for the above-mentioned materials. From extrusion process, SF pellets are prepared where fibers are arbitrarily oriented. LF pellets were prepared from pultrusion technique where fibers are well oriented along with the pellet length. Pellets were obtained from Saint-Gobain India, according to the product data sheet, same molecular weight was being possessed by the base resin epoxy and coupling agent having same amount of silane type was used for the carbon fibers in LF and SF pellets. Void is assumed to be same for both short and long fiber reinforced composites since the amount of void content is significantly small and intricate to quantify by the available test facility. Material behaviour deliberations were partial only to the fiber length since the examined reinforced materials have the same type and amount of coupling agent. To remove excess moisture, initially pellets were maintained at 80°C for 2 h, and later injection moulded in to cylindrical specimens as per ASTM

D 6110 standard. To investigate the adhesive friction wear performance for the chosen leaf spring materials, pin on disc tribometer exposed and utilized and as per ASTM G 99 standard, the testing was also completed. According to cylindrical pin of 5 mm diameter and 20 mm length, specimens relating to ASTM D 6110 standard were machined¹⁷⁻¹⁹. Physical properties of carbon fiber as shown in Table 1.

2.1. Adhesive friction wear

The adhesive friction wear performance for the chosen leaf spring materials, pin on disc tribometer exposed and utilized and as per ASTM G 99 standard, the testing was also carried out. According to the ASTM D 6110 standard the cylindrical pin of 5 mm diameter and 20 mm length specimens are machined.

In support of the counter material, stainless steel disc (AISI 314) having centre line average surface roughness (Ra) of 0.1433 µm was utilized. As per ASTM D 2240 standard, initial hardness of the test, materials were calculated. By means of the force transducer fixed on the loading lever arm, the friction force was calculated and by using a computer-based data acquisition system, it was stored. At 19.62 and 28.43 N normal loads with a stable sliding velocity of 0.5 m/s, and sliding distance of 3000 m carry out adhesive friction and wear performances. In the dry conditions (32±3°C, RH 57±6%) tests were executed. On behalf of friction force and displacement measurement, data sampling rate was set aside as 1 Hz. Toward polish the test specimen to the standard surface roughness value of 0.9 Ra, silica carbide emery paper was used well. By applying an electronic balance of 0.1 mg accuracy, test specimen mass was calculated. At similar test circumstances, as a minimum of three tests were conducted and the average values of frictional force and mass loss were used for the supplementary investigation. By using Equation 1, the specific wear rate (K) was calculated,

$$K = \frac{(m_1 - m_2)}{PS\rho_g} \times 1000 \quad (1)$$

Here m_1 and m_2 are specimen mass before and after testing in g, ρ_g is the density of the specimen (g/cm^3), P is the normal load in N and S is the sliding distance in m. Subsequent to sputtering with gold coating, worn out surfaces of the pins were identified with SEM²⁰⁻²².

2.1.1 Mechanism on the Transient Friction

It was made clear that there is an increase in friction coefficient in the initial period (1500 m) from the Figure 1, after that a steady state was obtained by the friction coefficient. Commonly, in influencing wear mechanism, a significant role is played by the formation of transfer film on the counter material. A steady state was reached by coefficient of friction on the counter face material only after the formation of transfer film Figure 2a-c.

Due to the asperities deformation, the actual area of contact increases as close as to the visible area of contact when the sliding distance increases. Primarily, their opposing asperities with maximum height come in contact when two surfaces approach each other. New pairs of asperities with

lesser height create contact forming individual spots when the time increases.

This behavior was established by the measurement of surface roughness before and after sliding was indicated in the Figure 3. When compared to UFPE, the reduction of surface roughness in fiber reinforced epoxy was impeded by the existence of fibers and the breakage of fibers during sliding over the steel counter face therefore when compared to its counterparts, Ra for soft UFPE was least. For the principal abrasive wear, more number of asperities contributes in

the early period of contact. The number of asperities was reduced by the increase in sliding distance/time, in which adhesion wear leads. Thus, for all the test materials, initially there was an increase in coefficient of friction owing to the dominant abrasive friction and later reaches constant value owing to the principal adhesive friction^{23,24}.

2.2 Effect of Fiber Length on the Friction

A considerable role is played by the fiber length in influencing the frictional coefficient of the examined materials after running in period (1500 m). Owing to the adhesion between the contacting surfaces, the material transfer phenomenon is become principal. By mechanical interlocking of polymer material to the metal asperities, the transfer of material is directed well. In general, from weaker to stronger material the particle shift is occurred. In the case of carbon fiber reinforced epoxy than unreinforced epoxy, transfer film thickness was discovered to be thin LF showed thin transfer film than SF among the reinforcements, owing to its superior fiber matrix bonding. Similar behavior of transfer film for the graphite filled composites, in which the frictional coefficient increased initially after that dropped to constant value, therefore the formation of a graphite transfer film on the counter face, was confirmed by it. LF exhibited greater mechanical characteristics than that of LF compared to SF despite identical category of fibers and identical quantity of coupling agent. In common, the interfacial shear strength is directly proportional to fiber length. The

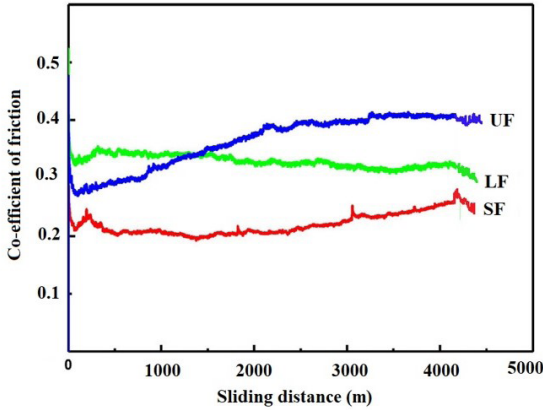


Figure 1. Coefficient of friction at 19.62N for materials under various loading parameters.

Table 1. Physical properties of carbon fiber.

Tensile strength (MPa)	Tensile modulus (GPa)	Elongation (%)	Density (g/cm ³)	Compressive strength (GPa)	Shear modulus (GPa)
4890	390	1.9	1.79	1.25	15.8

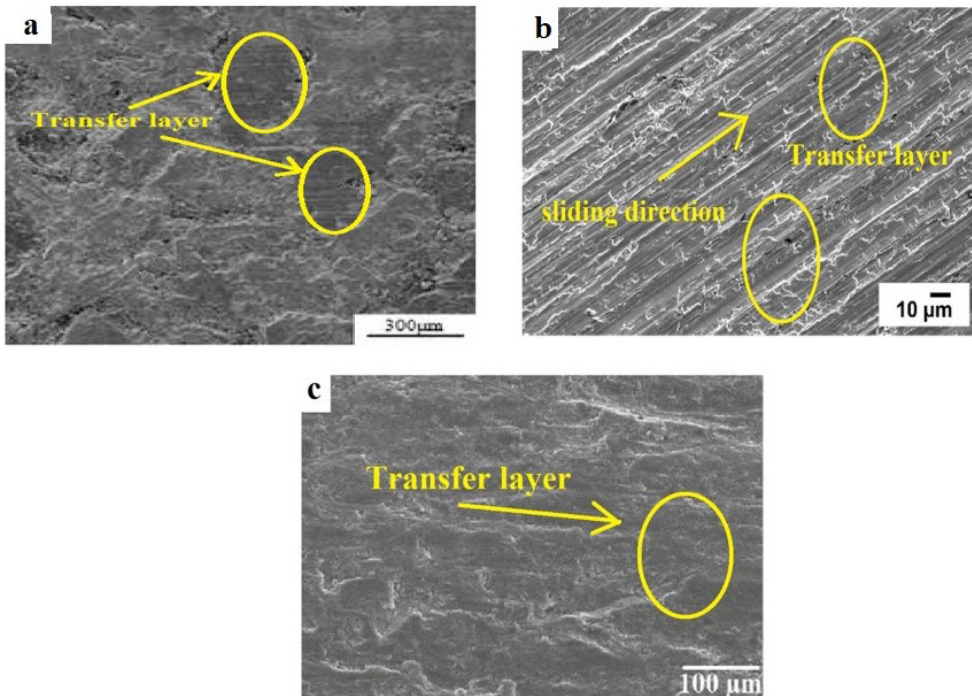


Figure 2. Transfer layers formed on stainless steel at 29.43 N for the material (a) UFPE, (b) SF (c) LF.

fiber should have a minimum length for effective composite strengthening, through which an efficient load transfer is feasible. Fibers which are shorter than this decisive length do not serve as load-bearing component. The fiber-matrix bonding was proved to be better which ultimately enhanced its mechanical properties since the fiber length in LF is three times more than SF. The above deliberations were authenticated by carrying out tensile test on fiber matrix bonding, on the selected material and to comprehend the fiber-matrix interface, fractured surfaces were examined thoroughly. At atmospheric condition (23 °C and 50% RH) the tests were executed. When the gauge length of the test material was 50 mm, the crosshead was moved at 1 mm/min speed. The stress-strain curve of the test materials is shown

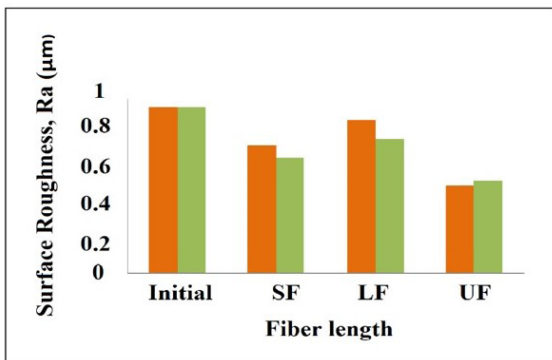


Figure 3. Influence of the fiber length on surface roughness.

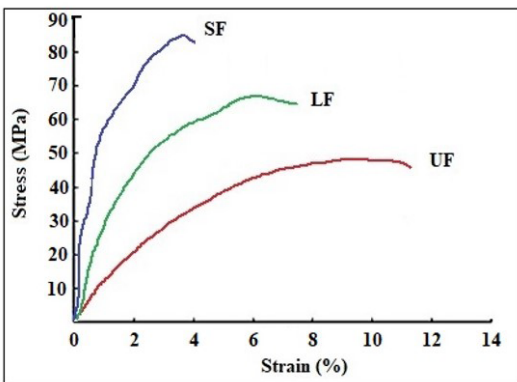


Figure 4. Stress-strain curve of pure and reinforced epoxy composites.

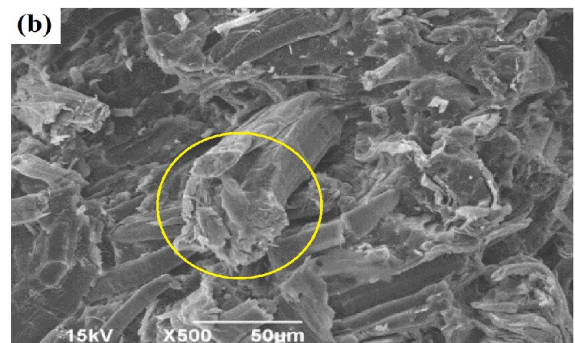
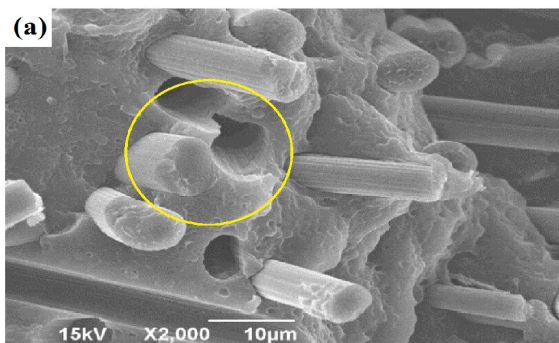


Figure 5. SEM of fractured surface of SF composites.

in Figure 4. The addition of reinforcement increased the material modulus and strength. SEM of LF showed hardly fiber pull out whereas SEM of SF exhibited more fiber pull out failures as indicated in Figure 5 and Figure 6. Hence, surface area of the fiber is increased by the increase in fiber length of LF material and fine interfacial bonding strength is also provided with the matrix and thus, fiber pullout was completely avoided.

When compared to short fibers in SF, the steady-state frictional coefficient significantly is lowered by the presence of long fibers in the LF. The test material hardness and fiber reinforcement increased material hardness are shown in the Figure 7.

2.3 Effect on the fiber loading condition on the coefficient of friction and its wear rate

In the Figure 8, the influence of load on the coefficient of friction has revealed clearly. All the considered test materials, the friction coefficient decreased slightly with increase in applied load. Owing to the low sliding resistance offered by the specimen asperities at higher loading condition was the sole reason for this behavior. Specific wear rate of all the test materials increased with the increase in PV despite the decrease in friction coefficient is shown in Figure 9. Due to the higher normal load acting on the specimen there was an increase in explicit wear rate. Less specific wear rate than unreinforced epoxy has revealed in both the load conditions/PV values, and reinforced epoxy.

The addition of carbon fiber to epoxy abridged the wear rate. LF exhibited less specific wear than SF and UF among the reinforced epoxy. The enhanced wear resistance in long carbon fiber epoxy was notified and owing to more surface area of the fiber in contact, the importance of higher aspect ratio in developing the adhesion between fiber and the matrix. The enhanced wear resistance in carbon fiber reinforced epoxy with the addition of maleic anhydride was envisaged as well as the enhanced fiber matrix bonding strength between fiber and matrix. Fine worn particles of carbon fiber was embedded with the smooth shiny surface, upon which the sliding smooth surface was created and that significantly abridged the specific wear rate than other two considered materials were all revealed in the Figure 10a.

The capability of long reinforced carbon fibers in enduring the tough protuberance owing to counter face is clearly

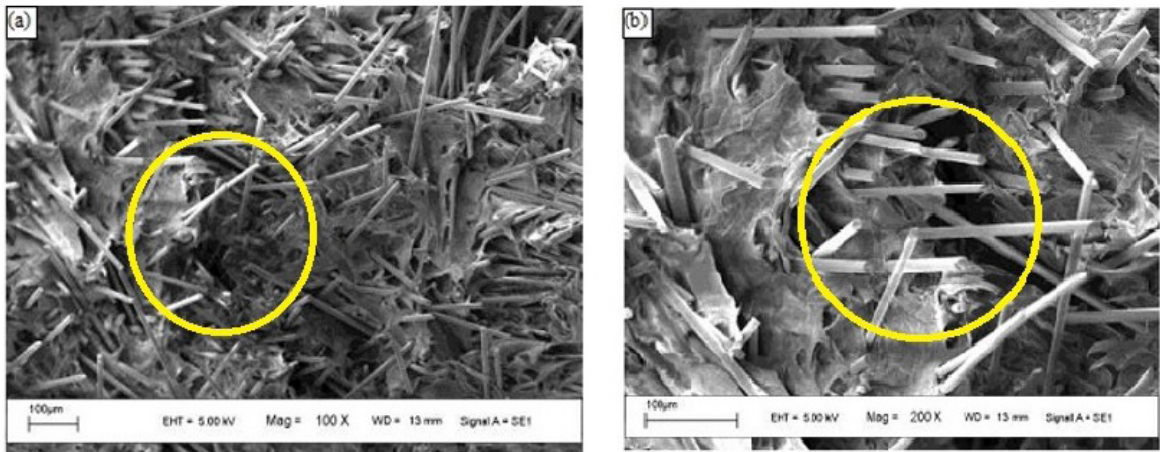


Figure 6. SEM of fractured surface of LF composites.

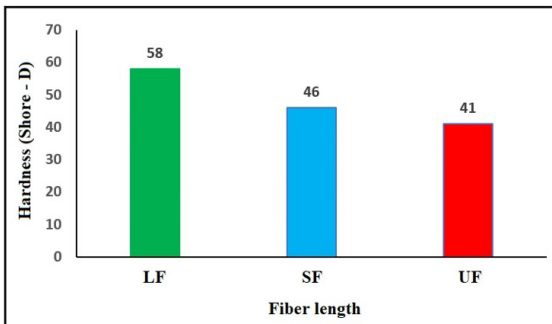


Figure 7. Hardness of the composites.

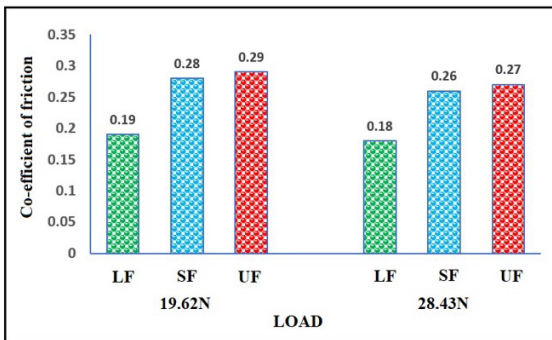


Figure 8. Influence of the load Vs coefficient of friction of the different composite materials.

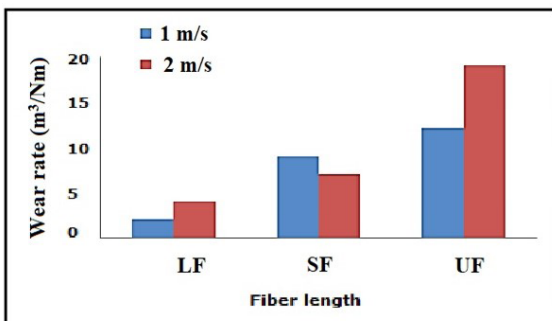


Figure 9. Influence of velocity Vs specific wear rate of the composite materials.

represented by the scratch marks in the sliding direction of long fiber reinforced epoxy as shown in Figure 10b.

2.4 Wear Mechanisms of the composite specimens

Figure 11a owing to de-bonding in the surface of SF, the fiber pullout was visibly indicated, the existence of more fiber ends as well as poor fiber matrix bonding strength were the reasons for this behavior. As a third body abrasive, the accumulated debris at the SF specimens was acted and the specific wear rate of SF as LF was also increased as represented in the Figure 11b. The frail bond between fiber and matrix was confirmed by the fibrils formed at SF as shown in the Figure 11c. Poor wear resistance was the outcome of the behavior of abrasive reinforced carbon fibers which were freely bounded to PTFE matrix. The effectiveness with which the fiber reinforces the matrix increases when the fiber length increases as well.

Fiber breakage failure can be anticipate while the load surpasses the greatest permissible fiber strength. As a stress concentration region, which assisted fiber breakage, the configuration of grooves and some patches of tranfiber film on the LF surface were served. Due to the adequately larger fiber length and enhanced fiber matrix bond, LF displayed broken fibers as indicated in the Figure 12a and fiber entanglement as represented in the Figure 12b in the current case. The good wear resistance is this sort of fiber breakage/entanglement in a surface leaves the result of the surface comparatively uninterrupted. The ductile wear was exhibited by unreinforced epoxy as shown in Figure 13a-b moreover it was subjugated by micro ploughing and as a result of the asperities of the mating steel disc, deep grooves were caused.

On the wear performance of leaf spring materials, adhesive wear performance of leaf spring materials confirmed the function of fiber length. Compared to that of short fiber reinforced and unreinforced material, the enhanced fiber matrix bonding, hardness and presence of less fiber ends in long fiber reinforced material reduced specific wear rate significantly. In adhesive mode, UF exhibited micro ploughing. In SF material at adhesive and abrasive mode fiber pullout and micro cutting were observed respectively. Under adhesive mode, LF exhibited fiber breakage.

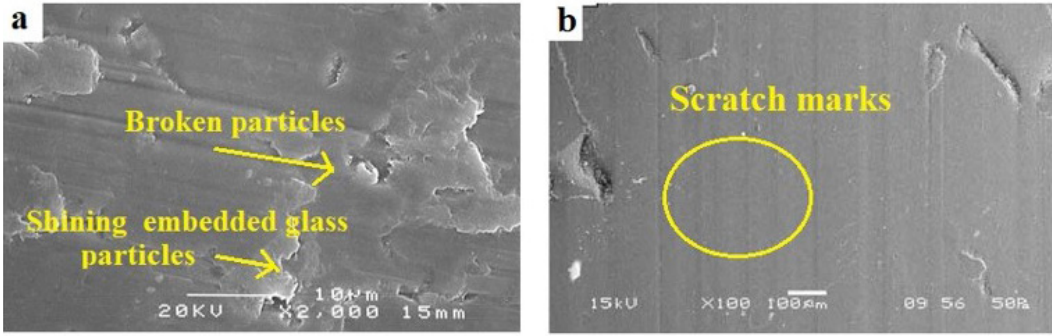


Figure 10. Morphological Structure of long fiber reinforced epoxy at 29.43N.

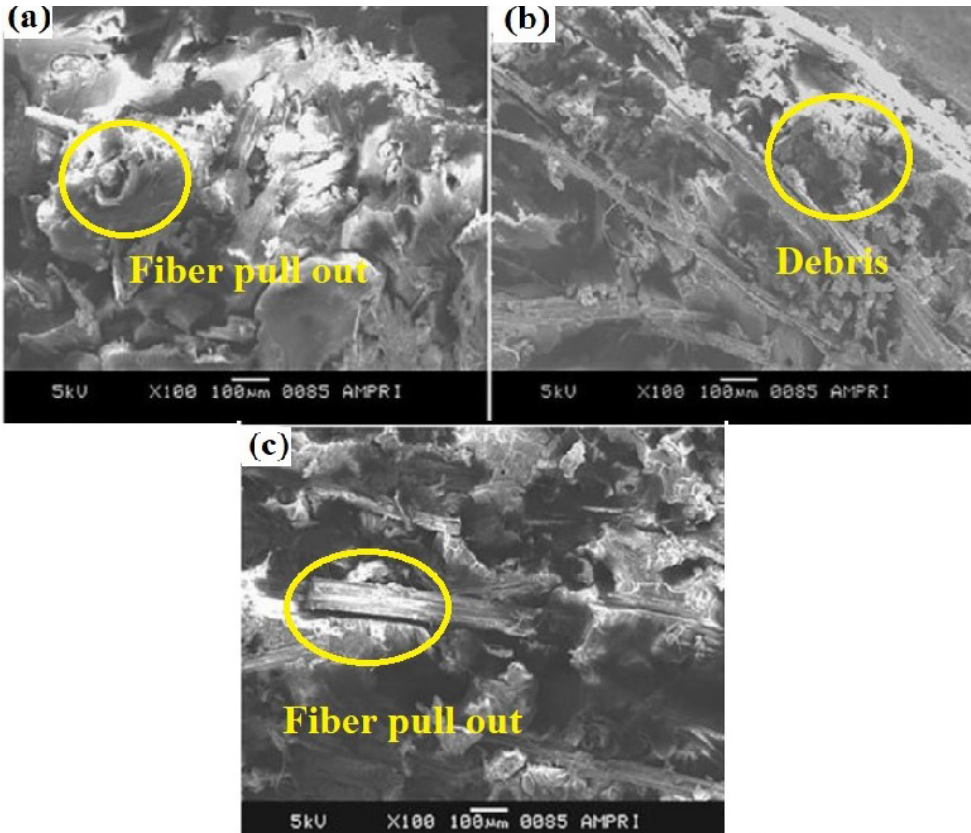


Figure 11. (a-c) SEM image of short fiber reinforced epoxy at 29.43N.

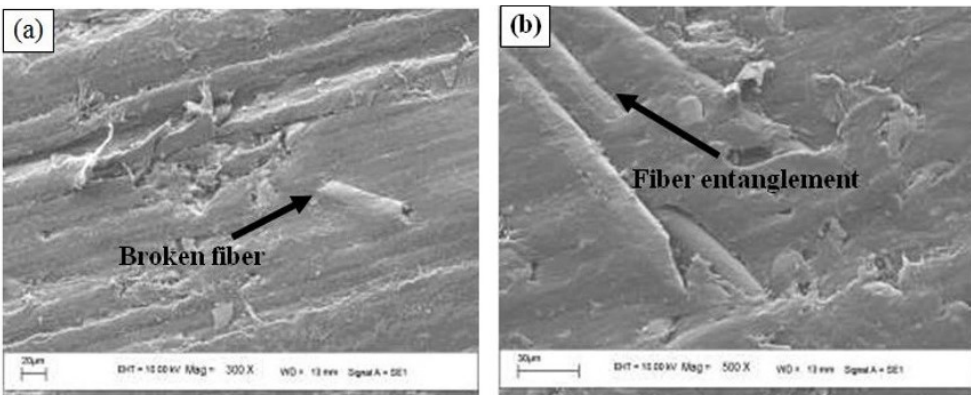


Figure 12. (a-b) Morphological Structure of long fiber reinforced epoxy at 29.43 N.

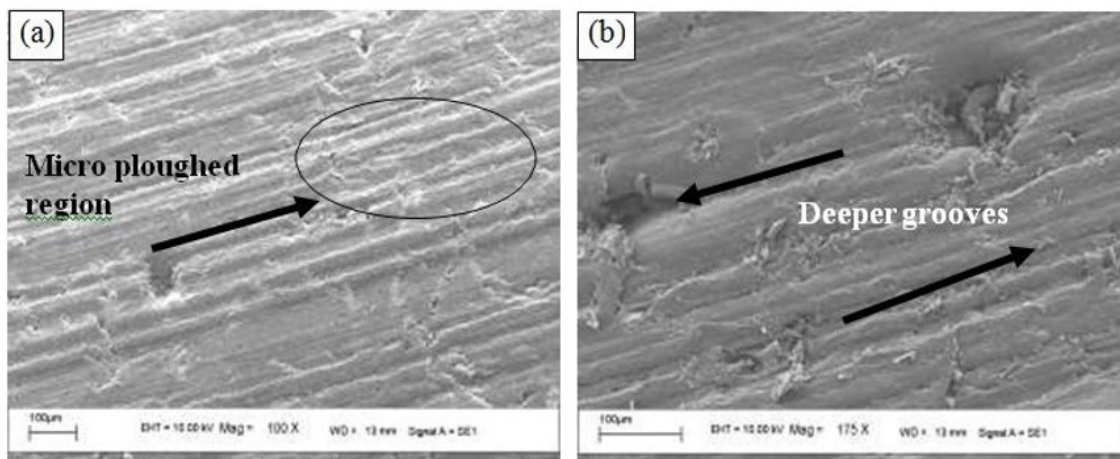


Figure 13. (a-b) SEM image of unreinforced epoxy material at 29.43 N.

5. Conclusion

For the leaf spring materials under adhesive mode using pin on disc test configuration, friction and wear characteristics were studied. The wear performance was interrelated with plastic deformation energy and crystallite size of the test materials.

- The hardness improved by fiber reinforcement and the coefficient of friction than unreinforced material reduced effectively. In adhesive mode when compared to SF, less specific wear rate shown by reinforcement LF.
- When compared to that of SF and UF, improved fiber matrix bonding and presence of less fiber ends in LF improved wear resistance. The increase in load during adhesive for all the materials, specific wear rate and wear volume of the test materials also increased.
- Significantly, friction-wear behavior was affected by the transfer film formation and clogging on the counter face during adhesive mode. In unreinforced material, transfer layer and clogged layer were found to be more distinct than reinforced material.
- By the resulted superior wear resistance compared to that of SF and UF, LF exhibited was improved.
- Due to the dominant failure morphology, UF, SF and LF exhibited micro ploughing, fiber pullout and fiber breakage respectively under abrasive mode.
- This type of composites can be used for automotive applications.

6. References

1. Beardmore P. Composite structures for automobiles. *Compos Struct.* 1986;5(3):163-76. [http://dx.doi.org/10.1016/0263-8223\(86\)90001-2](http://dx.doi.org/10.1016/0263-8223(86)90001-2).
2. Morris CJ. Composite integrated rear suspension. *Compos Struct.* 1986;5(3):233-42. [http://dx.doi.org/10.1016/0263-8223\(86\)90005-X](http://dx.doi.org/10.1016/0263-8223(86)90005-X).
3. Sancaktar E, Gratton M. Design, analysis, and optimization of composite leaf springs for light vehicle applications. *Compos Struct.* 1999;44(2-3):195-204. [http://dx.doi.org/10.1016/S0263-8223\(98\)00136-6](http://dx.doi.org/10.1016/S0263-8223(98)00136-6).
4. Rajendran I, Vijayarangan S. Optimal design of a composite leaf spring using genetic algorithms. *International Journal of Computers and Structures.* 2001;79(11):1121-9. [http://dx.doi.org/10.1016/S0045-7949\(00\)00174-7](http://dx.doi.org/10.1016/S0045-7949(00)00174-7).
5. Hou JP, Cherruault JY, Jeronimidis G, Mayer R. Design, testing, and simulation of fibre composite leaf springs for heavy axle loads. *J Strain Anal Eng Des.* 2005;40(6):497-504. <http://dx.doi.org/10.1243/030932405X30704>.
6. Mallick P. *Composites engineering handbook.* Boca Raton: CRC Press; 1997. <http://dx.doi.org/10.1201/9781482277739>.
7. Crawford RJ. *Plastics engineering.* Oxford: Butterworth Heinemann; 1998.
8. Beardmore P, Johnson CF. The potential for composites in structural automotive applications. *Compos Sci Technol.* 1986;26(4):251-81. [http://dx.doi.org/10.1016/0266-3538\(86\)90002-3](http://dx.doi.org/10.1016/0266-3538(86)90002-3).
9. Lhymn C, Tempelmeyer KE, Davis PK. The abrasive wear of short fibre composites. *Composites.* 1985;16(2):127-36. [http://dx.doi.org/10.1016/0010-4361\(85\)90619-6](http://dx.doi.org/10.1016/0010-4361(85)90619-6).
10. Cirino M, Pipes B, Friedrich K. The abrasive wear behaviour of continuous fibre polymer composites. *J Mater Sci.* 1987;22(7):2481-92. <http://dx.doi.org/10.1007/BF01082134>.
11. McGee AC, Dharan CKH, Finnie I. Abrasive wear of graphite fiber-reinforced polymer composite materials. *Wear.* 1997;114(1):97-107. [http://dx.doi.org/10.1016/0043-1648\(87\)90019-6](http://dx.doi.org/10.1016/0043-1648(87)90019-6).
12. Bijwe J, Indumathi J, John Rajesh J, Fahim M. Friction and wear behavior of polyetherimide composites in various wear modes. *Wear.* 2001;249(8):715-26. [http://dx.doi.org/10.1016/S0043-1648\(01\)00696-2](http://dx.doi.org/10.1016/S0043-1648(01)00696-2).
13. Barkoula NM, Karger-Kocsis J. Effects of fibre content and relative fibre-orientation on the solid particle erosion of GF/PP composites. *Wear.* 2002;252(1-2):80-7. [http://dx.doi.org/10.1016/S0043-1648\(01\)00855-9](http://dx.doi.org/10.1016/S0043-1648(01)00855-9).
14. Tong J, Ma J, Jiang M. Effects of the wollastonite fiber modification on the sliding wear behavior of the UHMWPE composites. *Wear.* 2003;255(1-6):734-41. [http://dx.doi.org/10.1016/S0043-1648\(03\)00221-7](http://dx.doi.org/10.1016/S0043-1648(03)00221-7).
15. Suresha B, Chandramohan G, Siddaramaiah, Samapthkumaran P, Seetharamu S. Three-body abrasive wear behaviour of carbon and glass fiber reinforced epoxy composites. *Mater Sci Eng A.* 2007;443(1-2):285-91. <http://dx.doi.org/10.1016/j.msea.2006.09.016>.
16. Kanagaraj S, Mathew MT, Fonseca A, Oliveira MSA, Simoes JAO, Rocha LA. Tribological characterisation of carbon nanotubes/ultrahigh molecular weight polyethylene composites: the effect of sliding distance. *Int J Surface Sci Eng.* 2010;4(4-6):305. <http://dx.doi.org/10.1504/IJSURFSE.2010.035138>.

17. Sathees Kumar S, Kanagaraj G. Investigation of characterization and mechanical performances of Al₂O₃ and SiC reinforced PA6 hybrid composites. *J Inorg Organomet Polym Mater*. 2016;26(4):788-98. <http://dx.doi.org/10.1007/s10904-016-0387-6>.
18. Kumar SS, Kanagaraj G. Evaluation of mechanical properties and characterization of silicon carbide-reinforced polyamide 6 polymer composites and their engineering applications. *Int J Polym Anal Charact*. 2016;21(5):378-86. <http://dx.doi.org/10.1080/1023666X.2016.1160671>.
19. Sathees Kumar S, Kanagaraj G. Investigation on mechanical and tribological behaviors of PA6 and graphite-reinforced PA6 polymer composites. *Arab J Sci Eng*. 2016;41(11):4347-57. <http://dx.doi.org/10.1007/s13369-016-2126-2>.
20. Sathees Kumar S, Kanagaraj G. Experimental investigation on tribological behaviours of PA6, PA6-reinforced Al₂O₃ and PA6-reinforced graphite polymer composites. *Bull Mater Sci*. 2016;39(6):1467-81. <http://dx.doi.org/10.1007/s12034-016-1296-6>.
21. Sathees Kumar S, Kanagaraj G. Effect of graphite and silicon carbide fillers on mechanical properties of PA6 polymer composites. *Journal of Polymer Engineering*. 2017;37(6):547-57. <http://dx.doi.org/10.1515/polyeng-2015-0441>.
22. Sudhagar S, Raja VM, Sathees Kumar S, Samuel AJ. The wear behavior and service life of Madar and Bauhinia Racemosa reinforced polyester hybrid composites for gear applications. *Mater. Today Proceedings*. 2019;19(Pt 2):589-93.
23. Raja VM, Kumar SS. Determination of static and fatigue characteristics of carbon fiber reinforced polyester composites for automobile applications. *Mater Res*. 2019;22(6):e20190458. <http://dx.doi.org/10.1590/1980-5373-mr-2019-0458>.
24. Sathees Kumar S. Effect of natural fiber loading on mechanical properties and thermal characteristics of hybrid polyester composites for industrial and construction fields. *Fibers Polym*. 2020;21(7):1508-14. <http://dx.doi.org/10.1007/s12221-020-9853-4>.

Tone Mapping High Dynamic Range Images by Hessian Multiset Canonical Correlations

Original Paper | Published: 20 January 2020 | 21, Article number: 8 (2020)



Sensing and Imaging

[Aims and scope](#) →

[Submit manuscript](#) →

N. Neelima  & Y. Ravi Kumar

 242 Accesses  2 Citations [Explore all metrics](#) →

[Cite this article](#)

Abstract

Tone mapping algorithms reproduce high dynamic range (HDR) images on low dynamic range images in the standard display devices such as LCD, CRT, projectors, and printers. In this paper, we propose a statistical clustering-based tone mapping technique that would be able to adapt the local content of an image as well as its color. At first, the HDR image is partitioned into many overlapped color patches and we disintegrate each color patch into

Access this article

[Log in via an institution](#) →

[Buy article PDF 39,95 €](#)

Price includes VAT (India)

Instant access to the full article PDF.

Rent this article via [DeepDyve](#) 

[Institutional subscriptions](#) →

<https://submission.nature.com/new-submission/11220/3>

PAPER • OPEN ACCESS

^{57}Fe Mossbauer and electrical studies of Mn doped YFeO_3 prepared via sol-gel technique

G Padmasree¹, S Shravan Kumar Reddy², J Ramesh³, P Yadagiri Reddy⁴ and Ch Gopal Reddy⁴ 

Published 27 November 2020 • © 2020 The Author(s). Published by IOP Publishing Ltd

[Materials Research Express](#), Volume 7, Number 11

Citation G Padmasree *et al* 2020 *Mater. Res. Express* 7 116103

DOI 10.1088/2053-1591/abcc2c



Figures ▾ References ▾

+ Article and author information

Abstract

Polycrystalline $\text{YFe}_{1-x}\text{Mn}_x\text{O}_3$ ($x = 0, 0.1, 0.2, 0.3, 0.4$ and 0.5) samples are prepared via sol-gel method. Structural characterization of these samples is done by x-ray diffraction (XRD) technique and Raman spectroscopic method. Intense peaks in XRD graphs show that the sample is crystalline in nature and Reitveld refined XRD data shows that the samples are formed in single phase. Raman spectroscopic study confirms the structure and phase purity of the samples. Room temperature ^{57}Fe Mossbauer studies confirm that Fe ion exists in ferric state. The hyperfine field (B_{hf}) values are found to decrease with increase in manganese (Mn) concentration. This decrease in B_{hf} value indicates the increase in antiferromagnetic nature of the samples, which arises due to the weakening of magnetic interactions between the Fe ions. From room temperature leakage current density (I - F) measurements, it is

This site uses cookies. By continuing to use this site you agree to our use of cookies. To find out more, see our [Privacy and Cookies](#) policy.

Article metrics

682 Total downloads



Submit

[Submit to this Journal](#)

MathJax

[Turn on MathJax](#)

Share this article



Abstract

1. Introduction

2. Experimental

3. Results and discussion

4. Conclusions

[Acknowledgments](#)

[References](#)

[↑ Back to top](#)

You may also like

JOURNAL ARTICLES

Local electronic and magnetic properties of pure and Mn-containing magnetocaloric $\text{LaFe}_{13-x}\text{Si}_x$ compounds inferred from Mössbauer spectroscopy and magnetometry

The effect of hybridization on local magnetic interactions at highly diluted Ce ions in tetragonal intermetallic compounds RERh_2Si_2 (RE=Ce, Pr, Nd, Gd, Tb, Dy)

A TDPAC study of static and dynamic magnetic behaviour

Oxidation states and the quality of lower interfaces in magnetic tunnel junctions: oxygen effect on crystallization of interfaces

Mössbauer spectroscopic study of spin reorientation in Mn-substituted yttrium orthoferrite

Interplay of 4f-3d magnetism and ferroelectricity in DyFeO_3



B. Yelamasetti, G. Rajyalakshmi: Properties of dissimilar weldments of Monel 400 and AISI 316

Balram Yelamasetti^a, G. Rajyalakshmi^b

^aDepartment of Mechanical Engineering, CMR Institute of Technology, Hyderabad, India

^bSchool of Mechanical Engineering, Vellore Institute of Technology, Vellore, India

Residual stress analysis, mechanical and metallurgical properties of dissimilar weldments of Monel 400 and AISI 316

This research manuscript explores the residual stress analysis, mechanical and metallurgical aspects of dissimilar welded joints between AISI 316 and Monel 400 developed by constant, pulse and Interpulse current TIG welding processes. The induced residual stresses have been measured experimentally by employing X-ray diffraction. The mechanical properties of welded joints have been determined by conducting tensile and Vickers hardness testing. The metallurgical properties of weldments have been analyzed by employing optical and scanning electron microscopy. From the experimental results, lower residual stresses have been observed in Interpulse current TIG weldment than the other two weldments. The tensile properties of the Interpulse current TIG weldment were observed to be higher than the other two weldments. In Interpulse TIG weldments, grain refinement and reduced heat affected zone near the fusion zone have been observed.

Keywords: Constant current TIG welding; Pulsed current TIG welding; Interpulse current TIG welding; Mechanical properties; Metallurgical properties

1. Introduction

Ni-Cu based alloy, Monel 400, is extensively used in various corrosive environments because it is resistant to stress corrosion cracking and also contributes to good cracking resistance under tensile loading conditions [1, 2]. This al-

loy has applications in marine industries, chemical processing equipment and boiler feedwater heaters. Similarly, 316 grade steels convey superior properties when exposed to cryogenic temperature, pitting and crevice corrosion [3]. Dissimilar welded joints of austenitic steel 316 and Monel 400 are extensively used in boilers and feed water heaters, nuclear, petrochemical and offshore industries where the welding roots are exposed to high pressure and hot corrosive environments [4, 5]. The resulting welded joints of dissimilar plates are really cumbersome to achieve and a challenging task because of their different chemical composition, phase structures and differences in thermal properties. During joining of dissimilar metals, the choice of filler metal plays a key role so as to suit both the base metals. The alloying elements of filler wire can influence phase formation, grain boundaries and the bead geometry, which further influence the mechanical behavior and the formation of hot cracks [6, 7]. Devendranath et al. [8] reported the effect of fillers on similar welding joint of AISI904L developed using the pulsed current tungsten inert gas welding (TIG) technique. The results indicate that the ERNiCrMo-14 filler weldment exhibited better mechanical and corrosion properties than the other two fillers ERNiCrMo-14 and ERNiCu-7 weldments. Ni-based filler wire is most suitable for the dissimilar joint of Monel 400 and austenitic stainless steels [9].

In the TIG welding process, uneven expansion and contraction occurs due to the heating and rapid cooling cycles, resulting in development of thermally induced residual

stresses (RS). These developed stresses remain within a welded component when external applied loads are removed [10]. The X-ray diffraction (XRD) method, one of the non-destructive techniques (NDT), is most suitable to measure the RS for welded structures [11]. This method is proven and useful for the determination of macro- and micro-RS and also capable of giving useful information about sub-micro stresses [12]. The magnitude and distribution of RS in welded structures mainly depends on total heat inputs, cooling rates and properties of base metals. In constant current TIG welding, a high level of thermal energy is continuously given to the base plates which leads to enlargement of the weld pool and heat affected region [13, 14]. Due to these uneven thermal cycles in the vicinity of the weld zone, expansion and sudden contraction takes place which leads to development of high RS [15]. Vasantharaja et al. [16] reported the effect of TIG and Activated-TIG welding on development of RS and distortions in similar joints of steel grade 316LN. Peak tensile RS and distortions are observed to be lower in A-TIG welding compared to those of TIG welded joints. Kohandeghan et al. [17] studied the residual stress development of AA5251 of TIG weldments and concluded that the magnitude of RS affects the mechanical properties and particularly in the heat affected zone (HAZ). Zhang et al. [18] studied the distribution of RS in Ni-based alloys by using XRD and neutron techniques. The cooling rates are proved to be a key parameter to induce the stresses in weldments. Ahmed et al. [19] investigated the development of RS in martensitic steels using XRD. Compressive RS are beneficial for the applications where weldments are susceptible to stress corrosion by closing the cracks. The RS distribution in the long length weldments mainly depends on welding segmental time. In these weldments the pre-heating effect can be caused due to the time lag between successive welding segmental times. The starting of the segmental welds mitigates the RS [20]. The thermal properties of base metals are also effect the development of RS during joining of dissimilar plates. Tapes et al. [21] measured the RS in dissimilar joints of AA5051 and AA6061 by using XRD. The maximum longitudinal and transverse stresses were observed in AA6061 than the AA5052. Murugan et al. [22] measured the RS in low carbon steel and SS 304 weldments by using XRD. The stress distribution is found to be more in SS 304 than low carbon steels after the first pass. However, the stress distribution is higher in low carbon steels after finishing all welding passes than the stainless steels. Ranjbarnodeh et al. [23] investigated the total heat input rates on development of RS in AISI 409 and carbon steel CK4. The higher RS are observed in plain carbon steel because of lower elastic modulus than the ferritic steels. Also, as the yield strength of carbon steel is higher, it offers resistance against the

contraction during cooling resulted in development of RS. The distortions in weldments develop because of sudden shrinkage due to uneven heating and cooling cycles that results in misalignment and gaps between the base plates [24, 25].

The heat input rates significantly affect the development of the weld bead and its characteristic constituents' microstructure, HAZ and weld zone. Pandit et al. [26] investigated the metallurgical evaluation of TIG weldments between Monel 400 and C-276 using ERNiCrMo-3 filler wire. The results indicated that coarse grains are formed at the HAZ of both the plates due to constant heat inputs. Coarse grains and segregation of alloying elements are formed near the HAZ of Monel 400 when TIG welding is employed for joining of Monel 400 and AISI 304 [27]. Micro-segregation of filler elements such as Cu and Cr occur near the weld interface in the dissimilar welds of AISI 304 and Monel 400 when TIG welding is employed. Continuous heat input rates in the TIG welding technique have caused the formation of secondary phases and micro-segregation of filler alloying elements, thus causing an overall reduction in quality of welds [28, 29]. Current being the main parameter to determine the heat input rates and arc characteristics, the arc current can be made to pulsate from low to high levels current for a given set of pulse frequencies by using pulse TIG welding technique. Some metallurgical improvements can be achieved by using pulse TIG welding, such as grain refinement, and improvement in mechanical behavior of weldments [30, 31]. Dev et al. [32] developed dissimilar welded joints between Inconel 718 and AISI 416 with pulsed TIG welding to study the metallurgical behavior. Lower segregation of alloying elements and reduced coarse grains are observed in pulse TIG welding process. Lower segregation of filler elements and reduced partially mixed zone are attained when pulse TIG welding is employed to join C-276 and Monel 400 [33]. Reddy et al. [34] developed pulse TIG aluminum welded joints to study the effect of pulse current on bead and thermal profiles. Grain refinement was observed in this welding process with enhanced tensile properties.

The Interpulse TIG welding technique uses high pulse frequency (20 kHz) modulation and a magnetic field to improve constricted welding arc characteristics which control the heat input rates [35]. This welding technique involves three different types of current, namely, main current, delta current and background current. The main current is the maximum weld current which can be used alone for straight arc mode to attain full penetration. The low current (background current) is used to maintain the arc stability during pulse arc mode. The pulse arc effect can be noticed if a higher difference is maintained between the main and background current. The delta current is used to generate precise electromagnetic force to constrict the welding arc to maintain a

Table 1. Chemical composition (by wt.%) of filler/base metals.

Filler/base metal	Ni	Cr	Fe	Cu	Mn	Mo	Si	C	Others
ERNiCrMo-3	58.95	21.5	5.0	0.5	0.5	9.0	0.5	0.1	Nb-3.13, Al-0.4, Ti-0.42
Monel 400	65.15	Nil	1.25	32	1.0	Nil	0.5	0.1	Nil
AISI 316	10.6	17.6	66.41	Nil	2.0	2.5	0.8	0.08	P-0.004

Table 2. Welding parameters of constant, pulsed and Interpulse current TIG welding techniques.

Parameters	Constant-TIG	Pulsed-TIG	Interpulse-TIG
Main current (I_m)	135 A	180 A	175 A
Delta current (I_d)	–	–	140 A
Background current (I_b)	–	90 A	110 A
Arc Voltage (V)	14 V	14 V	14 V
Pulse frequency (P_f)	–	4 Hz	–
Heat input rate (Q)	0.619 kJ mm ⁻¹	0.619 kJ mm ⁻¹	0.619 kJ mm ⁻¹

stiff, narrow welding arc during delta mode. This allows improved heat input rates on welds that are critical to achieving full penetration. The weldments of Ti-alloys produced by the Interpulse TIG welding technique are successful and the bead development and microstructures are similar to the plasma welding arc process [36]. Interpulse TIG welding can achieve controlled heat energy, reduced heat affected region and reduced RS in the vicinity of the fusion zone [37].

In this research, constant, pulsed and Interpulse current TIG welding techniques were used to join the dissimilar metals AISI 316 and Monel 400. Heat input rates and filler wires were the same in the three welding methods. The effect of variations in TIG welding current on development of RS in dissimilar welded joints were studied and compared. Further, mechanical behavior and metallurgical properties of the welded joints were studied.

2. Experimental details

2.1. Base/filler metals

The base metals, AISI 316 and Monel 400 with the size of 120 × 80 × 5 mm were considered for the development of dissimilar welded joints using constant current TIG, pulsed current TIG and Interpulse current TIG techniques. The chemical compositions in wt.% of the filler and base metals are given in Table 1. Standard butt V-groove configuration was made on the base metals to fill the 5 mm thick plates using ERNiCrMo-3 filler wire of 1.6 mm diameter. For maintaining a uniform root gap between base metals along the length of the joint, tack welding was conducted at the ends as well as middle of the joint. The welding parameters of the three welding methods listed in Table 2 were set before the joining of

dissimilar metals. The heat input rate values of three TIG welding techniques were calculated by using Eq. (1). During the welding process, back purging gas and shielding gas were maintained to prevent weld zone contamination. The developed dissimilar joints are shown in Fig. 1

$$Q_{\text{TIG/pulse TIG/Interpulse TIG}} = \frac{\eta \times V \times I / I_{\text{avg.}}}{v} \tag{1}$$

$$I_{\text{avg.}} = \frac{I_b \times T_b + I_m \times T_m}{T_b + T_m} \tag{2}$$

$$I_{\text{avg.}} = \frac{(I_m + I_d)/2 + (I_b + I_d)/2}{2} \tag{3}$$

Where, η = arc efficiency ($\eta = 60\%$) [38, 39], Q = heat input rates, kJ mm⁻¹; I_m = main current, A; I_d = delta current, A; I_b = background current, A; T_b = background current time, s and T_m = main current time, s.

The average welding current ($I_{\text{avg.}}$) of pulsed and Interpulse current TIG welding techniques is calculated from Eqs. (2) & (3), respectively.

2.2. Specimen preparation and testing

After welding, the welded samples were inspected using X-ray radiography testing (XRT) to determine any defects in dissimilar welded joints. In this research, a CEREM XRT machine was employed. After XRT analysis, residual stresses were measured experimentally using XRD. In this XRD technique, X-rays measure only the surface strains and from this the stresses are calculated using the $\sin^2\psi$ method (discussed in Section 3). After XRT and RS analyses, the weld-

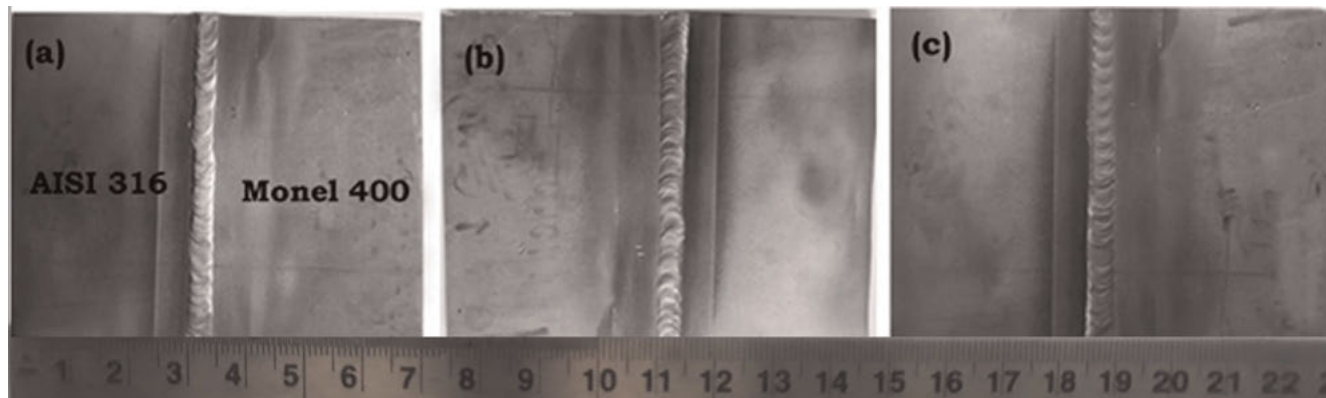


Fig. 1. Dissimilar joints of AISI 316 and Monel 400 joined by (a) Constant TIG, (b) Pulse TIG, (c) Interpulse TIG techniques.

ments were sliced transversely, i.e., perpendicular to the welding direction into different welding coupons to determine the mechanical and metallurgical properties. The tensile properties of weldments were determined by conducting a tensile test on a UTM machine as per the ASTM E/8 protocol. The microhardness values of weldments were measured with a Vickers hardness tester by setting the load with 100 gf for a constant dwell time of 10 s. The welding coupon of size 50 × 5 × 5 mm was polished with different emery papers coated with silicon carbide particles. Marble’s reagent was used at the HAZ and base plate of Monel 400 and fusion zone, whereas a combination of 10 cc HNO₃, 15 ml HCl and 10 ml CH₃COOH was used on the HAZ and base plate of steel 316. The microstructures of polished welding coupons were analyzed using scanning electron microscopes (SEM) and optical microscopes (OM). The chemical composition of the welded joints across the fusion zone and HAZ of base plates were analyzed using energy dispersive X-ray analysis (EDAX) in different zones.

3. XRD technique for residual stress measurement

The XRD technique involves change in the inter-planar spacing of a stressed specimen which can provide information on RS. The angle of reflection is selected to measure the change in the lattice inter-planar spacing by comparing the same with a stress-free sample that in turn is used to measure the sum of the principal stresses on the weld surface by using Bragg’s law Eq. (4). The peaks refer to the layer in the specimen whose plane follows Bragg’s law at a certain angle of incident of X-rays.

$$n\lambda = 2d \sin\theta \tag{4}$$

Where, *n* = order of reflection; *d* = planar space between two lattices; *λ* = X-ray wavelength (Å); and *θ* = angle between reflected planes and incident beam.

The welded sample was placed on the workbench of the XRD testing machine after electro chemical polishing. The surface under examination was mounted in the para-focusing position whenever possible in order to obtain sharp diffraction peaks. The radiation source vanadium filtered Cu-K_α was used as it suited both the base metals, which have the same ‘*hkl*’ plane {3 1 1} [40]. Changes in *d* (inter-planar spacing) lead to a shift in XRD peaks, which is taken as the measure of the RS. The RS value *σ*₀ can be calculated by substituting elastic modulus (*E*), Poisson’s ratio (*ν*), interplanar unstressed lattice space (*d*₀) and slope value (*m*) in Eq. (5).

$$\sigma_0 = \frac{m}{d_0} \left(\frac{E}{(1 + \nu)} \right) \tag{5}$$

The radiation wavelength *λ* = 1.07442 Å was deflected from plane (3 1 1) of the surface at 2*θ* = 156.12°. *ψ*-Angles were taken between -45° to 45° for measuring inter-planar lattice spacing. The RS were measured at the fusion line, and on either side (including base and heat affected region) of fusion at a distance of 12 and 50 mm, respectively. For example, the RS value in the weld zone of TIG weldment is calculated by using Eq. (5). The *m* value which is the slope derived from the *d* versus sin²*ψ* plot. The calculated RS value was found to be 189 MPa in compressive nature.

4. Experimental results and discussions

4.1. X-radiography test

The X-ray images of welded joints of dissimilar metals are given in Fig. 2. These XRT results show that the dissimilar

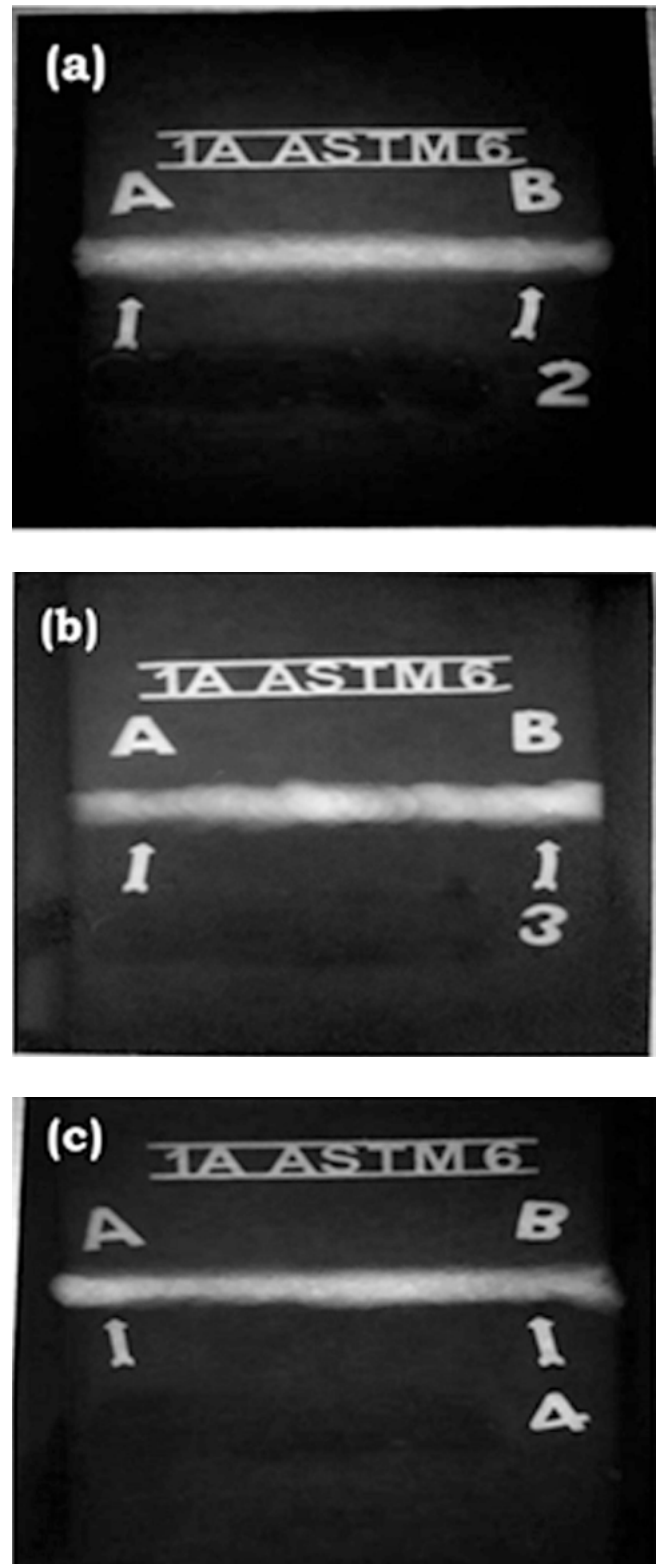


Fig. 2. XRT films of dissimilar joints joined by (a) Constant TIG, (b) Pulsed TIG, (c) Interpulse TIG techniques.

Table 3. Residual stress (MPa) values at different locations of dissimilar weldments.

Welding technique	AISI 316 (from fusion line)		Fusion zone	Monel 400 (from fusion line)	
	50 mm	12 mm		12 mm	50 mm
Constant TIG	-2.4	-44	-189	46	5.2
Pulsed TIG	1.2	-47	-101	35	2.1
Interpulse TIG	0	45	-53	37	0

welded joints developed using 3 welding techniques were free from surface and sub-surface defects like spatter, inclusions, porosity, etc. Uniform and complete bead profiles were observed in all the weldments.

4.2. Residual stresses

From the XRD analysis, the RS values of dissimilar weldments were calculated by using $\sin^2\psi$ method and the calculated values are listed in Table 3. The distributions of RS in welded joints of three welding techniques are shown in Fig. 3. The peak RS values, -189 MPa, -101 MPa and -53 MPa, were observed at the fusion zones of constant, pulsed and Interpulse current TIG weldments, respectively. Due to the variations in thermal properties, especially thermal conductivity values of the base metals, the uneven expansions and contractions occurred in the vicinity of the fusion boundary, which to the development of

compressive stresses [37]. Due to constant heat input rates to the welded joint in TIG welding high RS were observed. The RS values near the fusion zone were lower in the other two welding techniques due to the controlled total heat inputs. In all the weldments the state of RS is then changed from compressive nature to tensile nature for further distances in the Monel 400 side. In all the welding techniques the developed RS are self-balanced in the welded structure and within the yield limits only.

4.3. Mechanical properties

4.3.1. Tensile studies

The average tensile properties of welded joints and base plates were computed by conducting tensile tests on three tensile specimens of each welded joint, and are listed in Table 4. The stress-strain plots of base metals and welded joints are shown in Fig. 4. The maximum weld strength of 586 MPa was observed in Interpulse current TIG weldments. The yield stress of pulsed and Interpulse current TIG welded joints was observed to be higher than the con-

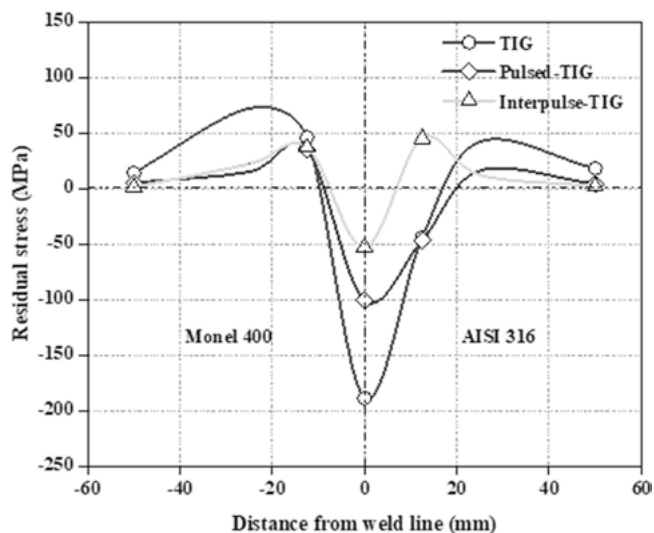


Fig. 3. Residual stress distribution along transverse direction in three welded joints.

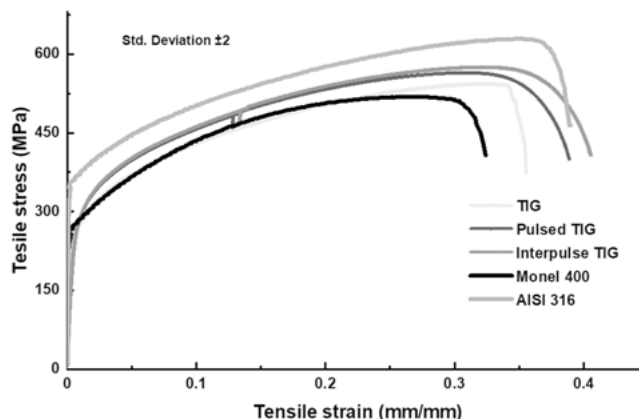


Fig. 4. Tensile stress-strain plots of base metals and dissimilar welded joints.

Table 4. Tensile properties of base plates and welded joints made of TIG, pulsed TIG and Interpulse TIG welding techniques.

Base/weldment	YS (MPa)	UTS (MPa)	% Reduction in area	% elongation	Failure location
Monel 400	215	516	49	34	-
AISI 316	350	632	60	45	-
Constant-TIG	253	544	58	41	Monel 400
Pulsed-TIG	343	554	64	40	Monel 400
Interpulse-TIG	356	586	60	33	Monel 400

stant current TIG welded joints, which could be attributed to the improvement of the factor of safety of welded joints. During tensile loading, the resistance against the applied load increased adequately at the vicinity of the weld area and the fracture occurred away from the weld zone. The ratio of yield strength (YS) to ultimate tensile strength (UTS) of pulsed and Interpulse current TIG welded joints was observed to be high when compared to both the non-welded base metals. Owing to the maximum Vickers hardness experienced in the welded zone due to Ni-Cu rich regions perceived from EDS analysis, the failure did not occur at the fusion boundary. This failure occurred in all the welded joints in the base metal Monel 400.

4.3.2. Hardness studies

The Vickers hardness values were measured on welded joints and measured values are plotted in Fig. 5. The average hardness value at the fusion zone of Interpulse TIG weldment (215 HV_{0.1}) was observed to be greater than constant TIG weldment (208 HV_{0.1}) and pulse TIG weldment (212 HV_{0.1}). The average micro-hardness value at the HAZ of AISI 316 was slightly decreased when employing constant current TIG welding and its EDS result showed the formation of low density alloying elements in HAZ. The hardness value at the heat affected region of base metal Monel 400 was improved in pulse and Inter-

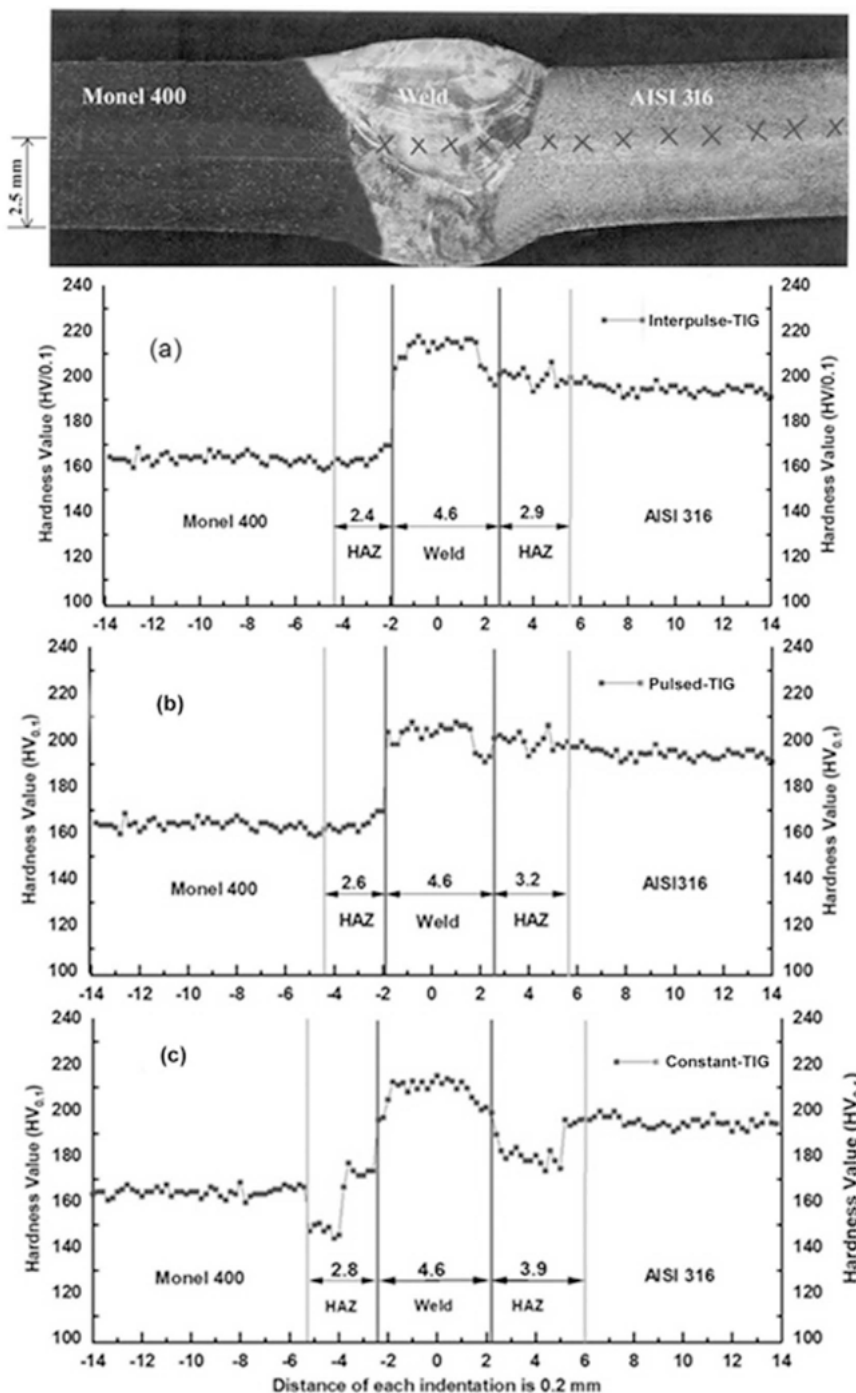


Fig. 5. Vickers microhardness profiles of (a) Interpulse TIG, (b) Pulsed TIG, (c) Constant TIG dissimilar weldments.

Table 5. Comparison of width and average Vickers microhardness value of TIG, pulsed and Interpulse current TIG weldments.

Welding technique	Monel 400		Weld zone		AISI 316	
	HAZ (mm)	HV _{0.1}	Fusion (mm)	HV _{0.1}	HAZ (mm)	HV _{0.1}
Constant-TIG	2.8	155	4.6	212	3.9	184
Pulsed-TIG	2.6	163	4.6	208	3.2	202
Interpulse-TIG	2.4	172	4.6	215	2.9	204

pulse TIG techniques due to controlled heat input rates, to which could be attributed the formation of fine grain structure near the fusion boundary. SEM/EDS analysis revealed the presence of main compositional elements such as nickel and iron at the weld zone, contributing towards the hardness of grains. The comparison was made of the heat affected region width and microhardness of three the weldments and results are listed in Table 5. The heat affected region was found to be narrower on both the base materials of Interpulse TIG welding technique compared to that of welded joints made using constant and pulsed current TIG welding techniques.

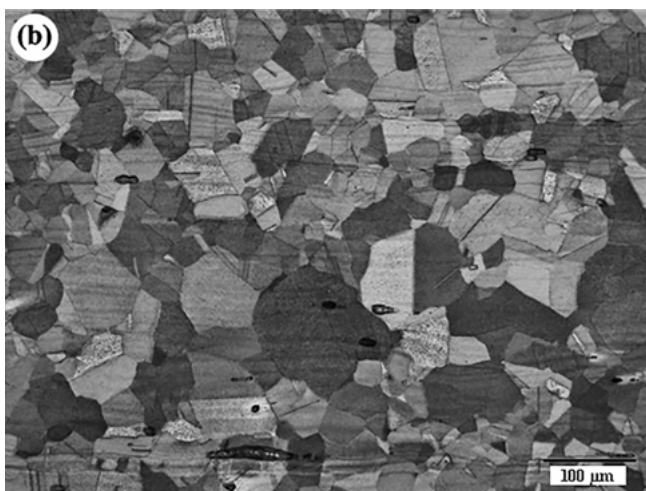
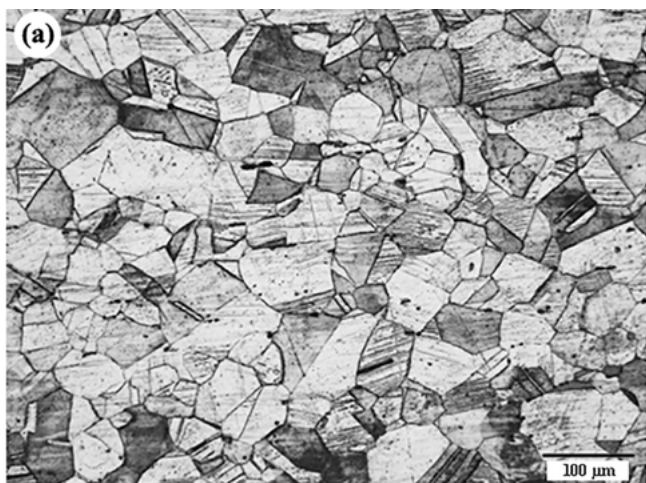


Fig. 6. Microstructures of base metals (a) Steel grade 316, (b) Monel 400.

4.4. Metallurgical studies

4.4.1. Base metals

The base metals, steel grade 316 and Monel 400, microstructures are shown in Fig. 6. The austenitic grains of mechanically deformed grains were identified in the microstructure of AISI 316 as shown in Fig. 6a. Single phase solid solution nickel–copper enriched structures with annealed grain boundaries were identified in the microstructure of Monel 400, as shown in Fig. 6b.

4.4.2. Constant current TIG weldment

Typical OM and SEM micrographs of various zones of AISI 316 and Monel 400 are shown in Fig. 7. It is observed that coarse grains were formed at the HAZ of both the base plates, which could be attributed due to continuous heat input rates. Migrated grain boundaries (MGBs) were also seen in the well-developed austenitic welds which emerged due to the reheating cycles during multiple passes. With the increase of heat input, the growth of substructures can also be clearly seen as a result of dislocation migration. The interface of steel grade 316 as shown in Fig. 7a and b reveals that the formation of clear grain boundaries and clear grain structures about 50 microns were observed in TIG weldments. The elemental micro-segregation of alloying elements was seen to have dark spots in the micro-graphs of Monel 400 interface as shown in Fig. 7c and d that might have been caused by differences in heating and cooling cycles. The weld zone of the TIG welded joint shows long dendritic structures and clear grain boundaries, as shown in Fig. 8, which could serve to increased hardness values at the weld zone. The addition of the elements from filler wire such as Mo and Nb has resulted in the expansion of the Ni-rich, face centered cubic lattice, further resulting in the net enhancement in the strength of the austenite phase. SEM/EDS analysis at the weld zone shown in Fig. 9 revealed that the fusion boundary was enriched with Cr, Ni, Fe and Mo. The intensity of the peaks of Ni, Cu, Fe, Cr and Mo was observed.

4.4.3. Pulsed current TIG weldment

Typical OM and SEM micrographs of the Monel 400 interface and AISI 316 interface of pulsed current TIG weldments are shown in Fig. 10. No grain coarsening was identified near the HAZ of Monel 400 from Fig. 10a and b, which could be attributed to the controlled total heat input and low pulse frequency (4 Hz). Also, columnar and long dendritic structures were observed at the HAZ of Monel 400. Clear grain boundaries and fine grain structures were observed at the interface of steel grade 316, as shown in Fig. 10c

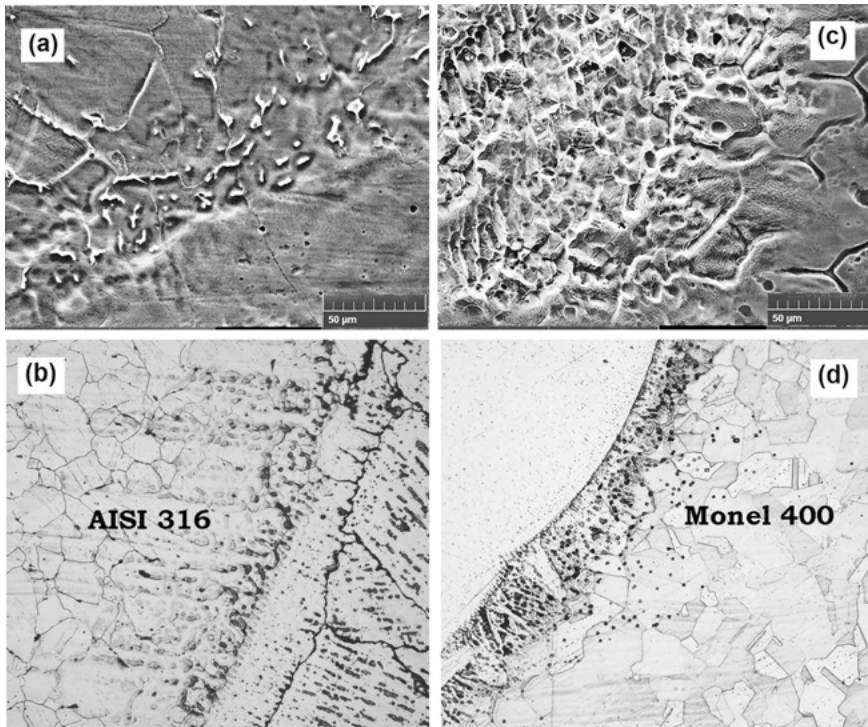


Fig. 7. SEM and OM micrographs of dissimilar TIG weldment (a, b) AISI 316, (c, d) Monel 400.

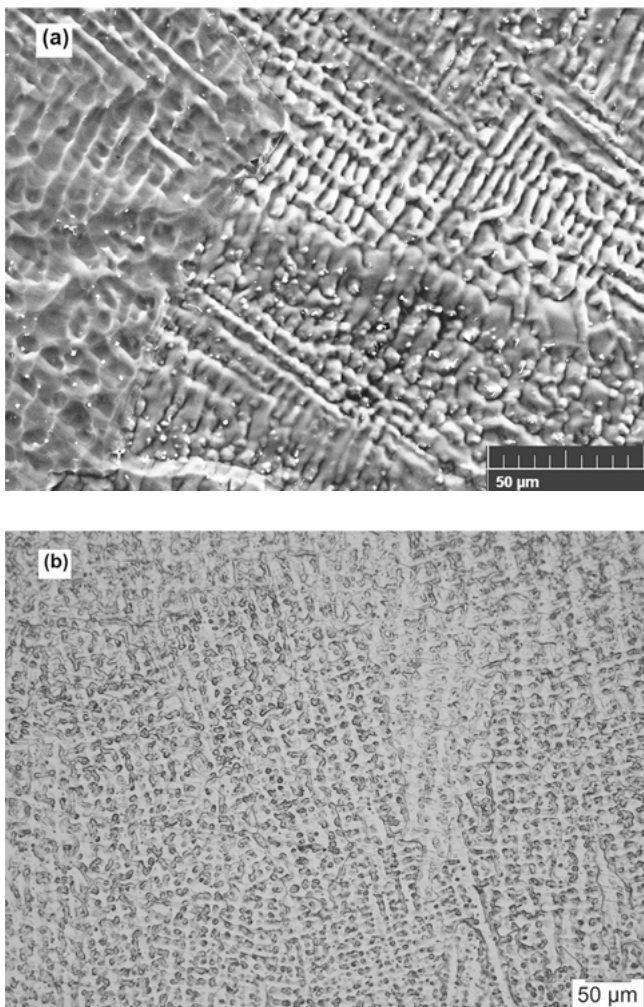


Fig. 8. ERNiCrMo-3 filler weld zone of dissimilar TIG weldment (a) SEM, (b) OM micrographs.

and d. The metallurgical studies also revealed that the fusion boundary has completely austenitic phase structures, as shown in Fig. 11. Secondary phase formation and isolation of alloying elements are greatly minimized in this welding technique. SEM/EDS analysis at the HAZ of Monel 400 and AISI 316 is shown in Fig. 12, which indicates that the weld boundary was enriched with Fe, Ni, Mo and Cr. The intensity of the peaks of Ni, Cu, Fe, Cr and Mo were observed.

4.4.4. Interpulse current TIG weldment

Typical OM and SEM micrographs of various zones of Interpulse TIG weldments of steel grade 316 and Monel 400 are shown in Fig. 13. The interface of Monel 400 in the Interpulse TIG weldment microstructure reveals well defined grain structures and equi-axed fine grain structure near the weld zone, as shown in Fig. 13a and b. Also, columnar and long dendritic structures were identified in the welded zone nearer to the interface of Monel 400. Grain refinement and grain boundaries, as shown in Fig. 13c and d, were formed near the weld zone at the interface of steel grade 316 due to the constricted arc and controlled heat input rates in the Interpulse TIG welding technique. The weld zone has completely austenitic phase structures, as shown in Fig. 14. Secondary phase formation and segregation of alloying elements are enormously controlled by utilizing an Interpulse welding process in welded joints. SEM/EDS analysis at the weld zone shown in Fig. 15 revealed that the fusion boundary was enriched with Cr, Ni, Fe and Mo. The intensity of the peaks of Ni, Cu, Fe, Cr and Mo was observed. The segregation of alloying elements, of filler wire was not found at the interface of both the base plates. The minimized segregation of alloying elements, as observed from Fig. 15 for Interpulse TIG welding, is attributed with the increase in the yield

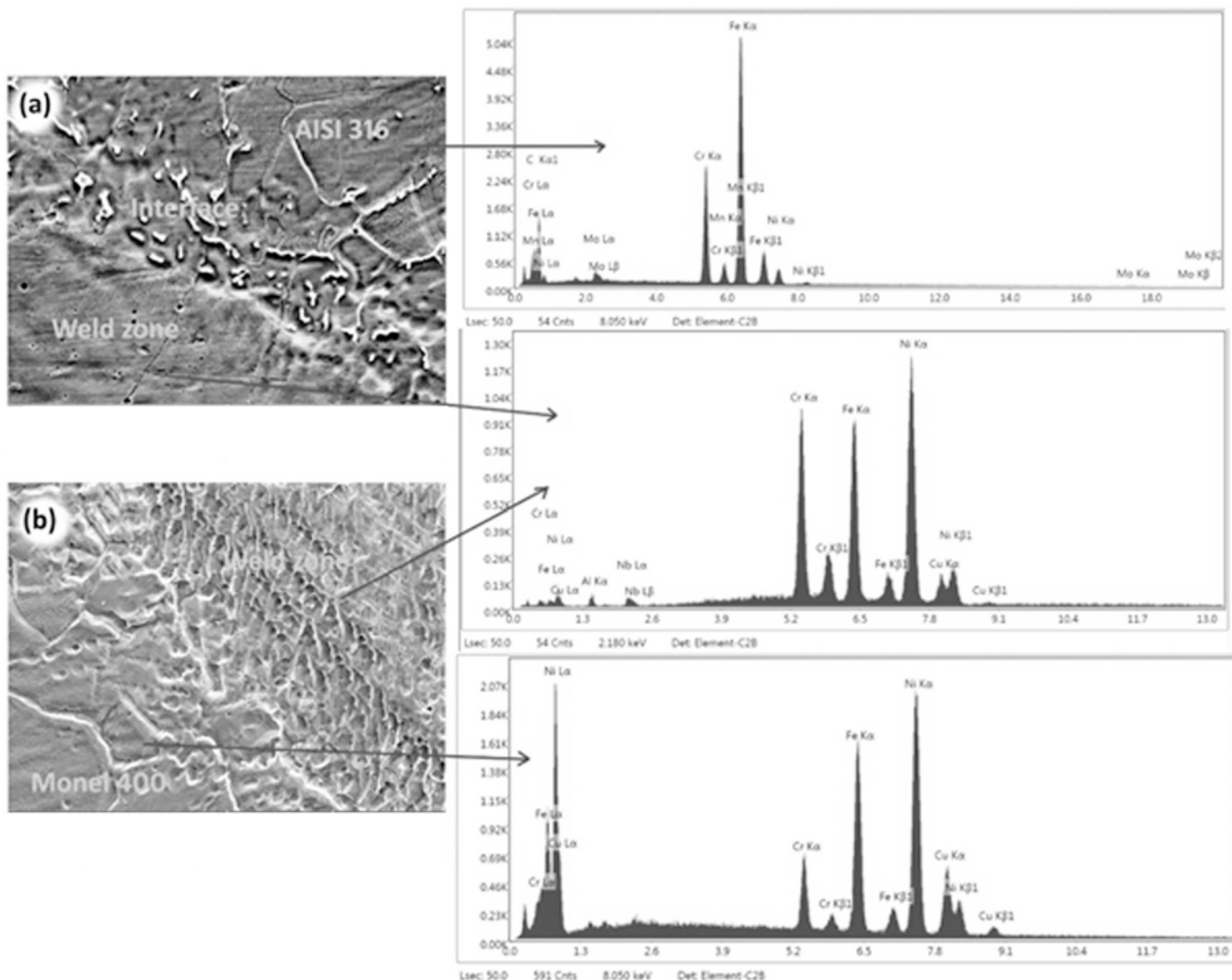


Fig. 9. SEM/EDS point analysis of dissimilar TIG weldment: (a) AISI 316, (b) Monel 400.

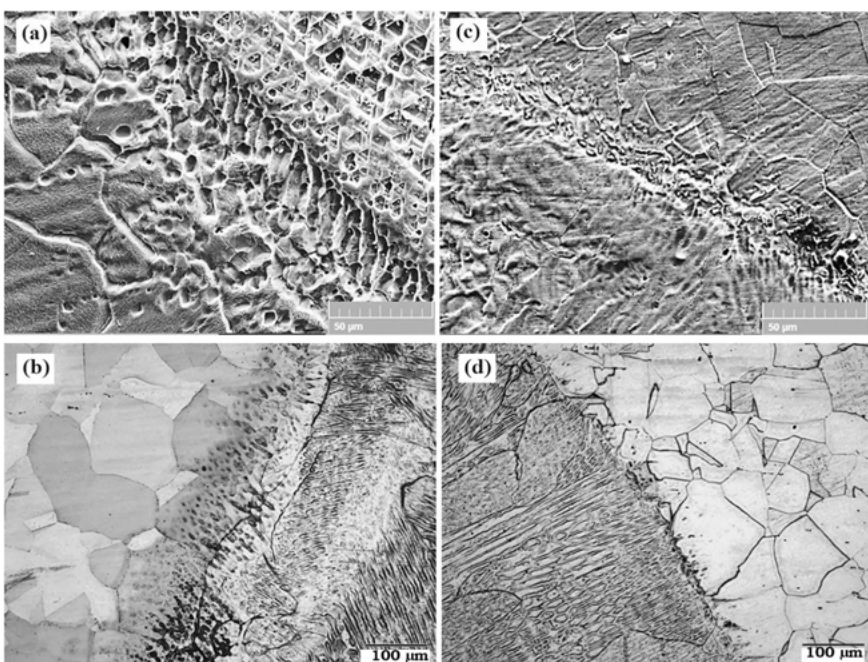


Fig. 10. SEM and OM micrographs of dissimilar pulsed TIG weldment: (a, b) Monel 400, (c, d) AISI 316.

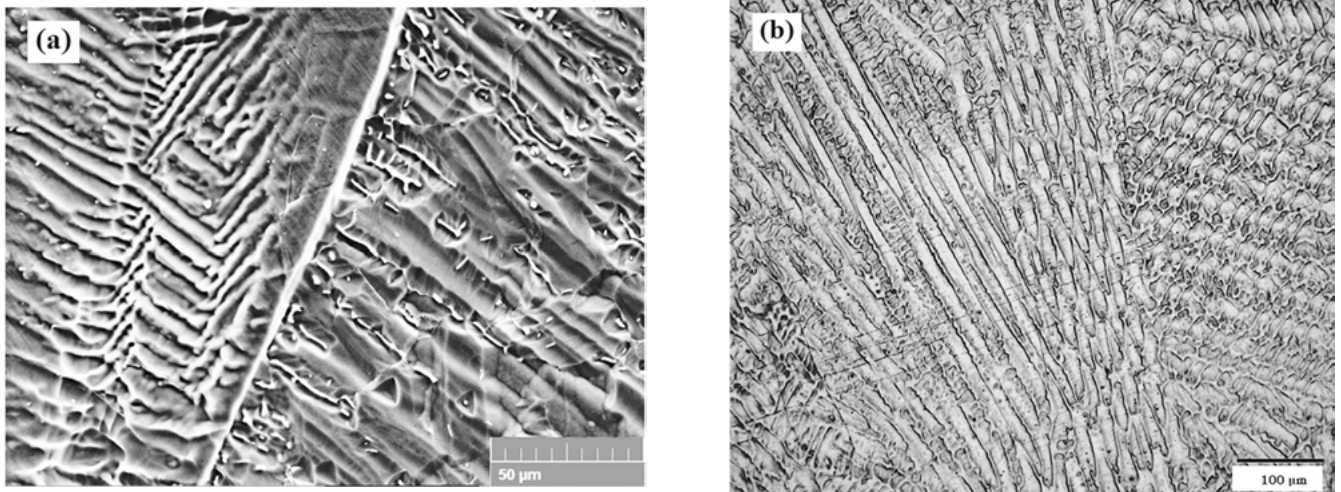


Fig. 11. Weld zone of dissimilar pulsed TIG weldment: (a) SEM, (b) OM micrographs.

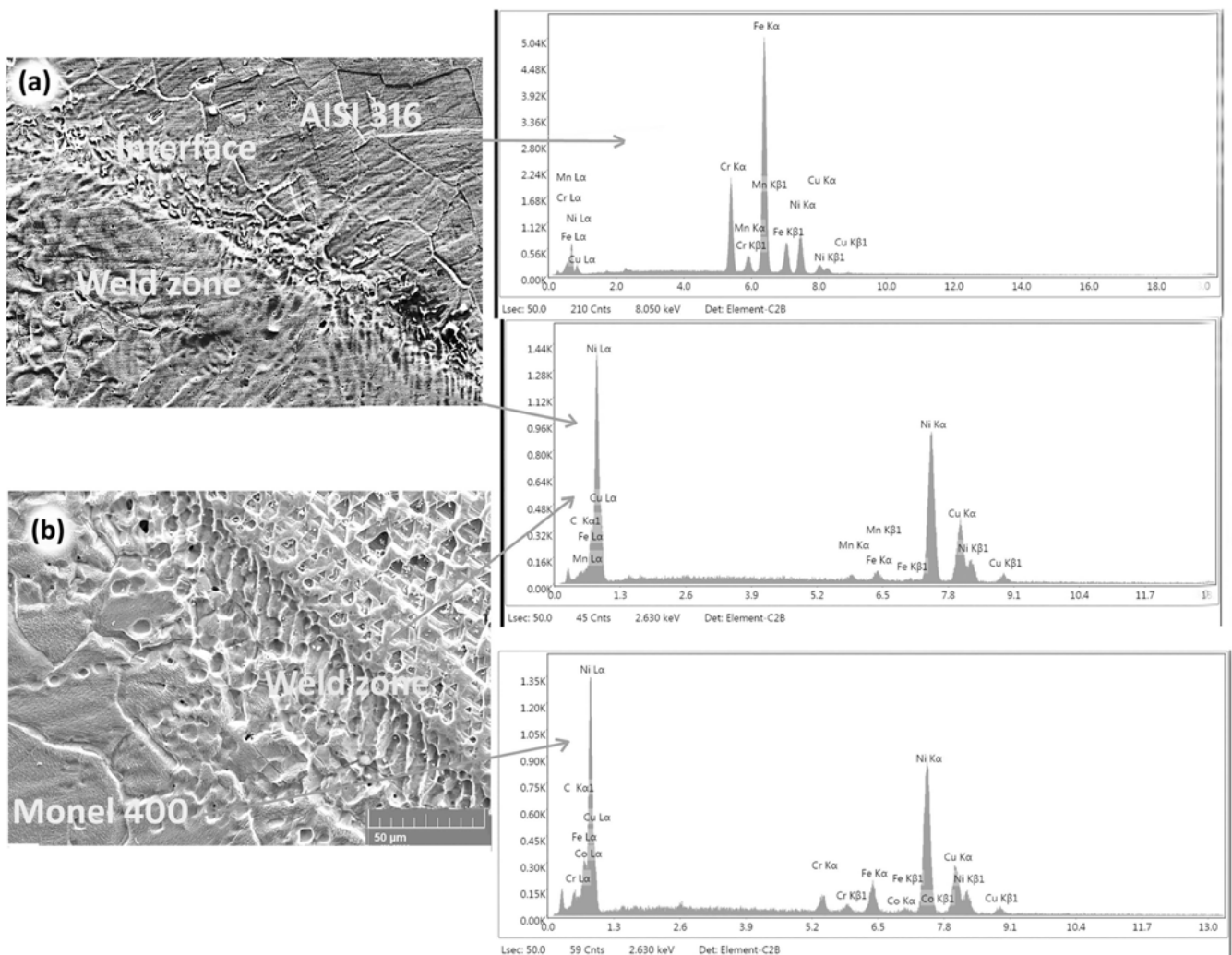


Fig. 12. SEM/EDS X-ray point analysis of dissimilar pulsed TIG weldment: (a) AISI 316, (b) Monel 400.

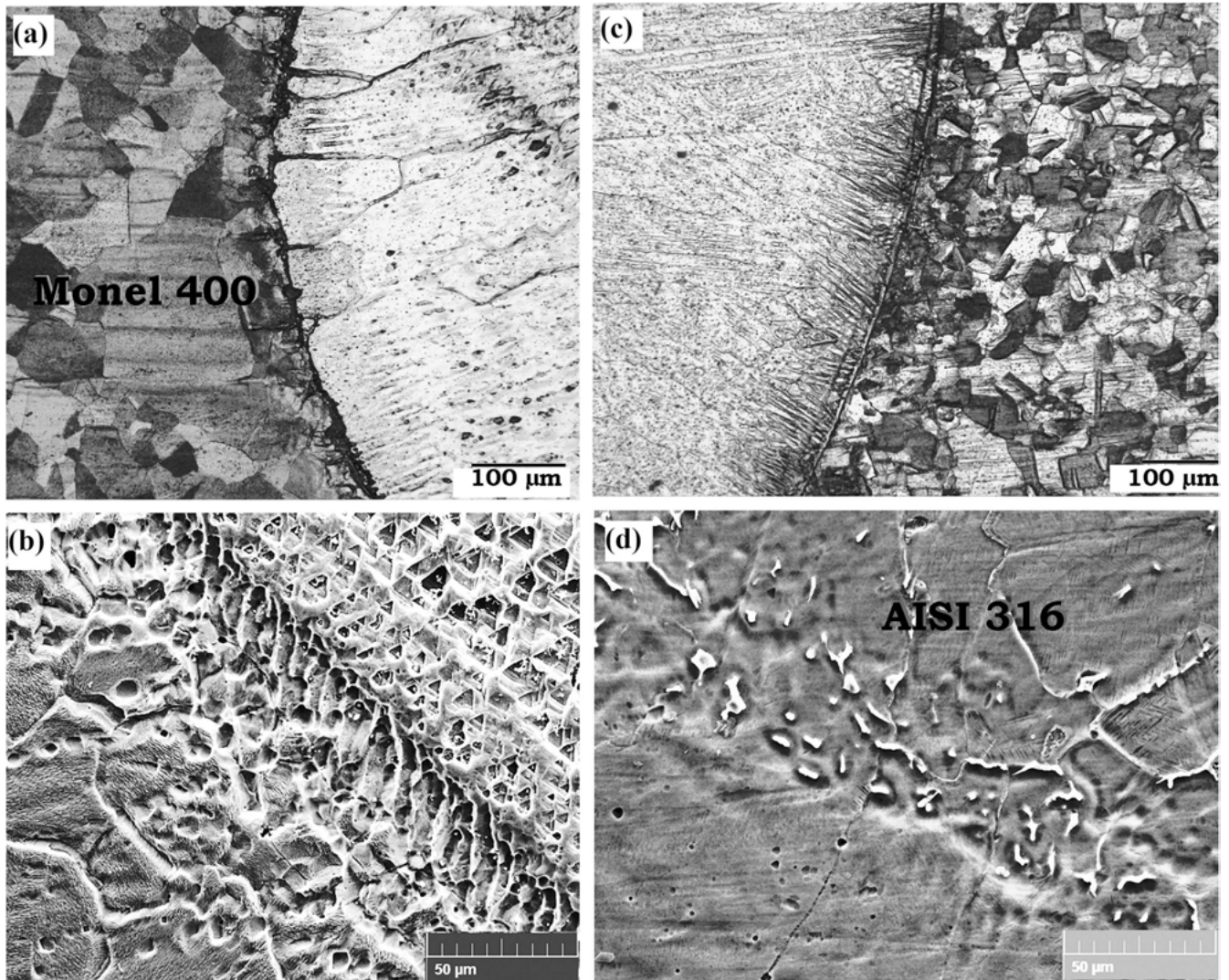


Fig. 13. OM and SEM HAZ microstructures of Interpulse TIG weldment: (a, b) Monel 400, (c, d) AISI 316.

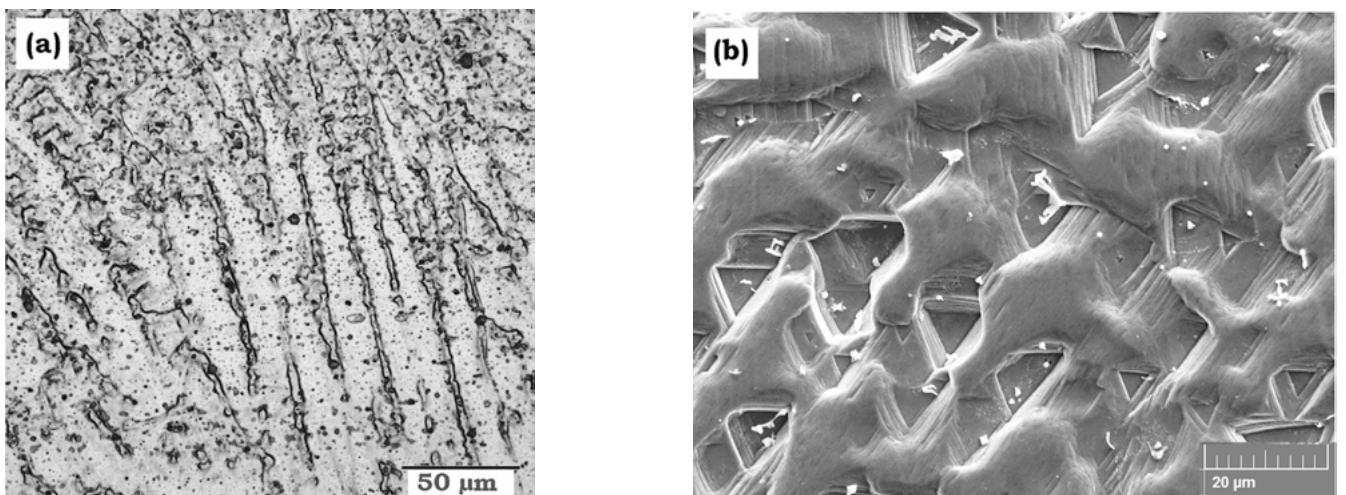


Fig. 14. Weld zone of dissimilar Interpulse TIG weldment: (a) OM, (b) SEM micrographs.

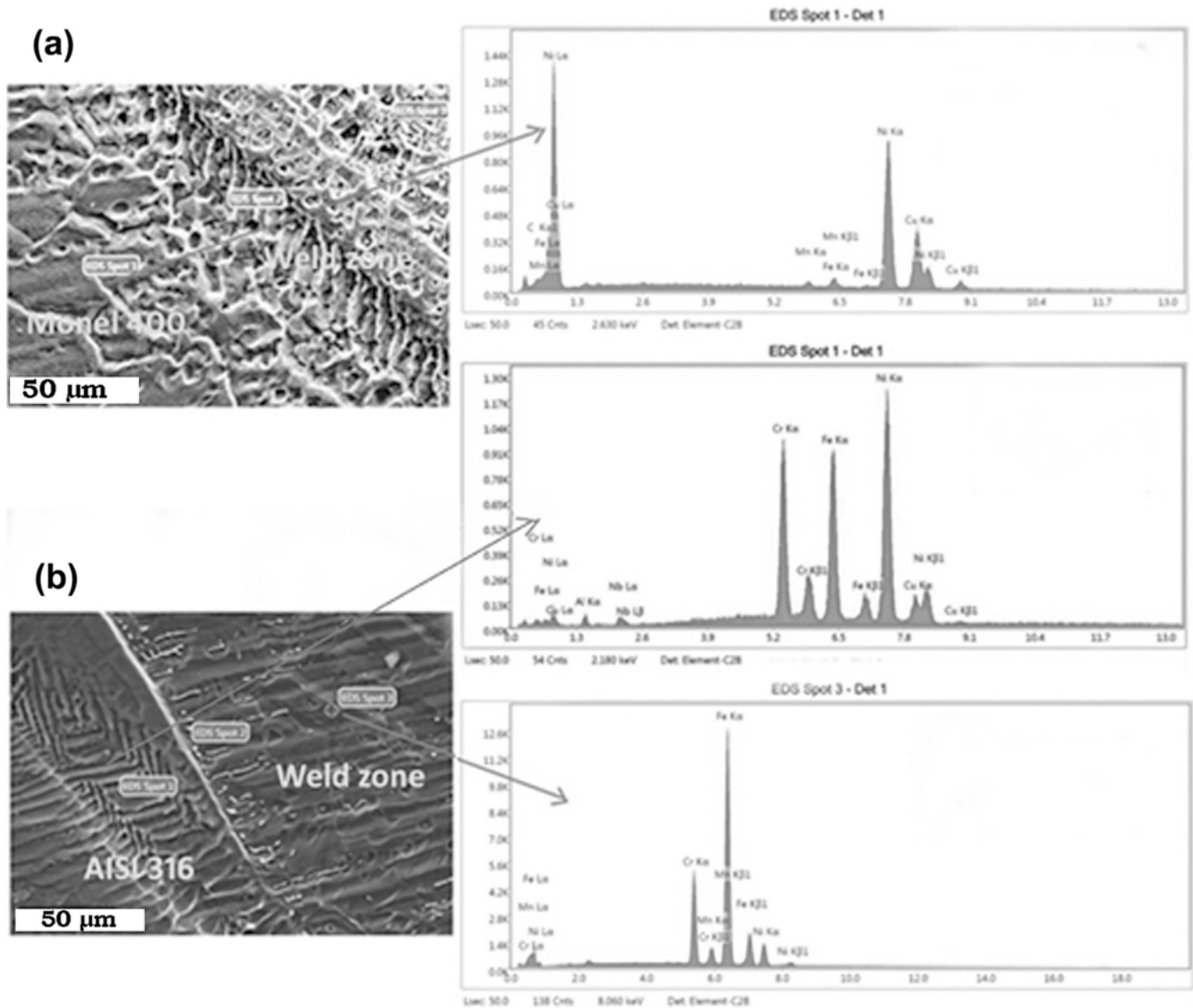


Fig. 15. SEM/EDS X-ray point analysis of dissimilar Interpulse TIG weldment: (a) Monel 400, (b) AISI 316.

strength. From the SEM/EDS point analysis, the chemical compositions of HAZ and weld zone of three dissimilar weldments are listed in Table 6. In the three welding techniques, niobium (Nb) alloying element was observed at the fusion zone which promotes the formation of carbides (NbC) during solidification which will improve the ductility dip cracking (DDC).

5. Conclusion

The constant, pulsed and Interpulse current TIG welding techniques have been used to join the dissimilar combination of AISI 316 and Monel 400 successfully by using ER-NiCrMo-3 filler wire. The conclusions drawn from the experimental studies are as follows;

- The residual stresses of constant, pulsed and Interpulse current TIG welding techniques were found to be 189 MPa, 101 MPa and 53 MPa, respectively, and compressive in nature. The developed residual stresses in these welded structures were self-balanced and within the yield limits only. Due to the constricted arc heat input rates in the Interpulse TIG welding technique the residual stresses

- were reduced by 51.3% and 71.9% when compared to pulse and constant current TIG techniques, respectively.
- The weld strength and microhardness of the Interpulse current TIG weldment are superior than the other two welded joints. The weld strength of Interpulse current TIG welding technique was improved by 5.7% and 7.7% when compared to pulsed and constant current TIG welding techniques, respectively.
- The ratio of yield strength to that of ultimate tensile strength was higher in pulsed current TIG weldment (0.62) and Interpulse current TIG weldment (0.61) than in constant current TIG weldment (0.46).
- The microhardness of constant, pulsed and Interpulse current TIG dissimilar weldments at the weld zone is increased by 30.8%, 28.4% and 32.7%, respectively when compared to the microhardness of base metal Monel 400.
- The HAZs on both sides of base metals were greatly reduced in Interpulse TIG welded joints compared to that of TIG welded joint. The HAZ width of Monel 400 and AISI 316 of Interpulse TIG weldment decreased by 14.28% and 25.64%, respectively when compared to the constant current TIG weldment.

Table 6. SEM/EDS point analysis (wt.%) of dissimilar weldments joined by three welding techniques.

(a) Constant-TIG								
Zone	Ni	Cr	Fe	Cu	Mo	Mn	Si	Others
Monel HAZ	60.61	2.17	6.1	29.02	0.5	1.34	0.23	–
Weld zone	47.21	20.06	18.42	9.01	2.2	1.71	0.2	Nb-0.96, Al-0.2
AISI HAZ	9.01	21.84	65.98	–	1.67	1.46	–	–
(b) Pulsed-TIG								
Zone	Ni	Cr	Fe	Cu	Mo	Mn	Si	Others
Monel HAZ	61.93	–	4.17	32.17	–	1.37	0.34	–
Weld zone	46.07	19.71	18.4	9.4	3.2	1.98	0.4	Nb-0.79
AISI HAZ	9.31	18.74	68.69	–	1.24	1.96	–	–
(c) Interpulse-TIG								
Zone	Ni	Cr	Fe	Cu	Mo	Mn	Si	Others
Monel HAZ	64.02	–	3.42	30.92	–	1.24	0.36	–
Weld zone	47.04	20.01	19.02	7.05	3.8	2.01	0.3	Nb-0.86
AISI HAZ	9.06	19.04	68.49	–	1.22	1.87	–	–

- The segregation of alloying elements at the interface of base plates and coarse grain structures were observed with the constant current TIG welding technique. Whereas the segregation of alloying elements was controlled in the pulsed TIG welding technique. Grain refinement and well-defined grain boundaries were observed in welded joints obtained from Interpulse current TIG welding.
- The Interpulse current TIG welding resulted in considerably reduced residual stresses and improved mechanical and metallurgical properties owing to its controlled total heat input during the process which will help to prevent inter-granular stress corrosion cracking.

References

[1] J.R. Davis: ASM Specialty Handbook, Epub ahead of print, USA (2000). (2000). DOI:10.1361/ncta2000p013,
 [2] J.N. DuPont, J.C. Lippold, S.D. Kiser: John Wiley & Sons, Inc., New Jersey. (2009) 53. DOI:10.1017/CBO9781107415324.004
 [3] J.C. Lippold, D.J. Kotecki: Wiley-Interscience, John Wiley & Sons, Inc., New Jersey (2005).
 [4] K.D. Ramkumar, S.V. Naren, P.V.R. Karthik, A. Tiwari, N. Arivazhagan: J. Manuf. Process. (2016). DOI:10.1016/j.jmappro.2015.10.004
 [5] Y. Balram, G. Rajyalakshmi: Mater. Res. Express. (2019). DOI:10.1088/2053-1591/ab23cf
 [6] K.D. Ramkumar, A. Chandrasekhar, A.K. Singh, S. Ahuja, N. Arivazhagan: Metallogr. Microstruct. Anal. (2015). DOI:10.1007/s13632-015-0236-y
 [7] Yelamasetti, Balram, Kumar, Sravan, B. Sridhar, T. Vishnu, V.R. Gunda: Mater.Today Proc. (2019). DOI:10.1016/j.matpr.2019.06.759
 [8] K.D. Ramkumar, A. Chandrasekhar, A. Srivastava, H. Preyas, S. Chandra, S. Dev, N. Arivazhagan: J. Manuf. Process. (2016). DOI:10.1016/j.jmappro.2016.07.006
 [9] K.D. Ramkumar, N. Arivazhagan, S. Narayanan: Mater. Des. (2012). DOI:10.1016/j.matdes.2012.03.024
 [10] P.J. Withers, H.K.D.H Bhadeshia: Mater. Sci. Technol. (2001). DOI:10.1179/026708301101509980
 [11] O. Anderoglu: Residual Stress Measurement Using X-Ray Diffraction, Texas A&M Univ. (2004) 64.
 [12] P.S. Prevey: Met. Handbook, Met. Park (1986) 513. DOI:10.1361/asmhba0001761

[13] S.A.A. Akbari, R. Miresmaeili: J. Mater. Process. Technol. (2008) 208. DOI:10.1016/j.jmatprotec.2008.01.015
 [14] Y. Balram, G. Rajyalakshmi: U.P.B. Sci. Bull., Ser. D. (2018) 80.
 [15] D. Deng, H. Murakawa, W. Liang: Comput. Methods Appl. Mech. Eng. (2007) 196. DOI:10.1016/j.cma.2007.05.023
 [16] P. Vasantharaja, V. Maduarimuthu, M. Vasudevan, P. Palanichamy: Mater. Manuf. Process. (2012) 27. DOI:10.1080/10426914.2012.663135
 [17] A.R. Kohandehghan, S. Serajzadeh, A.H. Kokabi: (2010) 25. DOI:10.1080/10426914.2010.481004
 [18] Z. Zhang, Y. Feng, Q. Tan, J. Zou, J. Li, X. Zhou, G. Sun, Y. Wang: (2019) 166. DOI:10.1016/j.matdes.2019.107603
 [19] I.I. Ahmed, J.A. Adebisi, S. Abdulkareem, A.H. Sherry: J. King Saud Univ. – Eng. Sci. (2018) 30. DOI:10.1016/j.jksues.2016.01.004
 [20] Y. Javadi, M. Ashoori M: Vessel. Mater. Des. (2015) 85. DOI:10.1016/j.matdes.2015.07.012
 [21] T. Bajpei, H. Chelladurai, M.Z. Ansari: J. Manuf. Process. (2017) 25. DOI:10.1016/j.jmappro.2016.12.017
 [22] S. Murugan, S.K. Rai, P.V. Kumar, T. Jayakumar, B. Raj, M.S.C. Bose: (2001) 78. DOI:10.1016/S0308-0161(01)00047-3
 [23] E. Ranjbarnodeh, S. Serajzadeh, K.A. Hosein, S. Hanke, A. Fischer: Int. J. Adv. Manuf. Technol. (2011) 55. DOI:10.1007/s00170-010-3095-3
 [24] V. Harinadh, G. Edison, A. Suresh, B.R. Kumar: Int. J. Eng. Technol. (2018) 7. DOI:10.14419/ijet.v7i4.10.20711
 [25] D. Deng, H. Murakawa, W. Liang: Comput. Mater. Sci. (2008) 42. DOI:10.1016/j.commatsci.2007.07.009
 [26] S. Pandit, V. Joshi, M. Agrawal, M. Manikandan, K.D. Ramkumar, N. Arivazhagan, S. Narayanan: Procedia Eng. (2014) 75. DOI:10.1016/j.proeng.2013.11.012
 [27] K.D. Devendranath, N. Arivazhagan, S. Narayanan: Kov. Mater. (2014) 52. DOI:10.4149/km-2014-5-287
 [28] Y. Balram, G. Rajyalakshmi, G.V. Ramana, B. Sridhar, V. Harinadh: Int. J. Adv. Manuf. Technol. (2020) 108. DOI:10.1007/s00170-020-05562-w
 [29] K.D. Ramkumar, G. Thiruvengatam, S.P. Sudharsan, D. Mishra, N. Arivazhagan, R. Sridhar: Mater. Des. (2014) 60. DOI:10.1016/j.matdes.2014.03.031
 [30] S. Pichumani, R. Srinivasan, V. Ramamoorthi: J. Mech. Sci. Technol. (2018) 32. DOI:10.1007/s12206-018-0130-4
 [31] S. Avinash, Y. Balram, B. Sridhar, G. Venkatramana: Mater. Today Proc. (2019). DOI:10.1016/j.matpr.2019.07.211
 [32] S. Dev, K.D. Ramkumar, N. Arivazhagan, R. Rajendran: J. Manuf. Process. (2018) 32. DOI:10.1016/j.jmappro.2018.03.035

- [33] K.D. Ramkumar, V. Joshi, S. Pandit, M. Agrawal, O.S. Kumar, S. Periwal, M. Manikandan, N. Arivazhagan: *Mater. Des.* (2014) 64. DOI:10.1016/j.matdes.2014.08.055
- [34] G.M. Reddy, A.A. Gokhale, K.P. Rao: *Mater. Sci. Technol.* (1998) 14. DOI:10.1179/mst.1998.14.1.61
- [35] Y. Balram, G. Rajyalakshmi: *Mater. Today Proc.* (2019). DOI:10.1016/j.matpr.2019.08.125
- [36] D. Mishra, A. Manjunath, K. Parthiban: *Ind. Welding Journal.* (2017) 50. DOI:10.22486/iwj/2017/v50/i4/162271
- [37] P.N. Kumar, Y. Bhaskar, P. Mastanaiah, C.V.S. Murthy: *Procedia Mater. Sci.* (2014) 5. DOI:10.1016/j.mspro.2014.07.483
- [38] Y. Balram, T.V. Vardhan, G.V. Ramana: *Proc. Inst. Mech. Eng. Part C J. Mech. Eng. Sci.* (2020). DOI:10.1177/0954406220960780
- [39] P.K. Giridharan, N. Murugan: *Int. J. Adv. Manuf. Technol.* (2009) 40. DOI:10.1007/s00170-008-1373-0
- [40] M. Fitzpatrick, A. Fry, P. Holdway, F. Kandil, J. Shackleton, L. Suominen: *Meas. Good Pract. Guid.* (2005) 74. DOI:10.1007/s00028-005-0194-y

(Received March 1, 2020; accepted August 6, 2020)

Correspondence address

Balram Yelamasetti
Assistant Professor
Full Postal Address: Department of Mechanical Engineering
CMR Institute of Technology
Medchal
Hyderabad-501401
Telangana
India
Tel.: +91 9951312204
E-mail: balram3072@gmail.com

Bibliography

DOI 10.3139/146.111961
Int. J. Mater. Res. (formerly Z. Metallkd.)
111 (2020) 11; page 880–893
© Carl Hanser Verlag GmbH & Co. KG
ISSN 1862-5282

Fuzzy-Taylor- Elephant Herd Optimization Inspired Deep Belief Network for DDoS Attack Detection and Comparison with State-of-the-Arts Algorithms

S. Velliangiri^a, Hari Mohan Pandey^b

^aDepartment of Computer Science, CMR Institute of Technology, Telangana, Hyderabad

velliangiris@gmail.com

^bDepartment of Computer Science, Edge Hill University, UK

Pandeyh@edgehill.ac.uk

Abstract: Cloud computing environment support resource sharing as cloud service over the internet. It enables the users to outsource data into the cloud server that can be accessed remotely from various devices distributed geographically. Accessing resources from the cloud causes various security issues as the attackers try to illegally access the data. The distributed denial of service (DDoS) attack is one of the security concern in the cloud server. DDoS is a kind of cyber attack which disrupt normal traffic of targeted cloud server (or any other servers). In this paper, we propose an effective fuzzy and taylor-elephant herd optimization (FT-EHO) inspired by deep belief network (DBN) classifier for detecting the DDoS attack. FT-EHO uses taylor series and elephant heard optimization algorithm along with a fuzzy classifier for rules learning. The performance of the proposed FT-EHO is evaluated through rigorous computer simulations. Three standard benchmark databases, namely, KDD cup, database1 and database2 are used during simulations. Four quality measures such as accuracy, detection accurarcy, precision and recall are considered as a performance metrics. FT-EHO's performance is compared against the state-of-the-art methods considering the evaluation metrics. Results reveals that the proposed FT-EHO showed significantly higher value of evaluation metrics (accuracy (93.811%), detection rate (97.200%), precision (94.981%) and recall (93.833%)) as compared to other methods.

Keywords: Selector Engine, Elephant Herd Optimization (EHO), fuzzy system, Deep Belief Network (DBN).

1. Introduction

Cloud Computing (CC) is a new form to compute resources. It provide various service such as storage services, hardware equipment, operating systems, software applications and entire network

infrastructure and delivers the internet-based services to the users with low cost [6]. CC refers to both the services and the applications delivered to the hardware, internet, and software system in the data center that provides the cloud services [15]. The internet-based technology and the cloud metaphor referenced the accessibility and the availability of the resources to be computed [6]. CC provides the organizational users and the computing resources to be deployed as private, public, and community on the hybrid cloud [3]. CC provides various services like platform as a service (PaaS), expert as a service (EaaS), infrastructure as a service (IaaS) and software as a service (SaaS). The on-demand services and the computing resources allocated to the users are operated in the cloud [6].

CC is a paradigm where the resources of computing are shared as a cloud service on the internet [18]. CC is used in many organizations in the worldwide level as it supports computation and data storage with high performance. The cloud service relies on creating various dependencies using the number of holes with incompatibilities and vulnerabilities [17]. CC is a continuous development technology with abundant challenges in the service of security. The major concern in a cloud environment is the management of the cloud services [14]. The resources that are to be computed as the on-demand services are allocated to the user through the cloud storage [6].

The CC is used at most of the places to solve the cyber attacks as various vulnerabilities are existing in a cloud environment. The distributed denial of service (DDoS) attack is a kind of cyber attack which disrupt normal traffic of targeted cloud server. Hence, the DDoS attack is the critical [2]. Main characteristics of the DDoS attacks are defined: (a) It is very rigid to detect as it contains the equivalent flow in the regular user. DDoS attacks can be completed using a solitary node with limited flow of data and it results in low cost; (b) DDoS is a target insensitive attack because the attacked node identifies the attacker node. Thus, it affects the cloud computing services massively. The DDoS attacker compromises and collects various susceptible hosts referred to as zombies to attack against the targeted node; (c) DDoS attack increases sophistication, size and identifying the extortion is a major motive of this attack [3] [9]; (d) DDoS defense approach generally classifies the data packets as either malicious or legitimate packets [3]; (e) The DDoS attack exhausts the services and resources of the organization and individual by forwarding the useless traffic. Hence, legitimate users cannot access the services [4]; and (f) The DDoS detectors are situated in each host and their respective packet filters are disseminated through the virtual machines (VM) [4].

For the non-intrusive traffic, the network profile is generated by the detectors based on the network attributes of the selected statistics [4].

For most of the web applications (e.g. online auctions and online retail sales), security of the network is a major factor in the internet services [1]. Intrusion detection system (IDS) was noted as an effective method to detect DDoS attack and ensures the functional cloud services [6]. IDS detects the computer attacks by investigating the records, which are collected from the internet [1]. IDS was categorized into two types: (a) anomaly-based detection; and (b) signature or misuse based intrusion detection. Signature-based detection method uses the attacker signatures that are present in the knowledge database for identifying the attacks [3]. It is an effective technique to detect the known attacks [3]. On the other hand, anomaly-based method uses the behavioral pattern of the normal traffic with a period to compute whether the relevant patterns are deviated from the accepted behaviour [3]. The anomaly detection potentially detects a few or zero-day attacks [3]. Anomaly detection specifies the deviations that are obtained from the regular patterns whereas the signature detection utilized the patterns, which are related to the attacks to detect the intrusions [1].

Intrusion detection (ID) in CC is considered as an NP-hard problem. Metaheuristic algorithms give the best solution to the NP-hard problems [1]. The IDS is classified based on the source data as follows: (a) Host based IDS (HIDS); (b) Network-based IDS (NIDS); and (c) Distributed IDS (DIDS). The host-based detection system detects the intrusion using the sensors in the single host, whereas the network-based detection system focuses on the network arrangement. DIDS integrates the sensors and classifies the IDS into mobile agent-based IDS and grid-based IDS [10] [11].

The primary focus of this research is to develop an algorithm for detecting the DDoS attack in the cloud. We propose an effective fuzzy and taylor-elephant herd optimization (FT-EHO) inspired by deep belief network (DBN) classifier for detecting the DDoS attack. The working of the FT-EHO involves three modules: (a) feature extraction; (b) feature selection; and (c) classification. The working starts when the user request is sent to the packet feature extraction module to extract the packet features. The packet informations such as *dest-bytes*, *duration*, *src-bytes*, and so on are extracted and the selective features are obtained by applying the holoentropy into the feature selector engine. Finally, selected features are further processed by the classification module. The classification module detects the DDoS attacks using a fuzzy and taylor-elephant herd optimization (FT-EHO) inspired by deep belief network (DBN) classifier.

Commented [HP1]: R3C2. Motivation of the paper is not clearly explained so explain in a more proper way.

Response: The motivation of the paper is clearly mentioned in the Introduction section of the revised manuscript.

The proposed FT-EHO based DBN classifier is the integration of the DBN and fuzzy classifier. The rule learning approach based on the fuzzy classifier where the genetic algorithm (GA) in the adaptive genetic fuzzy system (AGFS) is the standard form. Moreover, the genetic algorithm has no guarantee for optimal solution and its one of state-of-the-art algorithms. Therefore, the genetic algorithm is replaced with the T-EHO algorithm, which is the integration of Taylor series and EHO algorithm. EHO is one of the ideal algorithms for finding a global optimization solution. EHO has been applied various optimization benchmark problems and real-life applications showing promising. Based on the extracted packet features, the proposed classifier based on a fuzzy and DBN classifier detects the DDoS attack by determining the node as an intruder or not.

The key contributions are elaborated as follows.

- We present a FT-EHO based DBN classifier for DDoS attack detection. Our approach utilized the merits of both fuzzy and DBN classified. In FT-EHO, we integrated Taylor series and elephant herd optimization (EHO) algorithm along with fuzzy classifier for rules learning. In the proposed system, the traditional genetic algorithm (GA) is replaced by EHO algorithm.
- We systematically show how the packet features and packet information are extracted by the packet extraction module. The selective features are obtained by applying the holoentropy into the feature selector engine.
- A comprehensive discussion is presented on the rule learning approach based on the fuzzy classifier, where GA is replaced by Taylor series and EHO (T-EHO) algorithm.
- Extensive computer simulations are conducted to evaluate the performance of the proposed FT-EHO based DBN classifier. Three standard benchmark databases, namely, KDD cup database [25], database 1 and database 2 are used during simulations. Four quality measures such as accuracy, detection accuracy, precision and recall are selected as a performance metrics.
- Finally, the comparative results and analysis is presented. FT-EHO based DBN classifier is compared against the state-of-the-art methods. The result indicates that FT-EHO based DBN classifier outperforms other methods.

The rest of the paper is organized as follows: Section 2 elaborates related work; Section 3 discusses the proposed algorithm; Simulation model is presented in the Section 4; Section 5 shows the conclusion of this research work.

Commented [HP2]: R4C1. The author proposes a novel effective fuzzy and Taylor-Elephant Herd optimization (T-EHO)-based Deep Belief Network (DBN) classifier to detect the DDoS attack. This paper seems interesting and can be very beneficial on to detect DDoS attack. There are some recommendations which the author can use to improve the quality of the paper as follows:

1. The author need to explain in introduction section why Taylor series and Elephant Herd Optimization algorithm with fuzzy classifier for as rule learning approach is used over genetic algorithm.

Response: The rule learning approach based on the fuzzy classifier, where the genetic algorithm in the AGFS is the standard form. Moreover, genetic algorithm has no guarantee for optimal solution and its one of state-of-the-art algorithm. Therefore, genetic algorithm is replaced with the T-EHO algorithm, which is the integration of Taylor series and EHO algorithm. Based on the extracted packet features, the proposed classifier based on fuzzy and DBN classifier detects the DDoS attack by determining the node as an intruder or not.

Commented [HP3]: R1C1: Introductory section is overcrowded with both relevant and irrelevant details. This should be summarized to highlight the research motivations and the proposed research carried out.

Response: Appreciating you for notifying this comment. The introduction is improved, and unnecessary sentences are removed. The revised introduction highlight the research motivation and proposed research carried out.

2. Related work

The review of literatures are deliberated in this section. Yasir Ali *et al.* [1] developed a detection and migration approach to enhance the performance and stability of the Network Control System (NCS). The unknown packets are dropped from the network by applying the filtering process to enhance data integrity. However, this approach did not apply to the physical applications in the Cloud Control System (CCS). Kesavamoorthy and Ruba Soundar [2] proposed an autonomous multi-agent approach to improve communication among the agents to accurately make the decision. The multiple agents communicate themselves and update the coordinating agent to detect the DDoS attacks. The stochastic based filtering was not applied to achieve optimization. Opeyemi *et al.* [3] developed a feature selection approach to enhance the optimal selection. The important features were identified based on the counter and the threshold and enhanced the detection accuracy. However, the performance attained using the labeled datasets is very less. Pandey *et al.* [4] introduced a distributed network filtering approach to distributing the filters among the virtual machines. The DDoS attacks were effectively detected and provide high scalability, whereas, the real-time detection was not performed. Loukas *et al.* [5] developed a cloud-based intrusion detection system using the deep learning approach. This system attained high accuracy and better detection latency. Collecting the data for the attack or normal behaviour was not considered. Hajimirzaei and Navimipour [6] introduced an intrusion detection system to create the training subset. The normal and the abnormal packets were identified using the multilayer perceptron in the network traffic. This approach achieved better performance, but the meta-heuristic methods were not applied effectively. Deng *et al.* [7] developed a cyber physical power system for accurate identification and detection of intrusions. This approach attained better performance in terms of scaleup and speedup. Even though the computing nodes were increased, the type of the noise data was not accurately determined. Chen *et al.* [8] proposed a fuzzy-based clustering algorithm to partition the dataset into clusters. Each node perfectly forwards the data packets to the neighboring node. The proposed approach identifies the malicious nodes under heavy traffic conditions, but the structure using a large number of nodes was not considered.

Yan *et al.* [26] showed the characteristics of DDoS attacks in cloud computing and presented a comprehensive survey on the DDoS attacks protection methods using software-defined networking (SDN). Major part had been analyzed and the studies about launching DDoS attacks on SDN and the techniques to detect DDoS attacks in SDN were discussed. From a rigorous

analysis, authors [26] concluded that the conflicting relationship between SDN and DDoS attacks had not been well addressed in the previous literatures. Further, authors [26] had provided information about how to make full use of SDN to beat DDoS attacks in cloud computing environments and how to prevent SDN itself from becoming a victim of DDoS attacks. Somani *et al.* [27] introduced developments related to DDoS attack mitigation solutions in the cloud. They presented an inclusive survey with a thorough insight into the characterization, prevention, detection, and mitigation techniques of these attacks. Also, they presented an inclusive solution taxonomy for classifying DDoS attack solutions. The authors provided a definite guideline on effective solution building and detailed solution requirements to assist the cybersecurity research community in designing defense techniques.

Gao et al. [9] modelled a semi-supervised learning approach in the cloud-based robotic system for detecting the intrusion. It constructs the ensemble labeled data using the ensemble learning, and utilized the unlabeled data for data analysis. However, modelling the generalization and improving the detection performance is a challenging task in the intrusion detection system. Dey et al. [10] developed a machine learning approach for intrusion detection in the cloud environment. Identifying the attributes in the detection system is a challenging task in the cloud-based environment. A Machine learning based intrusion detection system was developed to intercept the network traffic in the physical layer [11]. Detecting the intrusion using the ensemble learning classifier results in several challenges in the central storage server. A conceptual cloud mitigation framework is modelled for detecting the attacks in the cloud. Providing security to the cloud server is a challenging task in the cloud services. The availability of the training and the testing dataset results in attack patterns to generate the optimal features [12]. Patil et al [13] developed a multi-threaded based intrusion detection system to extract the accurate features in the cloud system. Delivering the proper services to the cloud user results many challenges in the cloud computing. In the real time, if the selective features are not accurately extracted, the DDoS attack will not be detected.

In order to address the above challenged, we have proposed Fuzzy-Taylor-Elephant Herd Optimization based Deep Belief Neural Network (FT-EHO-DBN) classifier for detecting the DDoS attack. When compared with the state-of-the-art algorithms, DBN has the more advantage in the pre-training with the fine-tuning learning technique and a multi-layer structure. These advantages formulate the DBN to extract the deep attributes of the training data. Hence, the DBN

solves the problems of low training efficiency, local optimum, and complex network attack detection. Here, the T-EHO algorithm is developed by integrating the Taylor series in the existing EHO for selecting the optimal weights and biases for the DBN classifier. EHO is one of the ideal algorithms for finding a global optimization solution. EHO has been applied to various optimization benchmark problems and real-life applications showing promising. Hence, the proposed FT-EHO-DBN classifier addresses the challenges of the research problem

3. Proposed Model

In this paper, Taylor-Elephant Herd Optimization based Deep Belief Neural Network (TEHO-DBN) classifier is developed for detecting the DDoS Attack. When compared to the conventional neural networks, DBN has the merits of pre-training with the fine-tuning learning technique and a multi-layer structure. These merits formulate the DBN to extract the deep attributes of the training data. Hence, the DBN solves the problems of low training efficiency, local optimum, and complex network attack detection. Here, the TEHO algorithm is developed for selecting the optimal weights and biases for the DBN classifier. EHO is one of the ideal algorithms for finding a global optimization solution. EHO has been applied to various optimization benchmark problems and real-life applications showing promising results in finding optimal solutions. Since EHO does not resort to any type of relaxations, EHO outperforms the state-of-the-art optimization algorithms. Hence, the proposed TEHO-DBN classifier addresses the challenges of the research problem.

The DDoS attack is detected using the proposed FT-EHO-DBN classifier. The block diagram of the proposed DDoS attack detection is depicted in Figure 1. We have used DBN classifier which is consists of 21 hidden layers. The number of hidden layers (N_h) can be determined using equation (1).

$$N_h = N_s / (N_i + N_o) * \alpha\alpha \quad (1)$$

Where, N_i = number of input neurons; N_o = the number of output neurons; N_s = number of samples in the training data set and $\alpha\alpha$ = an arbitrary scaling factor, usually 2-10.

Commented [HP4]: R1C2. The related work needs to be elaborated more by adding more literature on deep networks for cloud computing security.

Response: The suggestion considered and therefore literatures have been added for cloud computing security.

Commented [HP5]: R2C1. In this paper authors have proposed an effective fuzzy and Taylor-Elephant Herd optimization (T-EHO)-based Deep Belief Network (DBN) classifier to detect the DDoS attack. The idea proposed in the paper is novel and well organized. Although, authors have covered most of the things but still the paper needs some improvement. My comments are on this paper is given as follows:

1. In section 2, a paragraph must be added at the end to show how this paper addresses the shortcoming of the existing algorithms.

Response: Thank you for pointing this to us. A paragraph is added to address this point.

Commented [HP6]: R3C1. The reason of replacing genetic algorithm need to be discussed.

Response: In this paper, Taylor-Elephant Herd Optimization based Deep Belief Neural Network (TEHO-DBN) classifier is developed for detecting the DDoS Attack. When compared to the conventional neural networks, DBN has the merits of pre-training with the fine-tuning learning technique and a multi-layer structure. These merits formulate the DBN to extract the deep attributes of the training data. Hence, the DBN solves the problems of low training efficiency, local optimum, and complex network attack detection. Here, the TEHO algorithm is developed for selecting the optimal weights and biases for the DBN classifier. EHO is one of the ideal algorithms for finding a global optimization solution. EHO has been applied to various optimization benchmark problems and real-life applications showing promising results in finding optimal solutions. Since EHO does not resort to any type of relaxations, EHO outperforms the state-of-the-art optimization algorithms. Hence, the proposed TEHO-DBN classifier addresses the challenges of the research problem.

Commented [HP7]: R1C4. Usually for Deep learning, the no of layers are at least 8 -10, how many layers in your proposed method?

Response: The number of hidden layers in the deep neural network is 21. The number layer can be calculated following equations.
 N_i = number of input neurons.
 N_o = the number of output neurons.
 N_s = number of samples in the training data set.
 $\alpha\alpha$ = an arbitrary scaling factor, usually 2-10.
 $N_h = N_s / (N_i + N_o) * \alpha\alpha$

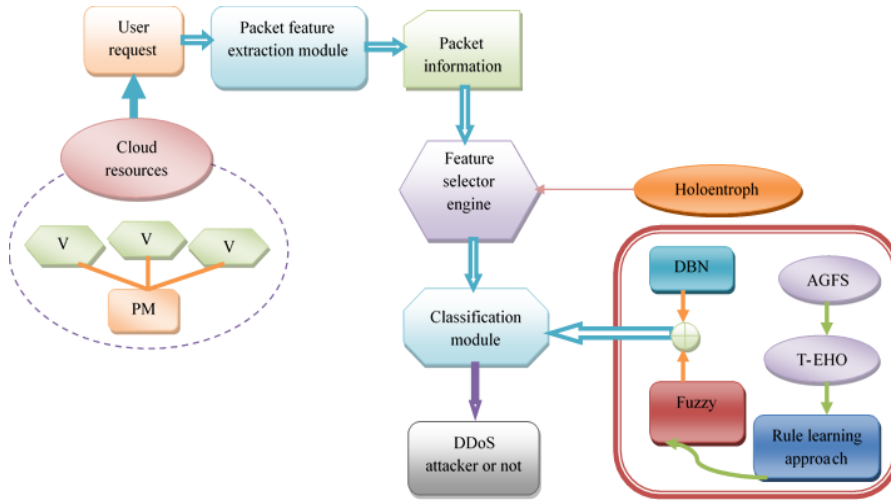


Figure 1. Architecture of the proposed DDOS attack detection.

The proposed DDOS attack detection classifier includes three modules are as follows: i) packet feature extraction module; ii) feature selector engine; and iii) classification module. Initially, the user request is send to the packet feature extraction module to extract the packet features. From each node, the packet information, like duration, dst-bytes, wrong fragment, and so on are extracted in the extraction module. The extracted features are passed into the feature selector engine, which selects the appropriate features accurately using the holoentrophy criteria. Finally, the selected features are further processed by the classification module. The classification module in the proposed approach detects the DDOS attacks using the FT-EHO-DBN classifiers, which is the hybridization of the DBN and fuzzy logic. The proposed FT-EHO-DBN classifier is employed for classification, where the training algorithm is based on T-EHO. In the fuzzy classifier, named AGFS [19], the genetic algorithm is replaced by the T-EHO algorithm, which is the rule learning approach. Based on the extracted packet features, the proposed classifier detects the DDOS attacks by determining the node as an intruder or not.

Initially, the log file is created in the attack detection module, and the created log file is represented as, H . The user utilizes the allocator or the resource scheduler to access the resources in the cloud model. In the resource allocation component, the devices are allocated to the user based on their requirement, and also it contains the device information. The resource scheduler records the log information of every user for creating the log file H .

Commented [HP8]: R1C3. The methodology discussed in section 3 looks interesting; however, this should be discussed in a manner that will facilitate understanding by a non-expert.

Response: We appreciate your concern on methodology. To improve big paragraph is divided in smaller one and an attempt is made to present the idea in lucid manner.

Commented [HP9]: R3C5. Figure 1 and 2 need more explanation so that the contribution needs to be explained in detailed manner.

Response: As per the reviewer suggestion, explanation is added in both Figure 1 and Figure 2.

Commented [HP10]: R2C2. Figure 1 needs explanation especially for different blocks used in the figure.

Response: We added explanation to cover different blocks used in Figure 1.

3.1 Packet feature extraction module

After creating the log file, packet features are extracted from the log file so that classifier can be trained. Extracted features are stored in the feature database, which is denoted as I . Extracted features are explained as follows:

duration: The duration is the first extracted packet feature, which is indicated in seconds, and it shows the time or length of the packet connection.

src-bytes: The nodes present in the cloud model is indicated as the source node or the destination node, as it performs the transmitting and receiving functions. The src-bytes indicate the total number of bytes transmitted from the sender to the receiver.

dst-bytes: This feature is similar to the src-bytes features, dst-bytes represents the total number of bytes transmitted from the receiver node to the sender node.

logged_in: logged_in feature is one of the discrete feature, when the user is log on to the system, then the logged_in feature is resulted as 1, otherwise the feature value will be 0.

count: This feature determines the total number of connections present in the same host.

srv-count: In certain cases, the nodes in the cloud model may provide the exact services, and is represented using the srv-count feature.

The connection of the node is situated under the rejection and the synchronization error, which is expressed using the below two features.

error-rate: This feature reflects the percentage of total connections exists in the cloud using the SYN error.

rerror-rate: This feature shows the percentage of total connections exists in the cloud using REJ error.

diff-srv-rate: This feature represents the percentage of connections made to the various hosts, where the service connections are offered to different hosts.

same-srv-rate: Some services may have the same host as the destination. This feature symbolizes the total number of connections made in the same destination.

srv-diff-host-rate: This feature shows the service connection from single node to various destination hosts.

3.2 Feature selector engine using holoentropy

The extracted packet features are subjected to the feature selector engine to select the considerable features using the holoentropy criteria [20]. The holoentropy used in the feature selector engine is denoted as $X(j_k, j_l)$ and can be determined using equation (1).

$$X(j_k, j_l) = J \cdot L(j_k, j_l) \quad (1)$$

where,

$$J = 2 \left[1 - \frac{1}{1 + \exp(-L(j_k, j_l))} \right] \quad (2)$$

$$L(j_k, j_l) = \sum_{k=1}^{m(j_l)} Y(j_k = k, j_l = l) \cdot \log(j_k = k, j_l = l) \quad (3)$$

Where, $m(j_l)$ represents the unique values of the selected features, j_k and j_l denotes the unique attributes of the selected features.

3.3 FT-EHO-DBN classifier for attack detection

The proposed FT-EHO-DBN classifier to detect the DDoS attack in the cloud environment is elaborated in this section [22] [23]. The proposed FT-EHO-DBN classifier is employed for classification where the training algorithm is based on T-EHO. In the fuzzy classifier, named AGFS, the genetic algorithm is replaced by the T-EHO algorithm, which is the rule learning approach. Based on the extracted packet features, the proposed classifier detects the DDoS attacks by determining the node as an intruder or not.

3.3.1 Fuzzy classifier based on rule learning approach

The rule learning approach, termed as Adaptive T-EHO-based fuzzy system is applied into the fuzzy classifier by replacing the genetic in the AGFS system with the T-EHO algorithm. The Adaptive T-EHO-based fuzzy system is offered by integrating the fuzzy set, and T-EHO with the Genetic Algorithm (GA). The Adaptive T-EHO-based fuzzy system performs the classification using the fuzzy classifier, and generates the optimized rules by GA. Let I denotes the database, which is partitioned into two sets, as training I_{tr} and testing data set I_{te} . The training data is used to design the fuzzy system, and to generate the fuzzy rules. The testing data set is considered in

evaluating the performance of the classification. The overall procedure of Adaptive T-EHO based fuzzy system to generate the fuzzy rules is elaborated as follows:

a) Discretization

Discretization is a process of data pre-processing, which changes the data and range of values into a specific interval. In the discretization function, the training data set $I_{tr} = o_{np}; 0 \leq n \leq r \text{ and } 0 \leq p \leq r$ with r number of **attributes are considered**. The minimum and the maximum values of the attributes are **computed and are** sorted in ascending order. However, the minimum and the maximum values are calculated for all the **classes** in the database, based on the vector.

b) An Algorithmic description of T-EHO algorithm for optimal weight selection

The T-EHO algorithm is introduced to select the optimal weight of the DBN classifier. The T-EHO algorithm is the integration of Taylor series [25] and the EHO [22] algorithm. The EHO algorithm uses the elephant herding characteristics to compute the optimal solution, and the solution space is updated **using two operators, as i) clan updating, and ii) separating operator**. The training process of the T-EHO algorithm is described as below:

Clan initialization: The solution space in the T-EHO algorithm is determined using the population of the clan. The solution space is considered with M population and is denoted as, P_{np} . In each clan, there exists various number of elephants.

Fitness evaluation: The fitness is evaluated by considering the position, clan and error-based fitness in the clan. The solution with the minimum error value is taken as the best fitness solution. Equation (4) is used to determine the fitness value.

$$N_{avg} = \frac{1}{r} \sum_{n=1}^r (h_i - o^n)^2 \quad (4)$$

Where, h_i is the output obtained from the classifier and o^n denotes the estimated output.

Solution update: Based on the matriarch elephant movement, the solution space is updated in the population. The updated solution space is represented using equation (5).

$$P_{new,qn,p} = P_{low,p} + \sigma \times (P_{best,qn} - P_{qn,p}) \times s \quad (5)$$

Where the elephant best position is represented as $P_{best,qn}$ and $P_{qn,p}$ is the old position of p^{th} elephant in clan qn and the term $P_{new,qn,p}$ represents the newly updated position and $P_{low,p}$ denotes the old position. The solution space in the clan is updated using the scaling factor s , with the value ranges from 0 to 1. The search space is refined by adopting the Taylor series. The equation (5) is rearranged as shown in equation (6).

$$P_{new,qn,p} = P_{qn,p} (1 - \sigma s) + \sigma \times P_{best,qn} \times s \quad (6)$$

The solution space based on the Taylor series is expressed using equation (7).

$$P(r+1) = 0.5P(r) + 1.3591P(r-1) - 1.359P(r-2) + 0.6795P(r-3) - 0.2259P(r-4) + 0.0555P(r-5) - 0.0104P(r-6) + 1.38e^{-3}P(r-7) - 9.92e^{-5}P(r-8) \quad (7)$$

Computing $P(r)$ from the above equation (7) is represented as equation (8).

$$P(r) = \frac{1}{0.5} \left[\frac{P(r+1) + 1.3591P(r-1) - 1.359P(r-2) + 0.6795P(r-3) - 0.2259P(r-4) + 0.0555P(r-5) - 0.0104P(r-6) + 1.38e^{-3}P(r-7) - 9.92e^{-5}P(r-8)}{0.5} \right] \quad (8)$$

Equation (8) is substituted in equation (6) to compute $P_{new,qn,p}$ as shown in equation (9).

$$P_{qn,p}(r+1) = \frac{(1 - \sigma s)}{0.5} \left[\begin{array}{l} P(r+1) + 1.3591P(r-1) - 1.359P(r-2) \\ + 0.6795P(r-3) - 0.2259P(r-4) + \\ 0.0555P(r-5) - 0.0104P(r-6) + 1.38e^{-3}P(r-7) \\ - 9.92e^{-5}P(r-8) \end{array} \right] + \sigma \times P_{best,qn} \times s \quad (9)$$

The value of $P_{qn,p}(n+1)$ is computed by solving the above equation as presented in equation (10).

$$P_{qn,p}(n+1) = \frac{(1 - \sigma s)}{0.5 + \sigma s} \left[\begin{array}{l} 1.3591P(r-1) - 1.359P(r-2) \\ + 0.6795P(r-3) - 0.2259P(r-4) + \\ 0.0555P(r-5) - 0.0104P(r-6) + 1.38e^{-3}P(r-7) \\ - 9.92e^{-5}P(r-8) \end{array} \right] + \sigma \times P_{best,qn} \times s \left(\frac{0.5}{0.5 + \sigma s} \right) \quad (10)$$

Equation (10) denotes the updated position of the matchairat elephant using Taylor series. The Taylor coefficient with degree six is used to enhance the optimization accuracy of T-EHO algorithm.

Computing the best solution: After the position gets updated, the optimal solution can be determined using equation (4).

Termination: The iteration to update the position is continued until; the best optimal solution is obtained.

c) Designing the fuzzy membership function

The fuzzy system is considered using the fuzzy rule and the fuzzy membership function.

i) Membership function of fuzzy: The fuzzy membership function is computed using the triangular function, which contains three vertices, as $s, t,$ and u in the $y(z)$ fuzzy set. The membership value is calculated using equation (11).

$$y(z) = \begin{cases} 0 & \text{if } v \leq s \\ \frac{v-s}{t-s} & \text{if } s \leq v \leq t \\ \frac{u-v}{u-t} & \text{if } t \leq v \leq u \\ 0 & \text{if } v \geq u \end{cases} \quad (11)$$

ii) Defining the membership function: The discretization function of each attributes is utilized to compute the number of membership function in the fuzzy classifier. The values of the vertices $s, t,$ and u is defined for each membership function. For each interval, the maximum value of u , and minimum value of s is selected to compute the value for t .

d) Classification using fuzzy system: The fuzzy membership function and the fuzzy rules are applied in the classification process of the fuzzy system.

i) Rule base in the fuzzy system: The fuzzy rule set is generated as $J = \{J_p; 1 \leq p \leq q - K\}$, which is ordered using the fuzzy rule based on the genetic algorithm. The rule base contains the fuzzy rule as, $L_1, L_2, L_3,$ and L_4 , respectively as low, medium, very low, and very low decision.

ii) Membership function of fuzzy: The membership function used for every attributes and their respective values for the triangular membership is also generated.

iii) *Classification using fuzzy data set*: In the testing data set, the test data is converted into the fuzzified value, and the input of the fuzzified is matched with the fuzzy rules to generate the linguistic value, which is then further transformed into the fuzzy score. The optimal value is generated using the fuzzy score, and the output attained using the fuzzy classifier is denoted as, h_j .

3.3.2 Deep Belief Network for attack detection

DBN classifier is developed by incorporating two RBM layers and one MLP layer, which is depicted in Figure 2. In DBN, the connections exist between the visible and the hidden neurons, but there is no connection lies between the hidden neurons, and the visible neurons. The feature vector A is applied as input into the visible layer of the first RBM in DBN. The output obtained from the RBM 1 hidden layer is passed as input to the second RBM, and the output obtained from RBM layer 2 is fed as input to the MLP layer.

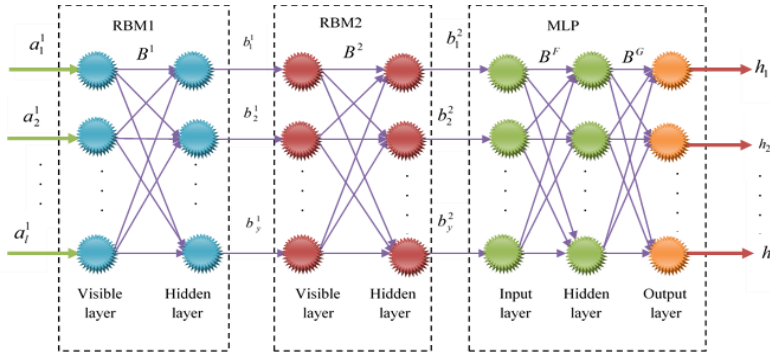


Figure 2. Architecture of DBN classifier.

The feature vector is the input to the visible layer of RBM1, and the output from the hidden layer of the RBM 1 is expressed as equation (12) and (13).

$$a^1 = \{a_1^1, a_2^1, \dots, a_x^1, \dots, a_{10}^1\}; 1 \leq x \leq l \quad (12)$$

$$b^1 = \{b_1^1, b_2^1, \dots, b_c^1, \dots, b_y^1\}; 1 \leq c \leq y \quad (13)$$

Where, b_c^1 denotes the c^{th} hidden neuron, a_x^1 is the x^{th} visible neuron of RBM 1, and y represents the number of hidden neurons. Each and every neuron in the hidden and the visible

Commented [HP11]: R2C3. Figure 2 need to be explained in detail.

Response: We added explanation for Figures 2.

Commented [HP12]: R3C5. Figure 1 and 2 need more explanation so that the contribution needs to be explained in detailed manner.

Response: As per the reviewer suggestion, explanation is added in both Figure 1 and Figure 2.

layer contains a bias. Let e and d represents the bias of the hidden and the visible layer. The two biases, which corresponds to the neurons of both the layers in RBM 1 is expressed as equation (14) and (15).

$$d^1 = \{d_1^1, d_2^1, \dots, d_x^1, \dots, d_j^1\} \quad (14)$$

$$e^1 = \{e_1^1, e_2^1, \dots, e_c^1, \dots, e_y^1\} \quad (15)$$

Where, e_c^1 denotes the bias of c^{th} hidden neuron, d_x^1 represents the bias of x^{th} visible neuron, and the weight of RBM 1 is represented as equation (16).

$$B^1 = \{B_{xc}^1\}; 1 \leq x \leq l; 1 \leq c \leq y \quad (16)$$

Where, B_{xc}^1 denotes the weight between the x^{th} visible neuron and the c^{th} hidden neuron, and the weight vector size is $l \times y$. Thus, the output of the first RBM hidden layer is calculated based on the weight and the bias associated with the visible neuron as represented as equation (17).

$$b_c^1 = \lambda \left[e_c^1 + \sum_x a_x^1 B_{xc}^1 \right] \quad (17)$$

Where, λ denotes the activation function. Therefore, the output attained from the first RBM is expressed as equation (18).

$$b^1 = \{b_c^1\}; 1 \leq c \leq y \quad (18)$$

The learning process for RBM 2 is started using the output of hidden layer from RBM 1. The output attained from the first RBM is passed as input to the RBM 2 visible layer. Hence, the number of visible neurons in RBM 2 is similar to the number of neurons in the hidden layer in RBM 1. Thus, it can be expressed as equation (19).

$$a^2 = \{a_1^2, a_2^2, \dots, a_y^2\} = \{b_c^1\}; 1 \leq c \leq y \quad (19)$$

Where, $\{b_c^1\}$ denotes the output vector of RBM 1. The hidden layer of RBM 2 is represented using equation (20).

$$b^2 = \{b_1^2, b_2^2, \dots, b_c^2, \dots, h_y^2\}; 1 \leq c \leq y \quad (20)$$

The bias of the visible layer, and the bias of the hidden layer are represented in the equation (14) and (15), and are represented as, d^2 and e^2 , respectively. The weight vector of the second RBM is expressed as equation (21).

$$B^2 = \{B_{cc}^2\}; 1 \leq c \leq y \quad (21)$$

Where, B_{cc}^2 is the weight between the c^{th} visible neuron and the c^{th} hidden neuron in RBM 2, hence the weight vector size is given as, $y \times y$. The output attained from the second RBM of c^{th} hidden neuron is expressed as equation (22).

$$b_c^2 = \lambda \left[e_c^2 + \sum_x a_x^2 B_{cc}^2 \right] \forall a_x^2 = b_c^1 \quad (22)$$

Where, e_c^2 denotes the bias of c^{th} hidden neuron. Therefore, the output of the hidden layer is denoted as, equation (23).

$$b^2 = \{b_c^2\}; 1 \leq c \leq y \quad (23)$$

The output attained from the second RBM is passed as input to the MLP, which contains the number of neurons in the input layer as, y . The input of the MLP is expressed as equation (24).

$$f = \{f_1, f_2, \dots, f_c, \dots, f_y\} = \{b_c^2\}; 1 \leq c \leq y \quad (24)$$

Where, y denotes the number of neurons present in the input layer passed by the output of RBM2 hidden layer $\{b_c^2\}$. The MLP hidden layer is expressed as equation (25).

$$g = \{g_1, g_2, \dots, g_C, \dots, g_D\}; 1 \leq C \leq D \quad (25)$$

Where, D represents the number of hidden neurons. Let us assume E_C as the bias of C^{th} hidden neuron, where $C = 1, 2, \dots, D$. The output layer of MLP is expressed as equation (26).

$$h = \{h_1, h_2, \dots, h_i, \dots, h_m\}; 1 \leq i \leq m \quad (26)$$

Where, m denotes the neurons of the output layer. The MLP contains two weight vectors, as one is defined between the input and the hidden layer, and the second is defined between the hidden and the output layer. Let B^F denotes the weight between the input and the hidden layer, and is expressed as equation (27).

$$B^F = \{B_{cc}^F\}; 1 \leq c \leq y; 1 \leq C \leq D \quad (27)$$

Where, B_{cc}^F represents the weight between c^{th} input neuron and C^{th} hidden neuron, thus the size of B^F is denoted as, $y \times D$. According, to the weight and bias of the neuron the output of the hidden layer is computed as equation (28).

$$g_C = \left[\sum_{c=1}^y B_{cc}^F * f_c \right] E_C \forall f_c = b_c^2 \quad (28)$$

Where, E_c denotes the bias of the hidden neuron and $f_c = b_c^2$, as the output of RBM 2 is the input of the MLP. The weight between the hidden and the output layer is represented as B^G and is expressed as equation (29).

$$B^G = \{B_{Ci}^G\}; 1 \leq C \leq D; 1 \leq i \leq m \quad (29)$$

Based on the output of the weight B^G and the hidden layer, the output vector is calculated as equation (30).

$$h_i = \sum_{C=1}^D B_{Ci}^G * g_C \quad (30)$$

Where, B_{Ci}^G denotes the weight between the C^{th} hidden neuron and i^{th} output neuron and the hidden layer output is denoted as, g_C .

The RBM uses the gradient descent method to achieve the unsupervised learning, whereas the MLP uses the T-EHO algorithm. The MLP layer is trained using the T-EHO algorithm, and the training procedure is elaborated as follows:

- i) The weight is applied to the input layer and then to the hidden layer using the random value.
- ii) The features are extracted and the output of RBM 2 is fed into the MLP layer.
- iii) The optimal weight is required in the MLP layer to compute the error value.
- iv) The weight of the hidden and the input layer is updated using the T-EHO algorithm, which is expressed in equation (27).

c) Detection output based on the proposed FT-EHO-DBN classifier

The detection output attained obtained using the proposed FT-EHO-DBN classifier is represented as equation (31).

$$Z = \alpha.h_i + \beta.h_j \quad (31)$$

Where, h_i denotes the output of the fuzzy classifier and h_j represents the output of the T-EHO-based DBN classifier. The extracted features and the packet information are processed by the feature selector engine by using the holoentropy. Moreover, the classification process is performed based on the fuzzy classifier and hence, the attack detection is achieved.

4. Simulation model

Extensive computer simulations have been performed to evaluate the performance of the proposed system. The proposed FT-EHO-DBN classifier is implemented in the tool MATLAB with the PC of windows 10 OS, intel I3 processor, and 4 GB RAM.

4.1 Database description

The proposed FT-EHO-DBN classifier considers three databases to detect the DDoS attack and are explained as follows:

KDD cup database: The KDD cup database [24] is the standard database used to perform anomaly detection. It offers various features and the data that exist in the network connections helps to identify the nodes under attack.

Database 1: The database 1 have the total data generated as 2500, and the total number of users as 100 for DDoS detection.

Database 2: The database 2 contains the server log information with the total information contents as 150,000.

4.2 Performance metrics

The proposed Fuzzy and TEHO-based DBN classifier uses the metrics, like accuracy, recall, precision, and detection accuracy to analyze the performance of DDoS detection. The metrics are elaborated as follows:

Detection accuracy: Detection accuracy refers to the ratio of detected DDoS attacks with the ground truth information.

Accuracy: The accuracy determines the accurateness of the performance, and is measured as,

$$Accuracy = \frac{S + T}{S + T + Y + Z} \quad (32)$$

Where, T and S , , denotes the true negative and true positive, Z and Y represents the false negative and false positive respectively.

Precision: It is the ratio of the detected nodes with the actual number of nodes.

Recall: The recall refers to the ratio of the measure of normal nodes in the cloud with the actual number of normal nodes.

4.3 State-of-the-art method for comparison

The analysis is performed by comparing the proposed FT-EHO-DBN classifier with the existing methods, like SVM [19], NN [20], Ensemble [21], EHO [22], and TEHO-based DBN. The SVM [19] classifier is mainly used to detect the attacks in the cloud environment by fixing the decision boundary. NN [20] detects the attack by using the weight of the optimization algorithm. The ensemble [21] classifier is used to select the features to perform the attack detection. EHO [22] algorithm is mainly used to train the DBN classifier [23] to perform the classification.

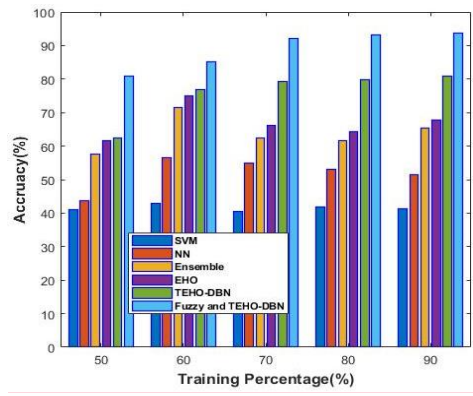
4.4 Results and Analysis

This section describes the comparative analysis of the proposed FT-EHO-DBN classifier and the results attained using different datasets are elaborated by varying the number of users and the percentage of data.

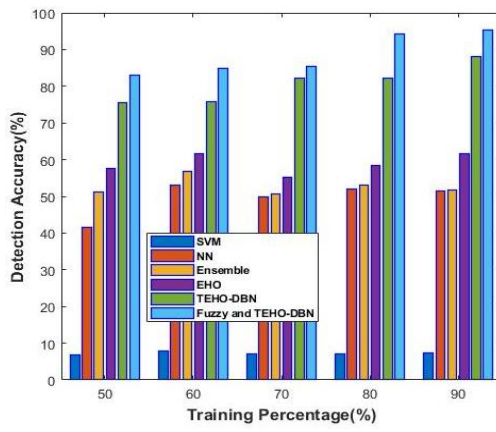
4.4.1 Comparative analysis using the KDD cup dataset

The comparative analysis using the KDD cup dataset for the proposed FT-EHO-DBN classifier is discussed briefly. In the comparative analysis, the percentage of data is varied with the large information in the KDD cup dataset. Figure 3 shows the comparative analysis of the proposed FT-EHO-DBN classifier by varying the percentage of data.

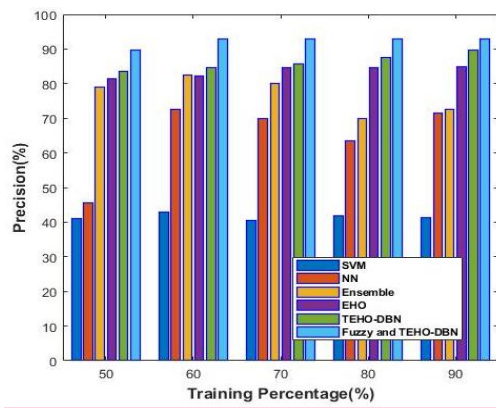
Figure 3 a) shows the analysis of accuracy by varying the percentage of data. When the training data is 60%, the accuracy attained by the existing methods, like SVM, NN, Ensemble, EHO, and TEHO-DBN is 42.9762%, 56.5476%, 71.4286%, 75.0%, and 76.9231%, whereas the proposed FT-EHO-DBN classifier obtain the accuracy value as 85.2786%. For 90% training data, the accuracy computed by the existing methods, namely SVM, NN, Ensemble, EHO, and TEHO-DBN is 41.389%, 51.587%, 65.385%, 67.857%, and 81.0%, while the proposed FT-EHO-DBN classifier obtained increased accuracy value as 93.645%, respectively.



(a)



(b)



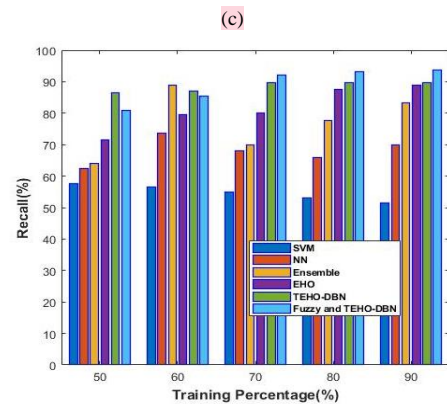


Figure 3. Comparative analysis using the KDD cup database by varying the percentage of data for (a) accuracy; (b) detection accuracy; (c) precision and (d) recall.

Figure 3 b) shows the analysis of detection accuracy by varying the percentage of data. When the percentage of training data is 60, the detection accuracy attained by the existing methods, like SVM, NN, Ensemble, EHO, and TEHO-DBN is 7.7844%, 53.2%, 56.6866%, 61.5385%, and 75.7633, whereas the proposed FT-EHO-DBN classifier obtained the detection accuracy value as 84.7872% respectively. For 90% training data, the detection accuracy computed by the existing methods, namely SVM, NN, Ensemble, EHO, and TEHO-DBN is 7.3852%, 51.6%, 51.6966%, 61.5385%, and 88.2353%, while the proposed FT-EHO-DBN classifier obtained increased detection accuracy value as 95.2697%, respectively.

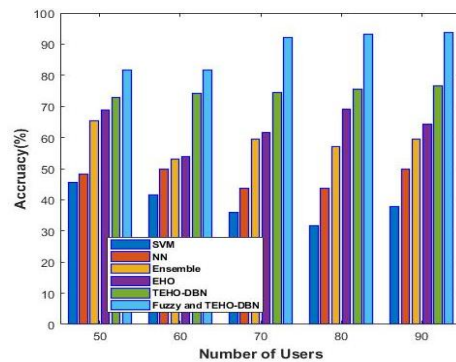
Figure 3 c) shows the analysis of precision by varying the percentage of data. When the training data is 60%, the precision attained by the existing methods, namely SVM, NN, Ensemble, EHO, and TEHO-DBN is 42.9880%, 72.7273%, 82.6087%, 82.1220%, and 84.6491%, whereas the proposed FT-EHO-DBN classifier obtained the precision value as 92.9672% respectively. For 90% training data, the precision value computed by the existing methods, namely SVM, NN, Ensemble, EHO, and TEHO-DBN is 41.3944%, 71.4286%, 72.7273%, 84.8718%, and 89.6154%, while the proposed FT-EHO-DBN classifier obtained better precision value as 92.9774%, respectively.

Figure 3 d) shows the analysis of recall by varying the percentage of data. When the training data is 60%, the recall attained by the existing methods, such as SVM, NN, Ensemble, EHO, and TEHO-DBN is 56.574%, 73.585%, 88.889%, 79.625%, and 87.048%, whereas the proposed FT-EHO-DBN classifier obtain the recall value as 85.297% respectively. For 90% training data, the

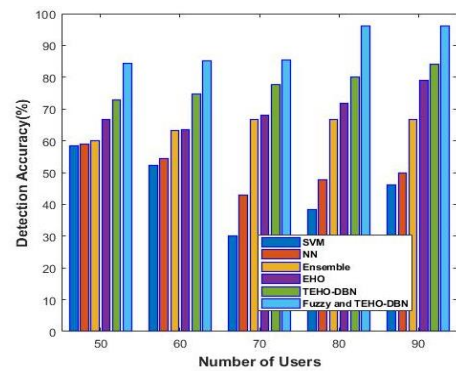
recall value computed by the existing methods, like SVM, NN, Ensemble, EHO, and TEHO-DBN is 51.594%, 69.811%, 83.333%, 88.889%, and 89.814, while the proposed FT-EHO-DBN classifier obtain better recall value as 93.670%, respectively.

4.4.2 Comparative analysis using the dataset 1

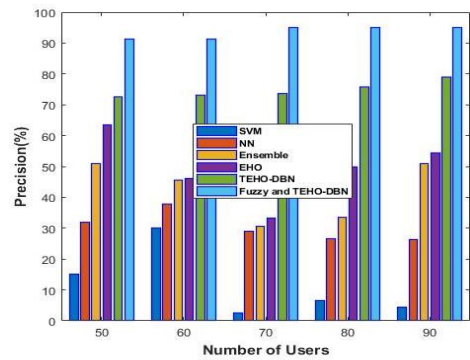
The comparative analysis of the proposed FT-EHO-DBN classifier using dataset 1 is discussed in this section. Figure 4 shows the analysis of the proposed FT-EHO-DBN classifier by varying the number of users.



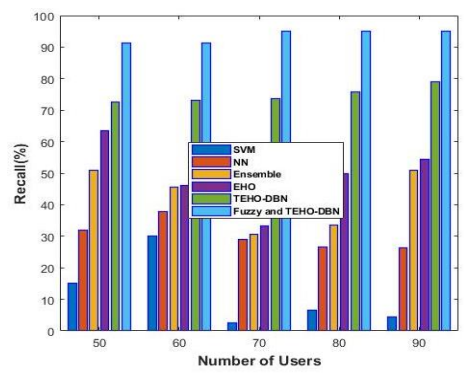
(a)



(b)



(c)



(d)

Figure 4. Comparative analysis using the database 1 by varying the number of users for (a) accuracy, (b) detection accuracy, (c) precision, and (d) recall.

Figure 4 a) shows the analysis of accuracy by varying the percentage of data. When the training data is 60%, the accuracy obtained by the existing methods, namely SVM, NN, Ensemble, EHO, and TEHO-DBN is 41.563%, 50.0%, 53.125%, 53.846%, and 74.186%, whereas the proposed FT-EHO-DBN classifier have the accuracy rate as 81.757% respectively. For 90% training data, the accuracy rate computed by the existing methods, namely SVM, NN, Ensemble, EHO, and TEHO-DBN is 37.872%, 50.0%, 59.574%, 64.286%, and 76.538%, while the proposed FT-EHO-DBN classifier obtain better accuracy value as 93.811%, respectively.

Figure 4 b) shows the analysis of detection rate by varying the percentage of data. When the percentage of training data is 60, the detection accuracy attained by the existing methods, like

SVM, NN, Ensemble, EHO, and TEHO-DBN is 52.381%, 54.545%, 63.158%, 63.636%, and 74.667%, whereas the proposed FT-EHO-DBN classifier obtain the detection accuracy value as 85.193% respectively. For 90% training data, the detection accuracy computed by the existing methods, namely SVM, NN, Ensemble, EHO, and TEHO-DBN is 46.154%, 50.0%, 66.667%, 78.947%, and 84.091%, while the proposed FT-EHO-DBN classifier obtain increased detection accuracy value as 96.030%, respectively.

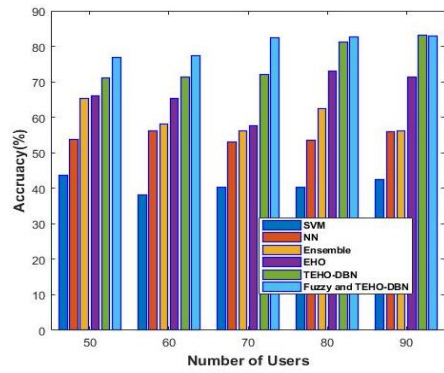
Figure 4 c) shows the analysis of precision by varying the percentage of data. When the training data is 60%, the precision value attained by the existing methods, namely SVM, NN, Ensemble, EHO, and TEHO-DBN is 30%, 37.826%, 45.555%, 46.153%, and 73%, whereas the proposed FT-EHO-DBN classifier have the precision value as 91.4% respectively. For 90% training data, the precision computed by the existing methods, namely SVM, NN, Ensemble, EHO, and TEHO-DBN is 4.444%, 26.364%, 50.870%, 54.545%, and 78.947%, while the proposed FT-EHO-DBN classifier obtain better precision value as 94.981%, respectively.

Figure 4 d) shows the analysis of recall by varying the percentage of data. When the training data is 60%, the recall value attained by the existing methods, namely SVM, NN, Ensemble, EHO, and TEHO-DBN is 26.667%, 60.0%, 60.870%, 66.667%, and 78.571%, whereas the proposed FT-EHO-DBN classifier obtain the recall value as 81.778% respectively. For 90% training data, the recall value computed by the existing methods, like SVM, NN, Ensemble, EHO, and TEHO-DBN is 15.926%, 25.0%, 66.667%, 75.0%, and 86.957, while the proposed FT-EHO-DBN classifier have better recall value as 93.833%, respectively.

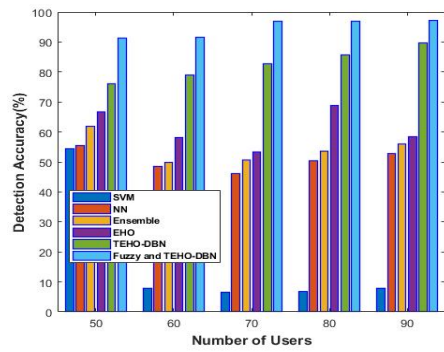
4.2.3 Comparative analysis using the dataset 2

The comparative analysis made using the dataset2 for the proposed FT-EHO-DBN classifier is discussed in this section. Figure 5 shows the analysis of the proposed FT-EHO-DBN classifier by varying the number of users.

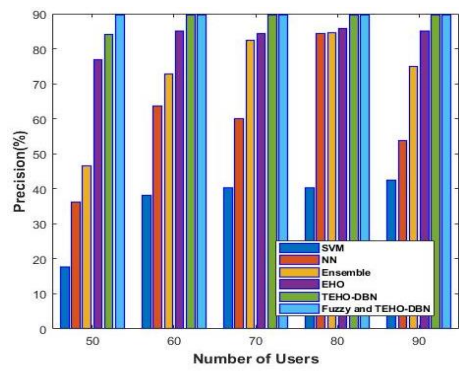
Figure 5 a) shows the analysis of accuracy by varying the percentage of data. When training data is 60%, the accuracy obtained by the existing methods, namely SVM, NN, Ensemble, EHO, and TEHO-DBN is 38.214%, 56.250%, 58.135%, 65.385%, and 71.429%, whereas the proposed FT-EHO-DBN classifier obtain the accuracy rate as 77.440% respectively. For 90% training data, the accuracy rate computed by the existing methods, namely SVM, NN, Ensemble, EHO, and TEHO-DBN is 42.579%, 55.952%, 56.250%, 71.429%, and 83.077%, while the proposed FT-EHO-DBN classifier obtain better accuracy value as 82.921%, respectively.



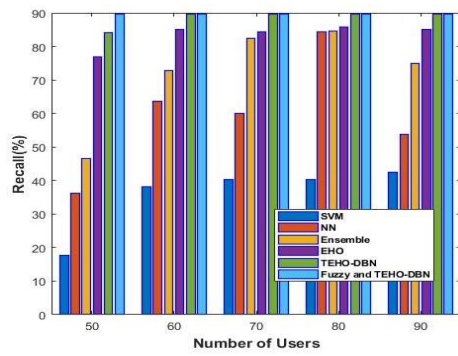
(a)



(b)



(c)



(d)

Figure 5. Comparative analysis using database 2 by varying the number of users for (a) accuracy, (b) detection accuracy, (c) precision, and (d) recall.

Figure 5 b) shows the analysis of detection rate by varying the percentage of data. When the percentage of training data is 60, the detection accuracy attained by the existing methods, like SVM, NN, Ensemble, EHO, and TEHO-DBN is 7.784%, 48.4%, 50.0%, 58.283%, and 78.889%, whereas the proposed FT-EHO-DBN classifier obtain the detection accuracy value as 91.710% respectively. For 90% training data, the detection accuracy computed by the existing methods, namely SVM, NN, Ensemble, EHO, and TEHO-DBN is 47.784%, 52.8%, 56.088%, 58.333%, and 89.657%, while the proposed FT-EHO-DBN classifier obtain increased detection accuracy value as 97.2%, respectively.

Figure 5 c) shows the analysis of precision by varying the percentage of data. When the training data is 60%, the precision value attained by the existing methods, namely SVM, NN, Ensemble, EHO, and TEHO-DBN is 38.207%, 63.636%, 72.727%, 85.122%, and 89.619%, whereas the proposed FT-EHO-DBN classifier obtain the precision value as 89.688% respectively. For 90% training data, the precision computed by the existing methods, namely SVM, NN, Ensemble, EHO, and TEHO-DBN is 42.590%, 53.846%, 75.0%, 85.122%, and 89.645%, while the proposed FT-EHO-DBN classifier obtained better precision value as 89.701%, respectively.

Figure 5 d) shows the analysis of recall by varying the percentage of data. When the percentage of training data is 60, the recall value attained by the existing methods, namely SVM, NN, Ensemble, EHO, and TEHO-DBN is 58.167%, 70.0%, 73.585%, 84.211%, and 82.588%, whereas the proposed FT-EHO-DBN classifier obtain the recall value as 77.460% respectively. For 90% training data, the recall value computed by the existing methods, like SVM, NN, Ensemble, EHO, and TEHO-DBN is 55.976%, 73.585%, 87.5%, 89.623%, and 89.474%, while the proposed FT-EHO-DBN classifier obtained better recall value as 82.931%, respectively.

4.3 Discussion

The comparative discussion of the proposed Fuzzy-Taylor-EHO inspired DBN classifier is elaborated in this section. Table I shows the comparative results based on various performance metrics. The values computed by the existing methods, namely SVM, NN, Ensemble, EHO, and T-EHO-based DBN are also presented Table 1. The proposed FT-EHO-DBN classifier attained better performance than the existing methods for the metrics, like accuracy, detection accuracy, precision, and recall with the values of 93.811%, 97.200%, 94.981%, and 93.833, respectively.

Commented [HP13]: R5C1. The paper presents a proposal of Fuzzy-Taylor- Elephant Herd Optimization Inspired Deep Belief Network for DDoS Attack Detection and Comparison with State-of-the-Arts Algorithms. Authors discuss their algorithm and perform some experiments.

The paper presents several problems. First of all, the motivation for the paper is well explained. Although it might be clear the relevance of DDoS attack detection in the context of cloud computing, it is clearly mentioned why the proposal presented in the paper addresses the challenges of the research problem. Also, the selection of the proposed technique looks somehow ad-hoc, since the authors are not explaining adequately why their approach makes sense in the context of the problem.

Response: The proposed method has the advantages of DBN, EHO, and Taylor series, which are provided in sub-section 4.4 of the revised manuscript. Due to the advantages of the utilized methods, the propose technique detects the DDoS attacks more precisely.

Table 1. Comparative discussion.

Comparative techniques	Evaluation metrics			
	Accuracy(%)	Detection rate (%)	Precision(%)	Recall (%)
SVM	45.556	58.333	42.988	58.167
NN	56.548	59.091	84.444	73.585
Ensemble	71.429	66.667	84.615	88.889
EHO algorithm	75.000	78.947	85.714	89.623
TEHO-DBN classifier	83.077	89.657	89.645	89.814
Proposed FT-EHO-DBN	93.811	97.200	94.981	93.833

This result reveals that SVM (accuracy = 45.556%) and NN (accuracy = 56.548%) showed the worst performance as far as accuracy is concerned. In addition, we noted that the precision value for SVM is 42.988% lowest than any other methods implemented in this paper. Results presented in Table I concludes that SVM showed the worst performance whereas Ensemble, EHO, and TEHO-DBN demonstrated moderate performance, whilst the proposed FT-EHO-DBN classifier has outperformed on the performance metrics. The overall performance has achieved through FT-EHO-DBN classifier is mainly because integrating Taylor series and EHO algorithm helped in reaching to global optimum without getting stuck at local optimum. Initially, the user request is send to the packet feature extraction module, where the packet features are extracted. The extracted features are subjected to the feature selector engine, where the selective features is extracted using the holoentropy criteria. The classification module uses the Deep Belief Network and the fuzzy classifier to detect the Distributed Denial of Service attack.

5. Conclusion

A FT-EHO-DBN classifier has been introduced in this paper to detect the DDoS attack. FT-EHO-DBN classifier has been developed by integrating the fuzzy and DBN classifier along with the T-EHO optimization algorithm. We showed the working of the proposed system in a well-organized manner so that researcher can utilize it in future. Initially, the user request is sent to the packet feature extraction module, where the packet features are extracted. The extracted features are subjected to the feature selector engine, where the selective features are extracted using the holoentropy criteria. The classification module uses the DBN and fuzzy classifier to detect the DDoS attack. In FT-EHO-DBN system, the T-EHO algorithm has been implemented as rule learning approach of the fuzzy classifier. T-EHO algorithm has been implement as replacement of an adaptive genetic fuzzy system. Rigorous computer simulations have been performed to evaluate the performance of the proposed FT-EHO-DBN classifier. Three standard databases, namely, KDD cup database, Database 1 and Database 2 have been used for the simulations. Four performance metrics, namely, accuracy, detection accuracy,

Commented [HP14]: R2C4. Experimental design is detailed, and results have been discussed in significant detail but I would suggest authors to include a paragraph why/how this improvements have been achieved.

Response: Many thanks on this comment. In the revised manuscript we have added details.

Commented [HP15]: R3C4. Results presented in Table I shows clearly that the proposed method has brought significant improvement but how/why this improvement is achieved need to be discussed.

Response: The overall performance has achieved through Fuzzy and Deep Belief Network classifier based on the Taylor-Elephant Herd optimization algorithm, which is the integration of Taylor series with the Elephant Herd optimization algorithm. Initially, the user request is sent to the packet feature extraction module, where the packet features are extracted. The extracted features are subjected to the feature selector engine, where the selective features are extracted using the holoentropy criteria. The classification module uses the Deep Belief Network and the fuzzy classifier to detect the Distributed Denial of Service attack.

Commented [HP16]: R4C3. A comparison results need to explain in the sense why the proposed method has brought improvement.

Response: Thank you for pointing this. It is included in the revised manuscript.

precision and recall have been identified to measure the result's quality. The performance of the FT-EHO-DBN DBN classifier was tested against the state-of-the-art methods and comparative results have been presented in Table I. The results reported in Table I reveals that the FT-EHO-DBN classifier outperformed over other state-of-the-art algorithms. Computational cost is found challenging during implementation mainly because of multiple hidden layers. Hence, **The immediate future scope is to explore the possibility of developing new optimization algorithm (or replace EHO with other swarm algorithms) and combine with the DBN so that performance in terms of accuracy and detection rate with less computational cost can be achieved.**

References

- [1]. Yasir Ali, Yuanqing Xia, Liang Ma, and Ahmad Hammad, " Secure design for cloud control system against distributed denial of service attack", Control Theory and Technology, vol.16, no.1, pp.14–24, February 2018.
- [2]. R. Kesavamoorthy and K. Ruba Soundar, "Swarm intelligence based autonomous DDoS attack detection and defense using multi agent system", Cluster Computing, pp.1-8, 13 March 2018.
- [3]. Opeyemi Osanaiye, Haibin Cai, Kim-Kwang Raymond Choo, Ali Dehghantanha, Zheng Xu, and Mqhele Dlodlo, " Ensemble-based multi-filter feature selection method for DDoS detection in cloud computing", EURASIP Journal on Wireless Communications and Networking, vol.2016, no.1, pp.130, 10 May 2016.
- [4]. Vikash C Pandey, Sateesh K Peddoju, and Prachi S Deshpande, " A statistical and distributed packet filter against DDoS attacks in Cloud environment", Sādhanā, 43:32, vol.43, no.3, pp.32, March 2018.
- [5]. Loukas G, Vuong T, Heartfield R, Sakellari G, Yoon Y and Gan D, "Cloud-based cyber-physical intrusion detection for vehicles using deep learning", IEEE Access, vol. 6, pp.3491-3508, 2018.
- [6]. Hajimirzaei B and Navimipour NJ, "Intrusion detection for cloud computing using neural networks and artificial bee colony optimization algorithm", ICT Express, 2018.
- [7]. Deng S, Zhou A.H, Yue D, Hu B and Zhu L.P, "Distributed intrusion detection based on hybrid gene expression programming and cloud computing in a cyber physical power system", IET Control Theory & Applications, vol. 11, no. 11, pp.1822-1829, 2017.

Commented [HP17]: R5C4. In the experiments section, the author has compared their results and performance state of the rat algorithm and its better accuracy and anyhow the author should mention their limitation in the proposed system.

Response: As per the suggestion, the limitation of the proposed system is added.

Commented [HP18]: R4C4. The author need to update the conclusion and highlight the future scope of this research.

Response: The immediate future scope is to explore the possibility of developing new optimization algorithm (or replace EHO with other swarm algorithms) and combine with the DBN so that performance in terms of accuracy and detection rate with less computational cost can be achieved.

Commented [HP19]: R5C2. A different aspect of the design such as the feature selection using Fuzzy-Taylor looks good. The operation process based on the creation of a log is also mentioned well. Considering the involvement of Deep Belief Networks, it would be important to evaluate whether the approach can operate in reasonable times, considering that the authors claim that it can detect the attack in earlier stages.

Response: In this research, we presented results on four quality measures, namely, accuracy, detection rate, precision and recall. Computational cost will be the agenda for further research and we highlighted this in the conclusion section.

- [8]. Chen M, Wang N, Zhou H and Chen Y, "FCM technique for efficient intrusion detection system for wireless networks in cloud environment", *Computers & Electrical Engineering*, vol. 71, pp.978-987, 2018.
- [9]. Gao Y, Liu Y, Jin Y, Chen J and Wu H, "A Novel Semi-Supervised Learning Approach for Network Intrusion Detection on Cloud-Based Robotic System", *IEEE Access*, vol. 6, pp. 50927-50938, 2018.
- [10]. Saurabh Dey, Qiang Ye, and Srinivas Sampalli, "A Machine Learning Based Intrusion Detection Scheme for Data Fusion in Mobile Clouds Involving Heterogeneous Client Networks", *Information Fusion*, vol. 49, ps. 205-215, September 2019.
- [11]. Idhammad M, Afdel K and Belouch M, "Distributed Intrusion Detection System for Cloud Environments based on Data Mining techniques", *Procedia Computer Science*, vol. 127, pp.35-41, 2018.
- [12]. Osanaiye O, Choo K.K.R and Dlodlo M, "Distributed denial of service (DDoS) resilience in cloud: review and conceptual cloud DDoS mitigation framework", *Journal of Network and Computer Applications*, vol. 67, pp.147-165, 2016.
- [13]. Patil R, Dudeja H, Gawade S and Modi C, "Protocol specific Multi-threaded Network Intrusion Detection System (PM-NIDS) for DDoS/DDoS Attack Detection in cloud", *IEEE International Conference on Computing, Communication and Networking Technologies (ICCCNT)*, pp. 1-7, July 2018.
- [14]. Lonea A.M, Popescu D.E and Tianfield H, "Detecting DDoS attacks in cloud computing environment", *International Journal of Computers Communications & Control*, vol. 8, no.1, pp.70-78, 2013.
- [15]. JoSEP A.D, Katz R, KonWinSKi A, Gunho L.E.E, PAttERSon D and RABKin A, "A view of cloud computing", *Communications of the ACM*, vol. 53, no. 4, 2010.
- [16]. Kholidy H.A. and Baiardi F, "CIDS: A framework for intrusion detection in cloud systems", In *IEEE Ninth International Conference on Information Technology-New Generations*, pp. 379-385, April 2012.
- [17]. Zhao, B, Fan P. and Ni M, "Mchain: A Blockchain-Based VM Measurements Secure Storage Approach in IaaS Cloud With Enhanced Integrity and Controllability", *IEEE Access*, vol. 6, pp.43758-43769, 2018.
- [18]. Hiremath S. and Kunte S, "A novel data auditing approach to achieve data privacy and data integrity in cloud computing", In *IEEE International Conference on Electrical, Electronics, Communication, Computer, and Optimization Techniques (ICEECCOT)*, pp. 306-310, December 2017.

- [19]. Dennis B. and Muthukrishnan S, "AGFS: Adaptive Genetic Fuzzy System for medical data classification", *Applied Soft Computing*, vol. 25, pp.242-252, 2014.
- [20]. Mane V.M. and Jadhav D.V., "Holoentropy enabled-decision tree for automatic classification of diabetic retinopathy using retinal fundus images", *Biomedical Engineering/Biomedizinische Technik*, vol. 62, no. 3, pp.321-332, 2017.
- [21]. Opeyemi Osanaiye, Haibin Cai, Kim-Kwang Raymond Choo, Ali Dehghantanha, Zheng Xu, and Mqhele Dlodlo, " Ensemble-based multi-filter feature selection method for DDoS detection in cloud computing", *EURASIP Journal on Wireless Communications and Networking*, vol.2016, no.1, pp.130, 10 May 2016.
- [22]. Gai-Ge Wang, Suash Deb, and Leandro dos S. Coelho, " Elephant Herding Optimization", In *Proceedings of the 3rd International Symposium on Computational and Business Intelligence (ISCBI)*, pp.1-5, 2015.
- [23]. Hinton, G.E., "Deep belief networks," *Scholarpedia*, vol. 4, no. 5, 2009.
- [24]. KDD cup database <http://kdd.ics.uci.edu/databases/kddcup99/kddcup99.html>, Accessed on November 2018.
- [25]. S. Alamelu Mangai, B. Ravi Sankar and K. Alagarsamy, "Taylor Series Prediction of Time Series Data with Error Propagated by Artificial Neural Network", *International Journal of Computer Applications (0975 – 8887)*, Vol. 89, no.1, March 2014.
- [26]. Yan, Q., Yu, F. R., Gong, Q., & Li, J. (2015). Software-defined networking (SDN) and distributed denial of service (DDoS) attacks in cloud computing environments: A survey, some research issues, and challenges. *IEEE communications surveys & tutorials*, 18(1), 602-622.
- [27]. Somani, G., Gaur, M. S., Sanghi, D., Conti, M., & Buyya, R. (2017). DDoS attacks in cloud computing: Issues, taxonomy, and future directions. *Computer Communications*, 107, 30-48

Commented [HP20]: R3C3. More recent references must be added to present state-of-the art.

Response: As per the suggestion, some recent work was added into state-of-the art.

Commented [HP21]: R4C2. I think the references used in the paper are old. The author must update the new references and make the paper up to date.

Response: As per the reviewer suggestion, the revised manuscript has updated

Commented [HP22]: R4C5. The authors should add more recent work in the literature section as most of the references are outdated in the paper so it's nice to update the references.

Response: The below mentioned references work were added into related work

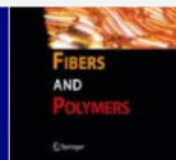
- Yan, Q., Yu, F. R., Gong, Q., & Li, J. (2015). Software-defined networking (SDN) and distributed denial of service (DDoS) attacks in cloud computing environments: A survey, some research issues, and challenges. *IEEE communications surveys & tutorials*, 18(1), 602-622.
- Somani, G., Gaur, M. S., Sanghi, D., Conti, M., & Buyya, R. (2017). DDoS attacks in cloud computing: Issues, taxonomy, and future directions. *Computer Communications*, 107, 30-48.

Commented [HP23]: R5C3. The literature review is incomplete. Authors are not considering important literature on the area of DDoS attack detection in the context of cloud computing. This reviewer suggests considering the following references:
Yan, Q., Yu, F. R., Gong, Q., & Li, J. (2015). Software-defined networking (SDN) and distributed denial of service (DDoS) attacks in cloud computing environments: A survey, some research issues, and challenges. *IEEE communications surveys & tutorials*, 18(1), 602-622.
Somani, G., Gaur, M. S., Sanghi, D., Conti, M., & Buyya, R. (2017). DDoS attacks in cloud computing: Issues, taxonomy, and future directions. *Computer Communications*, 107, 30-48.

Response: As per the recommendation, above mentioned references are updated in the revised manuscript.

Effect of Natural Fiber Loading on Mechanical Properties and Thermal Characteristics of Hybrid Polyester Composites for Industrial and Construction Fields

Published: 27 July 2020 | 21, 1508–1514 (2020)



[Fibers and Polymers](#)

[Aims and scope](#) →

[Submit manuscript](#) →

[S. Sathees Kumar](#)

287 Accesses 61 Citations [Explore all metrics](#) →

[Cite this article](#)

Abstract

In the present work tensile, flexural, impact and hardness properties of sorghum bicolor, sisal fiber and jute reinforced with polyester composites are described for the first time. The hybrid composite plates are fabricated for different fiber weights by hand lay-up method. To investigate the mechanical attributes tensile, flexural, impact and hardness tests were performed as per ASTM standard. The mechanical test results revealed a regular trend of an increase in tensile, flexural, impact and hardness properties to adding natural

Access this article

[Log in via an institution](#) →

[Buy article PDF 39,95 €](#)

Price includes VAT (India)
Instant access to the full article PDF.

Rent this article via [DeepDyve](#)

[Institutional subscriptions](#) →

[Sections](#)

[References](#)



Efficient Utilization of Virtual Instances by Suspend Resume Strategy in Cloud Data Center

A Nirmal Kumar*

Department of Computer Science and Engineering, CMR Institute of Technology, Hyderabad, Telangana, India

Received 1 June 2019; revised 17 February 2020; accepted 3 April 2020

The effective utilization of virtual instances by suspend resume policy in virtualized data center is analyzed in this paper. Cloud computing is a term that describes the means of delivering all information technology from computing power to computing infrastructure, applications, business process and personal collaboration to end users as a service wherever and whenever they need it. Here Infrastructure as a Service is used for open source cloud implementation. Open Stack provides architecture for cloud to build the virtual instances. Thus Virtual Machine allocates a single job, by dividing them to the grid systems. Suspend resume policy is used to provide the jobs to the virtual instances based on the usage. It helps in examining the weight flanked by the virtual instances as job arrived.

Keywords: Cloud, Virtual data centers, Openstack, Suspend resume policy

Introduction

The cloud in distributed computing is the arrangement of equipment, programming, systems, stockpiling, administrations and interfaces that join to convey parts of processing as assistance shared assets programming and data that are given to Personal Computers and different gadgets on request. It permits individuals to do things they like to do on a Personal Computer without the requirement for them to purchase and construct an Information Technology foundation on to comprehend the basic innovation.

There is a great need for it to help addressing, business challenges. Cloud computing can help in doing business more with less expenditure, providing high quality service, reducing risk, and ensuring breakthrough agility. The characteristics of the cloud are on-demand computing and ubiquitous computing etc. The services in the cloud are of 3 types. They are Infrastructure as a Service (IaaS), Platform as a Service (PaaS) and Service as a Service (SaaS). Grid computing is a group of computer from different locations to arrive at a universal goal. The network can be determined as a disseminated arrangement.

The open stack cloud architecture will build the Virtual Machine (VM). Virtual Instance (VI) is shaped in OpenStack by means of two methods. Virtual Instance is shaped openly in OpenStack. Instance is

created in OpenStack using dashboard or using j cloud Application Program Interface (API). If a solitary work is allocated to single virtual machine, power utilization will be very high and the response time will be more. Thus the work is alienated into manifold jobs. These jobs are allocated to the Grid of virtual instance. The job therefore reduces the response time and suspend resume policy is implemented to provide efficient energy consumption which will allocate the virtual machine based on the command. It helps in harmonizing the weight between the instances as the work arrives. There are totally 4 modules involved in it. They are OpenStack configuration, build and configure instance, launch an instances, and power management in grid computing.

Existing system

Cloud Computing is a term that describes the means of delivering any and all information technology from computing power to compute infrastructure, applications, business process and personal collaboration to end users as service whenever and wherever they need it. Here IaaS is used and the energy consumption is optimized by using three power saving policies to reduce the idle power of the server. Here N policy is used, in that when server machine will be turned on, only when the number of jobs in the queue is more or same as that of the specified N threshold. The three policies used are Integrated Server Nodes (ISN) policy, System Integration (SI) policy and Server Nodes (SN) policy.

*Author for Correspondence
E-mail: nirmalkumar@cmritonline.ac.in

In the Integrated Server Nodes, policy the server will enter into the busy mode when the job arrives and it will end its busy mode only when it completes all of its jobs. The server will be in the sleep mode until the number of jobs in the queue is less than that of the specified N threshold value. In the Server Nodes, the server will enter into the sleep mode only when there is no job in the specified machine, whereas in the System Integration policy, the server will be in the sleep mode for only a certain amount of time when the sleeping time of the server ends, it will enter into the idle mode. Thus, the consumption of idle power is efficiently reduced at the same time, thus more policies are used and in this the beginning cost will be high.¹

Here cloud as a service oriented platform dynamic allocation of resources is proposed by means of virtualization technology. In this technology, the resources are allocated dynamically to the system according to the need of the user. In order to allocate resources dynamically to the system and to determine the utilization of uneven multiple resources skewness is used. By using this skewness, the load between the virtual machine is balanced. Thus the overloading between the virtual machines is prevented by effective load balancing between the machines and at the same time physical machines should be capable enough to handle all the resource needs of the virtual machine, else overloading of the physical machine takes place and the virtual machine performance is decreased.²

For the past few years, consumption of energy has become the most difficult part in computing environment especially their data centres. Here the energy efficiency is improved in the web servers by determining the daily requests patterns sent to the web servers which indicate the resource provisioning in offline and will be more suitable for management of resources. Here two load distribution algorithms are used. They are relative load distribution, servers are utilized equally and the adaptive load distribution, the nodes are selected based on the power level. Mostly these two algorithms are used to view the usage of the Central Processing Unit (CPU) and level of power consumption in the web servers.³ Thus, at the end, shutting down of the idle nodes will save the energy. It is however difficult to make out this offline methodology without the daily request patterns. Thus in future it should be enhanced in such a way that the workload predictions should be based on online resource management.

The cloud computing has generally reshaped the cloud computing. Though the cloud provides more advanced features, still it is lagging in its operational cost because it is very high for both the public and the private clouds. Green computing is also very important with minimum resource and more demand. A framework is provided that ensures enhancements in the cloud architecture.⁴ By using less number of virtual machine, power aware scheduling techniques, proper resource management, and the cloud data center can be improved with minimum overhead. Thus, future enhancements should be done in such a way that all the fields that the proper resource management, scheduling techniques should be enhanced.

Data centers generally consume most amount of energy which is determined in terms of distribution of power and cooling of the systems. By dynamically adjusting the active machines, the resources can be efficiently used according to the system needs. Generally the data centers will have a wide variety of computer systems with varying energy consumption characteristics. Then, works performed by the system will be generally based on the priority, resource needed and the objective. Failure in any one of these characteristics will lead to a problem, thus here the heterogeneity aware resource management is presented for providing a dynamic work in the clouds. K means clustering algorithm is used for allocating the workload based on the similar characteristics in terms of requirements and resource. Here a novel technique is presented for adjusting the machines dynamically to minimize the power.⁵

Data centers consume more resources in the cloud computing epoch, which can be minimized by erasing the number of turned-on servers. A power-conscious scheduling technique for virtual data center resources uses this algorithm that periodically consolidates servers and changes the virtual machine placements in consolidation rounds to satisfy a Service Level Agreement (SLA). A power-aware datacenter simulator is constructed and validated using this methodology. Using this, Scheduling Algorithm simulator performance is analyzed. This strategy is more power efficient than the one based on events. Further simulation results show that in general, workload-based weight adjustment by virtual machine can allow power-aware schedulers to perform more efficiently under the SLA. This strategy increases the data center control budget by 35% for web-like

unintended workloads, and the data center progress budget by 22.7% for workloads with secure reserve criteria like ScaLAPACK.⁶

Cloud task consolidation has become an important strategy in streamlining resource usage and in effect improving energy efficiency. Resource utilization relates directly to energy use, modeled their relationship and established two energy-conscious task heuristics consolidation.⁷ Monitoring and controlling the behavior of Energy Management System (EMS) by fulfilling its purpose at the same time balancing certain constraints, including cost optimization, system reliability and environmental consideration.⁸ Examples of systems are building energy management, micro grid energy management and datacenter energy management. It shows promise in the improvement of energy savings across many domains. EMS is a proof of implementation in a wide variety of uses.

Electricity expenditures at Internet Data Centers (IDCs) are becoming an important category of operating costs. The overall energy cost minimization of IDCs in the smart grid environment is addressed here. The price maker in the electricity market should be high when the energy consumption is high. IDC will impact electricity price.^{9,10} The price varies with the load and the customers according to many observations. Then the cost of energy minimization issue is subjected to end-to-end delay constraints and energy optimization. Performance is evaluated to make the solution method more effective to turn the problem into a quadratic programming. The result shows that the total electricity cost of IDCs is minimized by handling the interaction between IDCs and smart grid.

Cloud computing is used as a service over the Internet to prove dramatically scalable and virtualized resources. Datacenters involve the realization of cloud computing in virtualization technology. As the server's rapid growth, quantity and scale in the datacenter, it is a huge challenge that is directly related to the number of servers hosted and their workloads. Designing and implementing the energy-efficient technologies for the 10 data center is very critical. Possible consolidation of server overhead performance investigates the consolidation strategies and explores the live migration process. These findings demonstrate that both systems are used with lower overhead efficiency to meet the energy-saving targets.

Research methodology of implementation

Proposed framework executes improved energy-effective green control (EGC) calculation which utilizes Suspend Resume arrangement for improving vitality effectiveness in lattice registering. Proposed framework utilizes open source cloud execution and OpenStack gives cloud design which is the best to fabricate the virtual instance. Virtual Instance is made in OpenStack utilizing two different ways:

- Virtual Instance is made legitimately in OpenStack Dashboard
- Using j clouds Application Program Interface, occurrence is made in OpenStack

In the event that a solitary occupation is dispensed to one virtual instance at any given moment, control utilization will be high and reaction time will be postponed. So as to give vitality productivity and low power utilization in a cloud, work is isolated into different little undertakings. These assignments are distributed to a framework of virtual instance. Matrix of virtual instance performs employment to lessen reaction time. The architecture of virtual machine migration is represented in Fig.1.

Suspend Resume approach is executed to give an effective green control which distributes virtual instance dependent on the utilization and can powerfully summon the virtual instance on demand. It additionally helps in adjusting the heap between the virtual instances as the activity arrives. The modules incorporate OpenStack arrangement, manufacture and design occurrence, dispatch a case and power the executives in framework registering.

A. Openstack Cloud Setup

In this module, router configuration will be completed. The following setting is done: switch IP

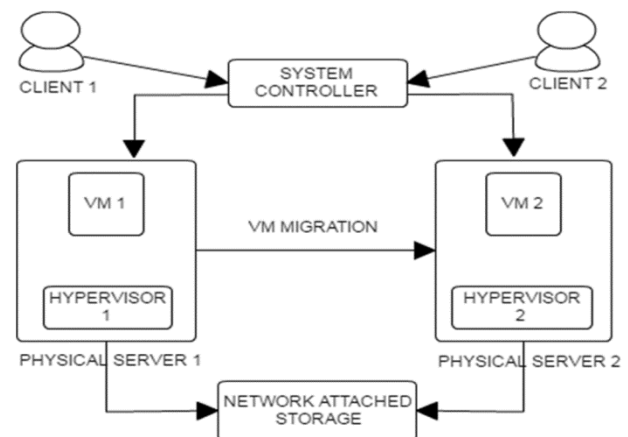


Fig. 1 — Architecture of Virtual Machine migration

address and Wireless Local Area Networks (WLAN) settings. After Router setup, virtualBox is introduced. Circle space will be distributed to virtualBox. Presently virtual apparatuses are imported in VirtualBox. Next processor and connector settings should be set. Confirmation step will be done in openStack. To begin server, the accompanying order to be utilized. /Stack. Sh. Server begins and it gives OpenStack IP and validation subtleties in terminal. To stop server, the accompanying order is to be utilized. /Unstuck. Sh.

B. Build and Configure Instance

In this module, picture and Instance will be made in openStack dashboard. To open dashboard, open program and type openStack IP. The dashboard gets opened. Give username and secret phrase and the page get diverted to openStack administrator page. On the left half of the dashboard, under administrator tab, click pictures connect. In picture connect, click make picture catch. A discourse box gets opened. Give name, depiction, select record in picture source and transfer a picture from the framework and select the arrangement as QCOW2.

At that point click open checkbox. Presently click make picture catch. The picture gets transferred to openStack. To dispatch an occasion, the accompanying strides to be pursued: at the left half of the dashboard, under venture tab, click cases connect. Snap dispatch an occurrence at the upper right of occasion page. Select accessibility zone as a nova, give occurrence name, season, boot from picture as case boot source and pick picture. Presently click dispatch catch. A virtual instance gets propelled in openstack dashboard.

C. Grid Computing and Application Development

In this module, example is propelled utilizing jclouds API. To dispatch an occasion in openStack utilizing jclouds API, give confirmation and openstack-nova supplier to jclouds. At that point give RAM, picture name and example name. Utilizing nodeMetaData, occasion will be propelled in openStack dashboard. A different IP will be made for every virtual instance.

To develop a Grid of virtual instance, administrator needs to give the absolute number of virtual instance to run, beginning virtual instance to be in running state and RAM determination. A network of examples will be made one by one for the absolute number of cases. The base number of occasions to be run is held and other virtual instance is put to rest state. The

client can exchange a web application to virtual instance. Presently client can send their web applications in virtual instance. Burden adjusting and Suspend Resume approach isn't actualized on virtual instance in Grid Computing which may prompt high over-burden and at last crashes the server examples. The power utilization and reaction time will likewise be high.

D. Power Management Grid Computing

Administrator will distribute occupations to virtual instance. This activity will put on First Come first Serve (FCFS) line and can be served in framework figuring condition. Occupation is part into little undertakings and designated to framework of running virtual instance. The memory for every virtual instance is observed ceaselessly to counteract over-burdening. Edge esteem will be checked with memory use and if any virtual instance surpasses, it will be accounted for to cloud administrator. Burden adjusting is accomplished by setting off the Suspend Resume Policy to stack another virtual instance which is in the rest state. This guarantees uniform circulation load among all the virtual instances that helps in avoiding high memory use which will definitely impact control utilization.

Result analysis

The evaluation of performance is carried out by number of experiments, and those are listed below. The installation of Kernel Virtual Machine (KVM) is depicted in Fig. 2. We will use a 64-bit kernel. A 2 GB RAM confinement for a given virtual machine will occur on a 32-bit kernel establishment. The order above causes the client to check whether or not the given part of the virtual machine bolsters 64-bit. On the off chance of 0 appearing as output, it means the

```

** (gdelt:18337): WARNING **: Set document metadata failed: Setting attribute metadata:gdelt-spell-enabled not supported
** (gdelt:18337): WARNING **: Set document metadata failed: Setting attribute metadata:gdelt-encoding not supported
** (gdelt:18337): WARNING **: Set document metadata failed: Setting attribute metadata:gdelt-spell-enabled not supported
** (gdelt:18337): WARNING **: Set document metadata failed: Setting attribute metadata:gdelt-encoding not supported
** (gdelt:18337): WARNING **: Set document metadata failed: Setting attribute metadata:gdelt-spell-enabled not supported
** (gdelt:18337): WARNING **: Set document metadata failed: Setting attribute metadata:gdelt-encoding not supported
** (gdelt:18337): WARNING **: Set document metadata failed: Setting attribute metadata:gdelt-spell-enabled not supported
** (gdelt:18337): WARNING **: Set document metadata failed: Setting attribute metadata:gdelt-encoding not supported
** (gdelt:18337): WARNING **: Set document metadata failed: Setting attribute metadata:gdelt-spell-enabled not supported
** (gdelt:18337): WARNING **: Set document metadata failed: Setting attribute metadata:gdelt-encoding not supported
** (gdelt:18337): WARNING **: Set document metadata failed: Setting attribute metadata:gdelt-spell-enabled not supported
** (gdelt:18337): WARNING **: Set document metadata failed: Setting attribute metadata:gdelt-encoding not supported
** (gdelt:18337): WARNING **: Set document metadata failed: Setting attribute metadata:gdelt-position not supported

Terminal 137: WARNING **: Set document metadata failed: Setting attribute metadata:gdelt-position not supported
#nodeData-mp-5 virsh -c qemu:///system list
virsh -c: command not found
error: Failed to connect to the hypervisor
error: Failed to connect socket to /var/run/libvirt/libvirt-sock: Permission denied
#nodeData-mp-5 sudo virsh -c qemu:///system list
id      name      state
-----
#nodeData-mp-5

```

Fig. 2 — Execution of Kernel Virtual Machine

CPU isn't 64-bit. If it is 1 or higher then it is a kernel of 64-bit. The following command `uname -m` is used to check whether the running kernel is less than or equivalent to 64-bit.

If the output is `x86_64` it shows the running kernel to be a 64-bit kernel at that point. In case the client sees other than that the client runs a 32-bit kernel at that point. The 32-bit kernel should not be utilized in light of the fact that it won't bolster the virtual machine. The five packages that are to be introduced are

- `qemu-kvm`
- `libvirt-bin`
- `bridge-utils`
- `virt-manager`
- `qemu-system`

The first module clarifies how kernel virtual machine (KVM) is established.¹ The initial step is to check if the CPU supports virtualization of the equipment.³ The command utilized to check the equipment support is `egrep -c '(vmx|svm)'/proc/cpuinfo`. The subsequent stage is to check whether the processor is 64-bit kernel. The command utilized for this rationale is `egrep -c 'lm'/proc/cpuinfo`.

The processor is not 64-bit kernel on the off chance that the output gets is 0. The processor is a 64-bit kernel on the off chance that the result obtained is 1 or more than 1, then. The next step is to introduce 5 bundles of vital aid to the KVM. It is not necessary to run a 64-bit kernel on the portion to make more than 2 GB of RAM available for the virtual machine which the client must render.

The `qemu-kvm` is used in the virtualization to run the information and yield. The device used to associate to the virtualization product is the `libvirt`. `Libvirt` is useful for the `qemu-kvm` run. It underpins numerous wide scope of hypervisor. As the VM supervisor the `virt-manager` is extended. Virtual machine supervisor is the Driving VM user interface. The `qemu-kvm` is linked with the `libvirt-bin` through `bridge utils`. In the design paper, the progressions about the development of virtual machine, holding alive break must be updated. You can open the design document by using the `sudo vim /etc / libvirt / libvirtd.conf` command. Once all 5 packages have

been set up, make the necessary changes in the setup document and then test the establishment using the `$virsh -c qemu:/system list` accompanying order.

Conclusion and future enhancement

The energy competence is achieved in openstack cloud by means of enhanced EGC algorithm by using grid computing to allocate the jobs to the grid of virtual instance by subdividing the single job into multiple jobs by means of divide and conquer algorithm. The jobs are selected based on the job which comes first, determined by using the FCFS algorithm. By using the SR policy, the virtual instance from the sleep mode is waken to busy mode when any one of the virtual instance has reached its threshold level and in need of another virtual instance. Thus here the energy is efficiently used and since the job is divided by grid computing the response time will be less.

References

- 1 Ahmad M, Hamid S & Madani, Virtual machine migration in cloud data centers: a review, taxonomy and open research issues, *J Supercomput*, **71** (2015) 2473–2515.
- 2 Haifeng J, Yanjing S, Renke & Hongli Xu, Fuzzy-Logic-Based Energy Optimized Routing for Wireless Sensor Networks, *Int J Distrib Sens Netw*, **1** (2013) 1–8.
- 3 Richa S, Vasudha V & Umang, EEFCMDE: energy-efficient clustering based on fuzzy C means and differential evolution algorithm in WSNs, *IET Commun*, **13** (2019) 996–1007.
- 4 Kumar A N, Kumar V, Efficient performance upsurge in live migration with downtime in the migration time and downtime, *Clust Comput*, **1** (2018) 455–467.
- 5 Ravikiran N & Deth, Improvements in Routing Algorithms to enhance Lifetime of Wireless Sensor Networks, *Int J Comp Net Commn*, **10** (2018) 1–10.
- 6 Ola A, Laila N & Etimad F, Fuzzy Clustering for Next Generation Wireless Sensor Networks, *Int J Adv Rsrchs in Comp Sci Elect Engg*, **8** (2019) 1–8.
- 7 Parwekar P & Rodda S, Location of Sensors by Base Station in Wireless Sensor Networks, *J Sci Ind Res*, **77(2)** (2018) 83–86.
- 8 Saravanan P & Kalpana P, A Novel Approach to Attack Smartcards Using Machine Learning Method, *J Sci Ind Res*, **76(2)** (2017) 95–99.
- 9 Singh M M & Basumatary H, MERAM-R: Multi- Clustered Energy Efficient Routing Algorithm with Randomly Moving Sink Node, *J Sci Ind Res*, **77(1)** (2018) 15–17.
- 10 Hassan K L, Mandal J K & Mondal S, Enhanced Trust-based Intrusion Detection System in MANET, *J Sci Ind Res*, **78(8)** (2019) 509–512.

Comparison of metallurgical and mechanical properties of dissimilar joint of AISI 316 and Monel 400 developed by pulsed and constant current gas tungsten arc welding processes

ORIGINAL ARTICLE | Published: 12 June 2020 | 108, 2633–2644 (2020)

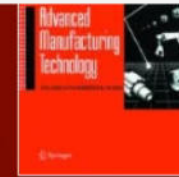
Balram Yelamasetti , Rajyalakshmi G, Venkat Ramana G, Sridhar Babu B & Harinadh Vemanaboina

 296 Accesses  23 Citations [Explore all metrics](#) →

[Cite this article](#)

Abstract

Dissimilar weldments of AISI 316 and Monel 400 are extensively used in boiler feed water heaters where the weld roots are exposed to high pressure and hot corrosive environments. In this research, metallurgical and mechanical properties of dissimilar weldments of AISI 316 and Monel 400 obtained by pulsed current gas tungsten arc welding (PCGTAW) and constant current gas tungsten arc welding (CCGTAW) processes were compared. The heat



[The International Journal of Advanced Manufacturing Technology](#)

[Aims and scope](#) →

[Submit manuscript](#) →

Access this article

[Log in via an institution](#) →

[Buy article PDF 39,95 €](#)

Price includes VAT (India)

Instant access to the full article PDF.

Rent this article via [DeepDyve](#) 

[Institutional subscriptions](#) →

View PDF

Download full issue

Search ScienceDirect

Outline

Abstract

Keywords

Value of the data

1. Data Description

2. Experimental Design, Materials, and Methods

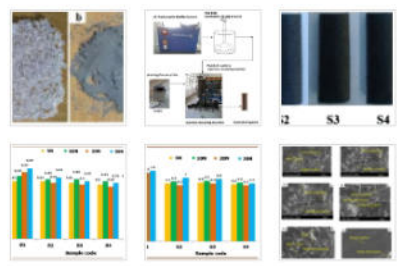
Conflict of Interest

References

Show full outline

Cited by (15)

Figures (8)



Data Article

Dataset on tribological, characterization and thermal properties of Silicon carbide reinforced polyamide composites for industrial applications

S. Sathees Kumar, T. Vishnu Vardhan, B. Sridhar Babu, CH. Nithin Chakravarthy, N. Prabhakar, K. Venkateswara Rao, K. Tirupathi

Show more

+ Add to Mendeley Share Cite

https://doi.org/10.1016/j.dib.2020.105662

Get rights and content

Under a Creative Commons license

open access

Abstract

This dataset comprises the characterizations, tribological and thermal properties of Silicon carbide (SiC) reinforced Nylon 6 (N6) or Polyamide 6 composites. The dataset illustrates the tribological properties such as coefficient of friction, wear and it also describes the characterizations and thermal stability of polyamide composites by varying the weight percentages from 5 - 30wt.% The composites samples were fabricated by injection moulding method. The tribological, characterization and thermal behaviors were determined by wear test, characterizations were carried out by Scanning Electron Microscope (SEM) and Fourier Transform Infrared (FTIR) Thermal stability degradation

U. Nagaraju, ..., T. Vishnu Vardan

Effect of FSW process parameters and tool profile on mechanical properties of AA 50...

Materials Today: Proceedings, Volume 46, Part 1, 2021, ... Venkat Ramana G., ..., Vishnu Vardhan T.

Performance analysis on synthesized reinforced carbon steel for structural...

Materials Today: Proceedings, Volume 33, Part 7, 2020, ... Lakshmi Keshav, ..., J. Vairamuthu

Show 3 more articles

Article Metrics

Citations

Citation Indexes: 15

Captures

Readers: 15



View details

FEEDBACK

Design and Implementation of Brick Making Machine Integrated with Smart IIoT Application

Premkumar, M.; Devi, G. Naga Rama; Sowmya, R.

DOI: <http://dx.doi.org/10.12785/ijcads/090311>

ISSN: 2210-142X

Date: 2020-05-01

Abstract:

Shelter is one of the basic needs and one of the most important challenges a man faces in his lifetime. As per the survey of PPP (Purchasing Power Parity), 21.9% of Indians are abysmal. The production of good quality, most efficient, and affordable bricks is paramount to solve housing problems in developing countries like India. This paper focuses on design, construction of an integrated machine that produces bricks for low-cost housing. With this smart and integrated machine, the production rate can be enhanced to 3600 bricks per day (8 working hours). It is an integrated machine which can produce different varieties of bricks such as clay bricks, concrete bricks, etc. Being automated through (Industrial Internet of Thing) IIoT, the speed, i.e., the production rate of bricks can be improved, which in turn improves the efficiency of the production. It produces the bricks based on the raw material fed to the machine. Assume that the raw materials provided to the machine are natural clay minerals, kaolin and shale then correspondingly produces a clay brick. This smart machine displays: i. the proportion in which the composition of raw materials is mixed, ii. The machine could be monitored via a mobile application. Also, it displays the count of bricks produced per 10 min. as well as the entire day. Thus, the machine is easily affordable for small scale enterprise (SME) with advanced features, and also the bricks produced are relatively cheap.

[Show full item record](#)

Files in this item



Name: paper 11.pdf
Size: 1.146Mb
Format: PDF

[View/Open](#)

All Journals

All Journals

This issue

[Advanced Search](#)

Browse

All of UOB Journals

[Journals, Volumes & Issues](#)

[By Issue Date](#)

[Authors](#)

[Titles](#)

[Subjects](#)

This Issue

[By Issue Date](#)

[Authors](#)

[Titles](#)

[Subjects](#)

Administrator Account

[Login](#)

Customize



Coplanar Waveguide Fed Multimode Resonant Switchable Antenna

Dr. Praveen Kumar Kancherla, B.Amulya, B.Venkateshwar Rao

Abstract

In current article active coplanar waveguide feed reconfigurable multiband antenna design and its operational characteristics are presented. The designed antenna covers S-band, Wi-MAX C-Band, X-band applications. A detail study was performed to characterize the switching operation by considering the wire bound effects. The circular ring is loading with (TSIR) T-shaped stepped impedance resonator and (PSLR) parallel stub loaded resonator. The proposed structure is resonating at 3.26GHz, 4.16GHz, 8.04GHz and 8.9GHz frequencies. Proposed structure exhibiting maximum gain of 5.94 dB at 8.04 GHz. The proposed antenna shows good impedance characteristics, low profile and compact size, which is suitable for wireless communication applications.

Keywords: TSIR, PSLR.

PDF

How to Cite

Dr. Praveen Kumar Kancherla, B.Amulya, B.Venkateshwar Rao. (2020). Coplanar Waveguide Fed Multimode Resonant Switchable Antenna. *International Journal of Advanced Science and Technology*, 29(06), 1986 - 1992. Retrieved from <http://serisc.org/journals/index.php/IJAST/article/view/13464>

More Citation Formats

Issue

[Vol. 29 No. 06 \(2020\): Vol. 29 No. 06 \(2020\)](#)

Section

Articles

International Journal of
Advanced Science and...

Not yet assigned
quartile

SJR 2022

0

powered by scimagojr.com

Make a Submission



ELSEVIER



Image Creator from Designer

Study on Assessment of Outcomes of Education


August 2020 · Journal of Engineering Education Transformations 3(4):38-44
DOI:10.16920/jeet/2020/v3i4/148741

Authors:

 **Aruna Govindan**
BMS Institute of Technology and Manage...

[Download citation](#) [Copy link](#)

[Citations \(1\)](#) [References \(5\)](#) [Figures \(2\)](#)



[Download full-text PDF](#)

[Read full-text](#)

Abstract and Figures

This paper describes the process for assessment of Course Outcomes (COs), Program and Program Specific Outcomes (POs & PSOs). Direct and indirect method was used to assess the COs, POs and PSOs. In the direct method, continuous internal evaluation test, assignment, seminar, end semester examination as well as in the indirect method, number of surveys were carried out to assess the outcomes. Threshold approach was followed for assessing the attainment. Based on the attainment, existing gap can be identified and filled by improving the curriculum, teach learning process and skills of the graduate.

Table 8. Comparison of CO attainment

Year	CO1	CO2	CO3	CO4
2017	78	79	77	79
2018	82	76	87	80
2019	71	88	74	85

ResearchGate

Discover the world's research

- 25+ million members
- 160+ million publication pages
- 2.3+ billion citations

[Join for free](#)

Advertisement

ResearchGate

Build the best teams in science and research.

[FIND OUT MORE →](#)

Find your next great hire on ResearchGate

We simplify hiring by helping you to target scientists based on their profiles, publications, and expertise.

[Find out more](#)

SURFACE ROUGHNESS MEASUREMENT ON AL-7075 REINFORCED WITH THE ZRO₂ POWDER BY USING BOX-BEHNKEN ANALYSIS

CH NITHIN CHAKRAVARTHY¹ & Dr. S. SATHEES KUMAR²

¹Assistant Professor, Department of Mechanical Engineering, CMR Institute of Technology, Hyderabad, Telangana, India

²Professor, Department of Mechanical Engineering, CMR Institute of Technology, Hyderabad, Telangana, India

ABSTRACT

In the present study, the surface roughness characteristics of Al-7075 require analysis due to the abrasive phase present in the reinforcement of Zro₂ particles. So the presence of nano particles in the metal increases hardness and strength. When the workpiece is machined, discontinuous chips are produced, resulting in different machining characteristics. So, by using surface roughness tester, the measured values are seen and by box-behnken analysis the various parameters are found.

KEYWORDS: Surface Roughness Measurement (Talysurf Instrument), Box-Behnken & Design Analysis

Received: Feb 12, 2020; **Accepted:** Mar 02, 2020; **Published:** Mar 31, 2020; **Paper Id.:** IJMPERDAPR202085

DETERMINATION OF FATIGUE ANALYSIS OF COMPRESSOR DISC IN GAS TURBINE

CH NITHIN CHAKRAVARTHY¹, K. ASHOK² & Dr. S. SATHEES KUMAR³

¹Assistant Professor, CMR Institute of Technology, Hyderabad, Telangana, India

²Research Scholar, CBIT, Hyderabad, Telangana, India

³Professor, CMR Institute of Technology, Hyderabad, Telangana, India

ABSTRACT

An abaqus software is used to evaluate fatigue testing of tie bolt holes in a typical gas turbine compressor disc. The material properties needed for the disk are taken as a grade TI-8AL-1MO-1V Titanium alloy. The research focus is on the impact of Uniaxial loading and cyclic rotation speed is subjected to the disc. A solution is fully obtained under uniaxial loading for a disc, numerical analysis measures the problems for the disc.

KEYWORDS: Rotating Disc, Uni-Axial Stresses & Fatigue Test

Received: Jan 11, 2020; **Accepted:** Jan 31, 2020; **Published:** Mar 19, 2020; **Paper Id.:** IJMPERDAPR202060

Soft computing based color image demosaicing for medical Image processing

Authors: D. R. Ramji, C. Anna Palagan, A. Nithya, Ahilan Appathurai, E. John Alex [Authors Info & Claims](#)

Multimedia Tools and Applications, Volume 79, Issue 15-16 • Apr 2020 • pp 10047–10063 • <https://doi.org/10.1007/s11042-019-08091-1>

Published: 01 April 2020 [Publication History](#)

4 0

Feedback

Multimedia Tools and Applications
Volume 79, Issue 15-16

[← Previous](#) [Next →](#)

- Abstract
- Abstract
- References
- Cited By
- Recommendations

Abstract

ABSTRACT

As digital cameras become more enhanced and small, CCD sensors can relate to only one color of a pixel. This color mosaic pattern is called as Bayer Pattern(BP) which requires processing to obtain a color image with a higher resolution. Each image pixel that undergoes interpolation has a full color spectrum based on surrounding pixel colors. Here we introduce Adaptive CFA(ACFA) interpolation model. For normal image regions hue technique is used while edge regions adapt the new technique. It

Vertical sidebar navigation icons: info, share, eye, 34, and grid.

Stub Column Tests of Cold-Formed Steel Built-Up Square Sections with Intermediate Stiffeners

Published: 09 June 2020 | 52, 281–290 (2020)



Strength of Materials

[Aims and scope](#) →

G. Aruna

134 Accesses 4 Citations [Explore all metrics](#) →

[Cite this article](#)

This paper describes the experimental and theoretical investigation on ultimate strength of cold-formed steel built-up square stub columns under axial compression. In total, fifteen stub columns were tested by varying the cross-sectional dimensions of specimens. Local buckling, distortion, and interaction of these buckling modes were observed. The strengths obtained from the experiment are compared to the design strengths calculated using the effective width method, which is a direct strength method in the North American Specification for cold-formed steel structures. It was observed that the effective width method conservatively predicted the strength of specimens. The reliability analysis was carried out to evaluate the appropriateness of the design standards.

Access this article

[Log in via an institution](#) →

[Buy article PDF 39,95 €](#)

Price includes VAT (India)

Instant access to the full article PDF.

[Rent this article via DeepDyve](#)

[Institutional subscriptions](#) →

[Sections](#)

[Figures](#)

[References](#)

Efficient Classification Of Cardiogram Data By Improved Bi-Model Neural Network

Dr. A. Nirmal Kumar, Kamineni B.T. Sundari, A Mahalakshmi

Abstract: In this paper, an Elaborate literature survey and background study was made on existing clustering and classification algorithms and CTG data classification methods. An Evaluation on Automated Classification Methods for the Clustering and Classification of Cardiogram Data was made and the results has been presented. An Outlier Based Bi-Model Neural Network (BM-NN) based Classification System for Improved Classification of Cardiogram Data has been presented. A PCA based Improved Bi-Model Neural Network (IBM-NN) based Classification System for Improved Classification of Cardiogram Data has been presented.

Index Terms: Cloud, Virtual Data Centers, Openstack, Suspend resume policy.

1 INTRODUCTION

In this work, present the improved classification models which will consider outliers in the data and eliminate them from training phase of the classification process. This model is almost similar to the previous BM-NN Model. But here use the Eigen Vectors of the training data to reduce the dimension of the training data as well as testing data. The proposed idea also considerably improved the performance in classifying Normal, Suspicious and Pathologic CTG patterns¹.

2 LITERATURE SURVEY

Cloud Computing is a term that describes the means of delivering any and all information technology from computing power to compute infrastructure, applications, business process and personal collaboration to end users as service whenever and wherever they need it. Here IaaS is used and the energy consumption is optimized by using three power saving policies to reduce the idle power of the server. Here N policy is used, in that when server machine will be turned on, only when the number of jobs in the queue is more or same as that of the specified N threshold. The three policies used are ISN policy, SI policy and SN policy. In the ISN, policy the server will enter into the busy mode when the job arrives and it will end its busy mode only when it completes all of its jobs. The server will be in the sleep mode until the number of jobs in the queue is less than that of the specified N threshold value. In the SN, the server will enter into the sleep mode only when there is no job in the specified machine, whereas in the SI policy, the server will be in the sleep mode for only a certain amount of time when the sleeping time of the server ends, it will enter into the idle mode.

Thus, the consumption of idle power is efficiently reduced at the same this, thus more policies are used and in this the beginning cost will be high (Chiang et al. 2015). Here cloud as a service oriented platform dynamic allocation of resources is proposed by means of virtualization technology. In this technology, the resources are allocated dynamically to the system according to the need of the user. In order to allocate resources dynamically to the system and to determine the utilization of uneven multiple resources skewness is used. By using this skewness, the load between the VM is balanced. Thus the overloading between the VMs is prevented by effective load balancing between the machines and at the same time physical machines should be capable enough to handle all the resource needs of the VM, else overloading of the physical machine takes place and the VM performance is decreased (Nagpure et al. 2015). For the past few years, consumption of energy has become the most difficult part in computing environment especially their data centres. Here the energy efficiency is improved in the web servers by determining the daily requests patterns sent to the web servers which indicate the resource provisioning in offline and will be more suitable for management of resources. Here two load distribution algorithms are used. They are relative load distribution, servers are utilized equally and the adaptive load distribution, the nodes are selected based on the power level. Mostly these two algorithms are used to view the usage of the CPU and level of power consumption in the web servers. Thus, at the end, shutting down of the idle nodes will save the energy. It is however difficult to make out this offline methodology without the daily request patterns. Thus in future it should be enhanced in such a way that the workload predictions should be based on online resource management (Chen et al. 2015). The cloud computing has generally reshaped the cloud computing. Though the cloud provides more advanced features, still it is lagging in its operational cost because it is very high for both the public and the private clouds. Green computing is also very important with minimum resource and more demand. A framework is provided that provides enhancements in the cloud architecture. By using less number of VM, power aware scheduling techniques, proper resource management, and the cloud data center can be improved with minimum overhead. Thus, future enhancements should be done in such a way that all the fields that the proper resource management, scheduling

- Dr. A. Nirmal Kumar is currently working as Associate Professor in Department of Computer Science and Engineering, CMR Institute of Technology, Hyderabad, Telangana, India. E-mail: nirmalkumar@cmronline.ac.in
- Kamineni B.T. Sundari is currently working as Assistant Professor in Department of Computer Science and Engineering, Kommuri Pratap Reddy Institute of Technology, Ghatkesar, Telangana, India. E-mail: kamineniabala@gmail.com
- A. Mahalakshmi is currently working as Assistant Professor in Department of Computer Science and Engineering, CMR Institute of Technology, Hyderabad, Telangana, India. E-mail: mahalakshmi.valliri09@gmail.com

techniques should be enhanced (Younge et al. 2010). Data centers generally consume most amount of energy which is determined in terms of distribution of power and cooling of the systems. By dynamically adjusting the active machines, the resources can be efficiently used according to the system needs. Generally the data centers will have a wide variety of computer systems with varying energy consumption characteristics. Then, works performed by the system will be generally based on the priority, resource needed and the objective. Failure in any one of these characteristics will lead to a problem, thus here the heterogeneity aware resource management is presented for providing a dynamic work in the clouds. K means clustering algorithm is used for allocating the workload based on the similar characteristics in terms of requirements and resource. Here a novel technique is presented for adjusting the machines dynamically to minimize the power (Zhang et al. 2014). In the epoch of cloud computing, data centres consumes more power that can be reduced by obliterating the number of turned-on servers. A power aware virtual datacenter resource scheduling strategy is using this algorithm that consolidates servers periodically and adjusts the VM placements between consolidation rounds to honor a SLA. This methodology is used to construct and validate a power-aware datacenter simulator. Using this, the simulator performance of scheduling algorithm is analyzed. This strategy is more power-efficient than event-based. Further simulation results show that in general, VM weight adjustment according to workload can enable power-aware schedulers to perform more efficiently under the SLA. This approach improves data center control budget by 35% for accidental workloads resembling web-requests, and progress data center budget by 22.7% for workloads exhibiting stable reserve requirements including ScaLAPACK (Zu et al. 2013). Task consolidation in the cloud has become an important approach to streamline resource usage and in turn improve energy efficiency. Resource utilization directly relates to energy consumption, modeled their relationship and developed two energies-conscious task consolidation heuristics. The cost functions incorporated into these heuristics effectively capture energy-saving possibilities and their capability has been verified by evaluation. The results show that the study should not have only a direct impact on the reduction of electricity bills of cloud infrastructure providers with better resource provisioning in other operational costs (Lee & Zomaya 2012). Monitoring and controlling the behavior of Energy Management System (EMS) by fulfilling its purpose at the same time balancing certain constraints, including cost optimization, system reliability and environmental consideration. Examples of systems are building energy management, micro grid energy management and datacenter energy management. It shows promise in the improvement of energy savings across many domains. EMS is a proof of implementation in a wide variety of uses (Duggan & Young 2012). At Internet Data Centers (IDCs) electricity expense is becoming a major category of operational cost. Here problem addresses the total energy cost minimization of IDCs in the smart grid environment. When the electricity usage is high, the price maker in the electricity market will be high. IDC will affect the price of electricity. By several observations, the price varies with load and consumers. Then by contrive the cost of electricity minimization problem and optimization of electricity is

subjected to end-to-end delay constraints. In order to make it more efficient solution method to transform the problem to a quadratic programming, performance is evaluated. The result shows that the total electricity cost of IDCs is minimized by handling the interaction between IDCs and smart grid (Wang et al. 2011). Cloud Computing is used to prove dramatically scalable and virtualized resource as a service over the internet. Datacenters involve in virtualization technology to realize cloud computing. As the rapid growth of server, quantity and scale in the datacenter, it is a great challenge which is directly related to the number of hosted servers and their workloads. It is very important to design and deploy the energy efficient technologies for the data center. Potential consolidation of performance overheads of the server investigates the consolidation strategies and explores the process of live migration. These results show both the two technologies are used to implement the energy saving goals with lower performance overheads (Ye et al. 2010).

3 RESEARCH METHODOLOGY OF IMPLEMENTATION

Proposed framework executes improved Energy-effective Green Control (EGC) calculation which utilizes SR arrangement for improving vitality effectiveness in lattice registering. Proposed framework utilizes open source cloud execution and OpenStack gives cloud design which is the best to fabricate VI. VI is made in OpenStack utilizing two different ways:

- VI is made legitimately in OpenStack Dashboard
- Using jclouds API, occurrence is made in OpenStack

In the event that a solitary occupation is dispensed to one VI at any given moment, control utilization will be high and reaction time will be postponed. So as to give vitality productivity and low power utilization in a cloud, work is isolated into different little undertakings. These assignments are distributed to a framework of VI. Matrix of VI performs employment to lessen reaction time. SR approach is executed to give an effective green control which distributes VI dependent on the utilization and can powerfully summon the VI on demand. It additionally helps in adjusting the heap between the VI as the activity arrives. The modules incorporate OpenStack arrangement, manufacture and design occurrence, dispatch a case and power the executives in framework registering.

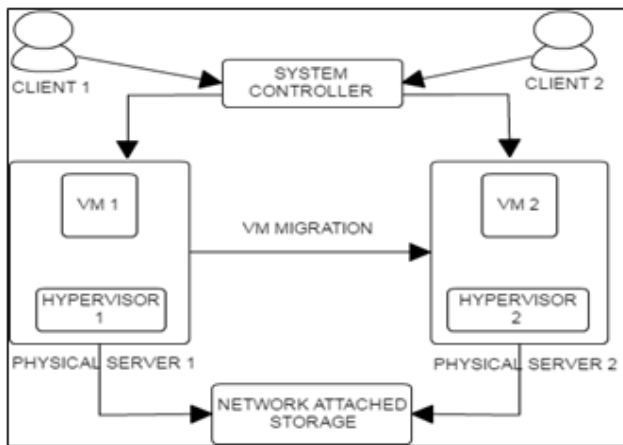


Fig.1 Architecture of VM migration

3.1 Openstack Cloud Setup

In this module, router configuration will be completed. The following setting is done: switch IP address and WLAN settings. After Router setup, virtualBox is introduced. Circle space will be distributed to virtualBox. Presently virtual apparatuses are imported in VirtualBox. Next processor and connector settings should be set. Confirmation step will be done in openStack. To begin server, the accompanying order to be utilized. /Stack. Sh. Server begin and it gives OpenStack IP and validation subtleties in terminal. To stop server, the accompanying order is to be utilized. /Unstuck. Sh.

3.2 Build and Configure Instance

In this module, picture and Instance will be made in openStack dashboard. To open dashboard, open program and type openStack IP. The dashboard gets opened. Give username and secret phrase and the page gets diverted to openStack administrator page. On the left half of the dashboard, under administrator tab, click pictures connect. In picture connect, click make picture catch. A discourse box gets opened. Give name, depiction, select record in picture source and transfer a picture from the framework and select the arrangement as QCOW2. At that point click open checkbox. Presently click make picture catch. The picture gets transferred to openStack. To dispatch an occasion, the accompanying strides to be pursued: at the left half of the dashboard, under venture tab, click cases connect. Snap dispatch an occurrence at the upper right of occasion page. Select accessibility zone as a nova, give occurrence name, season, boot from picture as case boot source and pick picture. Presently click dispatch catch. A VI gets propelled in openstack dashboard.

3.3 Grid Computing and Application Development

In this module, example is propelled utilizing jclouds API. To dispatch an occasion in openStack utilizing jclouds API, give confirmation and openstack-nova supplier to jclouds. At that point give RAM, picture name and example name. Utilizing nodeMeta Data, occasion will be propelled in openStack dashboard. A different IP will be made for every VI. To develop a Grid of VI, administrator needs to give the absolute number of VI to run, beginning VI to be in running state and RAM determination. A network of examples will be made one by one for the absolute number of cases. The base number of occasions to be run is held and other VI is put to rest state. The client can exchange a web application to VI. Presently

client can send their web applications in VI. Burden adjusting and SR approach isn't actualized on VI in Grid Computing which may prompt high over-burden and at last crashes the server examples. The power utilization and reaction time will likewise be high.

3.4 Power Management Grid Computing

Administrator will distribute occupations to VI. This activity will put on FCFS line and can be served in framework figuring condition. Occupation is part into little undertakings and designated to framework of running VI. The memory for every VI is observed ceaselessly to counteract over-burdening. Edge esteem will be checked with memory use and if any VI surpasses, it will be accounted for to cloud administrator. Burden adjusting is accomplished by setting off the SR Policy to stack another VI which is in the rest state. This guarantees uniform circulation load among all the VI that helps in avoiding high memory use which will definitely impact control utilization.

4 RESULTS AND DISCUSSION

The performance evaluation is carried by number of experiments and those are listed below. The first module clarifies the establishment of Kernel Virtual Machine (KVM) (Akiyama et al. 2014). The initial step is to check whether the CPU bolsters the equipment virtualization (Kumar & Schwan 2008). The command utilized to check the equipment support is `egrep-c '(vmxsvm)/proc/cpuinfo`. The subsequent stage is to check whether the processor is 64 bit kernel. The command utilized for this rationale is `egrep-c 'lm/proc/cpuinfo`. On the off chance that the output got is 0, then the processor is not 64bit kernel. On the off chance that the output obtained is 1 or more than 1, then the processor is a 64bit kernel. The following stage is to introduce 5 vital bundles to help the KVM. Running a 64 bit kernel on the portion is not required to make the accessibility of more than 2GB of RAM for the VM which the client will make (Shetty et al. 2012).

```

hp-p@ubuntu-pp:~$ sudo virsh -c qemu:///system list
No VMs are present
hp-p@ubuntu-pp:~$ sudo virsh -c qemu:///system list
No VMs are present
hp-p@ubuntu-pp:~$ sudo virsh -c qemu:///system list
No VMs are present
  
```

Fig.2 KVM

Figure.2 shows KVM installation. A 64-bit kernel should be utilized. On a 32-bit kernel establishment, there will be a confinement of 2GB RAM for a given VM. The above order causes the client to check whether the given VM bolsters 64bit part or not. On the off chance that 0 is appeared as output, it implies that the CPU is not 64-bit. If 1 or higher, then it is a 64 bit kernel. To check whether the running kernel is lesser than or equivalent to 64-bit, the following command

uname -m is used. If the output is x86_64, at that point it shows that the running kernel is a 64-bit kernel. In the event that the client sees other than that, at that point the client is running a 32-bit kernel. The 32 bit kernel should not be utilized in light of the fact that it won't bolster the VM. The five packages that are to be introduced are

- qemu-kvm
- libvirt-bin
- bridge-utils
- virt-manager
- qemu-system

The qemu-kvm is utilized to run the information and yield in the virtualization. The instrument that is utilized to associate with the product for virtualization is the libvirt. Libvirt is useful in running the qemu-kvm. It underpins numerous wide scope of hypervisor. The virt-manager is extended as the VM supervisor. VM supervisor is the user interface for driving VM. The bridge-utils associates the qemu-kvm with the libvirt-bin. The progressions with respect to the formation of VM, keep alive break must be changed in the design document. The design document can be opened by utilizing the command `sudo vim /etc/libvirt/libvirtd.conf`. After the establishment of all the 5 packages, make the important changes in the setup document and after that the establishment is checked utilizing the accompanying command `$ virsh -c qemu:///system list`.

5 CONCLUSION

The energy competence is achieved in openstack cloud by means of enhanced EGC algorithm by means of using grid computing to allocate the jobs to the grid of VI by subdividing the single job into multiple jobs by means of using divide and conquer algorithm and the jobs will be selected based on the jobs which comes first which is determined by using the FCFS algorithm. By using the SR policy, the VI from the sleep mode is waken to busy mode when any one of the VI has reached its threshold level and in need of another VI thus here the energy is efficiently used by waking the VI only when there is a need and since the job is divided by grid computing the response time which will be less.

REFERENCES

- [1] Ahmad, RW, Gani, A, Hamid, SHA, Shiraz, M, Xia, F & Madani, SA 2015, „Virtual machine migration in cloud data centers: a review, taxonomy and open research issues“, *The Journal of Supercomputing*, vol. 71, no. 7, pp. 2473-2515.
- [2] Al-Shayegi, MH & Samrajesh, MD 2012, „An energy-aware virtual machine migration algorithm“, In *IEEE International Conference on Advances in Computing and Communications*, pp. 242-246.
- [3] Buyya, R, Broberg, J & Goscinski, AM 2010, „Cloud computing: Principles and paradigms“, *John Wiley & Sons*, vol. 87.
- [4] Chiang, YJ, Ouyang, YC & Hsu, CHR 2015, „An efficient green control algorithm in cloud computing for cost optimization“, *IEEE Transactions on Cloud Computing*, vol.

- 3, no. 2, pp. 145-155.
- [5] Dalvi, R & Madria, SK 2015, „Energy efficient scheduling of fine-granularity tasks in a sensor cloud“, In *International Conference on Database Systems for Advanced Applications*, Springer, pp. 498-513.
- [6] Duggan, GP & Young, PM 2012, „A resource allocation model for energy management systems“, In *IEEE International Systems Conference SysCon*, pp. 1-3.
- [7] Fakhfakh, M, Cherkaoui, O, Bedhief, IL & Frikha, M 2009, „High availability in IMS virtualized network“, In *First IEEE International Conference on Communications and Networking*, pp. 1-6.
- [8] Liu, Z, Qu, W, Liu, W & Li, K 2010, „Xen live migration with slowdown scheduling algorithm“, In *IEEE International Conference on Parallel and Distributed Computing, Applications and Technologies*, pp. 215-221.
- [9] Piyare, R & Lee, SR 2013, „Towards internet of things (IOTs): Integration of wireless sensor network to cloud services for data collection and sharing“, *International Journal of Computer Networks & Communications*, vol. 5, no. 5, pp. 59-72.
- [10] Shetty, J, Anala, MR & Shobha, G 2012, „A survey on techniques of secure live migration of virtual machine“, *International Journal of Computer Applications*, vol. 39, no. 12, pp. 34-39.
- [11] Travostino, F, Daspit, P, Gommans, L, Jog, C, De-Laat, C, Mambretti, J & Wang, PY 2006, „Seamless live migration of virtual machines over the MAN/WAN“, *Future Generation Computer Systems*, vol. 22, no. 8, pp. 901-907.
- [12] Ye, K, Jiang, X, Huang, D, Chen, J & Wang, B 2011, „Live migration of multiple virtual machines with resource reservation in cloud computing environments“, In *IEEE 4th International Conference on Cloud Computing*, pp. 267-274.
- [13] Zhang, P, Sun, H & Yan, Z 2013, „A novel architecture based on cloud computing for wireless sensor network“, In *Proceedings of the 2nd International Conference on Computer Science and Electronics Engineering Atlantis Press*, pp. 472-475.
- [14] Zhang, Q, Zhani, MF, Boutaba, R & Hellerstein, JL 2014, „Dynamic heterogeneity-aware resource provisioning in the cloud“, *IEEE transactions on cloud computing*, vol. 2, no.1, pp. 14-28.
- [15] Zu, Y, Huang, T & Zhu, Y 2013, „An efficient power-aware resource scheduling strategy in virtualized datacenters“, In *IEEE International Conference on Parallel and Distributed Systems*, pp. 110-117.

Lowest emission sustainable aviation biofuels as the potential replacement for the Jet-A fuels

Anderson A., Karthikeyan A., Ramesh Kumar C., Ramachandran S., Praveenkumar T.R. ▾

Aircraft Engineering and Aerospace Technology

ISSN: 0002-2667

DOWNLOADS



Article publication date: 23 October 2020 Permissions

Issue publication date: 23 June 2021

Abstract

Purpose

The purpose of this study is to predict the performance and emission characteristics of micro gas turbine engines powered by alternate fuels. The micro gas turbine engine performance, combustion and emission characteristics are analyzed for the jet fuel with different additives.

Design/methodology/approach

The experimental investigation was carried out with Jet A-1 fuel on the gas turbine engines at different load conditions. The primary blends of the Jet A-1 fuels are from canola and solid waste pyrolysis oil. Then the ultrasonication of highly concentrated multiwall carbon nanotubes is carried with the primary blends of canola (Jet-A fuel 70%, canola 20% and 10% ethanol) and P20E (Jet-A 70% fuel, 20% PO and 10% ethanol)

Related articles

Combustion analysis of biodiesel-powered propeller engine for least environmental concerns in aviation industry
Balaji V. et al., Aircraft Engin and Aeros Techn, 2022

Influence of high oxygenated biofuels on micro-gas turbine engine for reduced emission
Booma Devi et al., Aircraft Engin and Aeros Techn, 2020

Role of spirulina microalgae blends in the micro gas turbine engine performance and

A Novel Forgery Detection in Image Frames of the Videos Using Enhanced Convolutional Neural Network in Face Images

S. Velliangiri^{1,*} and J. Premalatha²

¹CMR Institute of Technology, Hyderabad, 501401, India

²Kongu Engineering College, Erode, 638052, India

*Corresponding Author: S. Velliangiri. Email: velliangiris@gmail.com

Received: 02 April 2020; Accepted: 14 June 2020

Abstract: Different devices in the recent era generated a vast amount of digital video. Generally, it has been seen in recent years that people are forging the video to use it as proof of evidence in the court of justice. Many kinds of researches on forensic detection have been presented, and it provides less accuracy. This paper proposed a novel forgery detection technique in image frames of the videos using enhanced Convolutional Neural Network (CNN). In the initial stage, the input video is taken as of the dataset and then converts the videos into image frames. Next, perform pre-sampling using the Adaptive Rood Pattern Search (ARPS) algorithm intended for reducing the useless frames. In the next stage, perform pre-processing for enhancing the image frames. Then, face detection is done as of the image utilizing the Viola–Jones algorithm. Finally, the improved Crow Search Algorithm (ICSA) has been used to select the extorted features and inputted to the Enhanced Convolutional Neural Network (ECNN) classifier for detecting the forged image frames. The experimental outcome of the proposed system has achieved 97.21% accuracy compared to other existing methods.

Keywords: Adaptive Rood Pattern Search (ARPS); Improved Crow Search Algorithm (ICSA); Enhanced Convolutional Neural Network (ECNN); Viola Jones algorithm Speeded Up Robust Feature (SURF)

1 Introduction

The rapid development in video editing application has ended video forgery an easy task. Hence, the trustworthiness of hypermedia matters, particularly videos, as a proof is a cumbersome task. The growth of images processing software and the progression in cameras (digital) has brought about a significant amount of doctored images with no noticeable traces, creating a high demand for automatic forgery detection algorithms to ascertain the honesty of a candidate image [1]. Nowadays, it produces considerable difficulty in authenticating images. Image forgery implies the manipulation of the image (digital) to cover some essential or helpful information as of it [2]. Many research works focused on image forgery detection (IFD). The disclosure of the forgery algorithm will depend on the image source [3].



This work is licensed under a Creative Commons Attribution 4.0 International License, which permits unrestricted use, distribution, and reproduction in any medium, provided the original work is properly cited.

Forgery detection could well be developed as active or passive [4]. Active approaches were traditionally utilized by engaging data hiding (watermarking) or digital signatures [5]. Usually, the image watermarking is either embedded at the interval [6] of the time of the image acquisition or advanced after further processing of the real image. Contrary to active approaches, passive approaches do not count on pre-registration or pre-embedded information, and no meticulous research has been done on them. Passive methods for image forensic work on the dearth of any signature or water-mark [7].

Prior research has exhibited that copy-paste forgery can well be detected via finding localized inconsistencies in intrinsic image features such as traces of re-sampling, JPEG compression [8], median filtering [9], contrast enhancement, along with sensor noise. The forgery detection's output could well be of '2' types: (a) classifying the image as genuine or else forged (no localization), (b) localizing the forged region, on the off-chance of the image is not genuine [10]. Mainly '2' classes of CMFD are presented. One is centered on block-wise division and the next one on key-point extraction [11].

Every forgery detecting methods pursue a specific pattern, i.e., feature extraction, matching and post-processing. Since its last century, object features detectors are quite well-liked devices throughout the area of computer vision. They are incorporated in different applications such as object representation, object detection and matching, image recognition and recovery, 3D scene creation, activity recognition, text classification and biometric systems [12]. To encourage this, video forgery ought to develop either adequate information to streamline the production of precise altering veils or discharge the covers themselves. Moreover, video information ought to be dispersed to limit further preparation. Video preparing, for example, compression and correcting, can viably disguise altering. While the location of such an enemy of crime scene investigation is a significant research course, handling can be applied to video freely after dataset distribution, yet just if the first dataset is distributed to evade unnecessary handling. Much deep learning method has been proposed to solve this issue. As the assortment of video control procedures extends and propels, the altered and engineered video will get unclear from the original video to human eyes. Based on the review of different approaches, new procedures are required which either arrange altered video agreeing to its altering type or perform altering identification independent of the kind of altering. Keep up trust in the credibility of video content in the future, and it is vital to create procedures that can distinguish and limit video handling and control. For the most part, the techniques created to address one sort of tampering are not fit for tending to different sorts of imitations. The presentation of this technique relies upon the codecs utilized for compression and the video content. For instance, strategies fit for identifying tampering in quick movement recording will fail in slow movement recordings, and static foundations will bomb in dynamic foundation recordings and so forth.

The paper structure is organized as follows. Section 2 surveys the associated works regarding the method proposed. In sections 3, a concise discussion about the proposed methodology is given, section 4, explore the Investigational outcome, and also Section 5 concludes the paper with future directions.

2 Related Work

Hu et al. [13] suggested an IFD system for efficiently identifying a tampered background or foreground image utilizing image watermarking along with alpha mattes. This approach had '2' parts: (i) watermark embedding and (ii) identification of tempered images. The component-hue-difference-centered spectral matting was first utilized to attain the alpha matte. Subsequently, DWT-DCT-SVD-centered image watermarking was utilized to include the watermarks. Lastly, the difference betwixt the attained singular values was utilized for detecting the tempered background and foreground images.

Bhartiya et al. [14] presented a technique to detect sham on the JPEG image. An algorithm was designed to categorize the image blocks as non-forged or forged centered on an exacting feature that existed in multiple-compressed [JPEG] images. This approach modeled the characters present in the histograms of double compressed JPEG images for detecting forgery using feature-based clustering. The method performed was superior to the prior works that used the probability centered system for detecting a forgery on JPEG images. This approach showed the accuracy centered on quantitatively and qualitatively analysis only.

Mahmood et al. [15] recommended a robust method aimed at Copy-Moves Forgery detection (CMFD) along with localization on digital images. This approach consists of three steps: pre-processing, FE as of the image blocks, feature matching, along with filtering. In the pre-processing, the inputted image (RGB) was transformed into YC_bC_r the FE phase, and the image was split into blocks. In feature matching, the process was performed for image block pairs, and the post-processing was performed via morphological operation.

Elsharkawy et al. [16] presented an efficient blind IFD algorithm. Primarily, the image was attained with digital cameras together with scanned images. Subsequently, the logarithmic operation was applied to the input image for obtaining the illumination and also reflectance elements. Afterward, the low-pass filter image's histogram was estimated. Then, differentiation was implemented to the attained histogram for detecting the changes in illumination. Lastly, Support Vectors Machine (SVM) was utilized for training and testing to attain the feature vector. The Comparison outcomes proves the performance of this system.

Oommen et al. [17] offered a blind or passive approach to CMFD. This approach has seven steps, preprocessing, FE with LFD, image segmentation, organize segment in B+ Tree, Estimate SVD, Image blocks matching using SVD, and Filtering along with highlighting. The FE was done by using Local Fractals Dimension (LFD), and the LFD was estimated using Differential Box-Counting. The block matching was applied centered on Singular Values Decomposition (SVD). Youseph et al. [18] introduces techniques of detecting forged images using illuminant color assessment. It helps to detect the canny edges and extracts the shape features by HOG edge. Moreover, this technique has advantages of a minimum quantity of human interaction and improved the accuracy performance.

Pun et al. [19] propounded a CMF scheme utilizing adaptive over-segmentation and features-point matching. Initially, this was implemented for segmenting the [host] image into non-overlapping. Subsequently, the Scale Invariants Feature Transforms (SIFT) was applied in every block to extort the SIFT feature points. Lastly, the Forgery Region Extractions method was used for detecting the fake region as of the host image as per the extorted Labeled Features Points (LFP).

Zhong et al. [20] presented an enhanced block-centered efficient technique for CMFD. Initially, the suspicious image was inputted to pre-processing. Next, the step was the block

segmentation. The image was split into the overlapped circular block. Then, the features vector of every block was extorted by utilizing Discrete Radial Harmonics (DRHMs). The SVD and 2 Nearest Neighbors (2NN) was implemented for block matching. Lastly, the forgery regions were signified by white pixels.

Barani et al. [21,22] designed a digital image tamper detection algorithm based on integer wavelet transform. Proposed techniques recognize altered locales in different pictures, and furthermore, the technique has high inserting visual quality. The proposed technique assessed on various picture datasets and the outcomes as far as location execution are adequate, yet in individual assaults, the confirmation strategy has high recognition errors. These errors are self-explanatory in individual assaults, for example, JPEG pressure at high-pressure rates, what is more, salt and pepper at low commotion rates.

Hong et al. [23] recommended a detection of frame deletion in HEVC-Coded video. The proposed technique is triple. To begin with, it examines and recognizes video phony in the packed space, making it straightforward also, quick. Second, it arranges video as certifiable or produced without requiring recognition of the creases created upon outline erasure, making it hearty against a crease concealing handling. The trial results show that the proposed method altogether beats the current strategies and stays hearty in different erasure circumstances.

Uliyan et al. [24] reported the Anti-spoofing method for fingerprint recognition using a patch-based deep learning machine, which discusses with complex surface examples in a friendly manner because of its probabilistic multilayer engineering. KNN classifier is applied with the component vectors of the ROIs removed by the DBM to look at parody fabrications. The examination results show that the Deep learning model is hearty against various types of parody imitations. The exhibition assessment of the DRBM + DBM strategy accomplished best in class brings about three open unique mark acknowledgment benchmarks.

Bi et al. [25,26] proposed a quick duplicate move fraud detection using local bidirectional coherency error refinement. The proposed technique can hold excellent execution under various phony situations. Duplicate move falsification identification approach, setting up high-light correspondence under various assaults, is cultivated very well by the upgraded coherency delicate-looking.

3 Proposed Methodology

3.1 Forgery Detection in Image Frames of the Videos

Rapid development in digitalization causes spread of image along with video processing tools, such as Photoshop, Adobe Premiere, and also Final Cut Pro makes it easy to manipulate with digital visual media without any changes in existence. Nowadays, most of the legal and social issues were probably might occur due to malicious tampering. Major portions are tampered images and recordings used for false evidence in the trial and spread the rumors or false news among the people about political leaders or mislead the information. Meanwhile, the huge volume of digital knowledge makes it more difficult to identify interference through empirical observation alone. For detection, this work proposed forgery detection on image frames of the videos using Enhanced CNN. This work takes the Youtube8M as the dataset. Initially, the inputted video is transmuted into frames, and then the frames are pre-sampled for reducing the useless frames using ADPS. Preprocessing is performed for enhancing the image frames. Next, the features are extracted, and then the necessary features are selected as of the extorted features using ICOSA.

Finally, the image frame is classified centered on the chosen features using ECNN. The structural design of the proposed work is shown in Fig. 1.

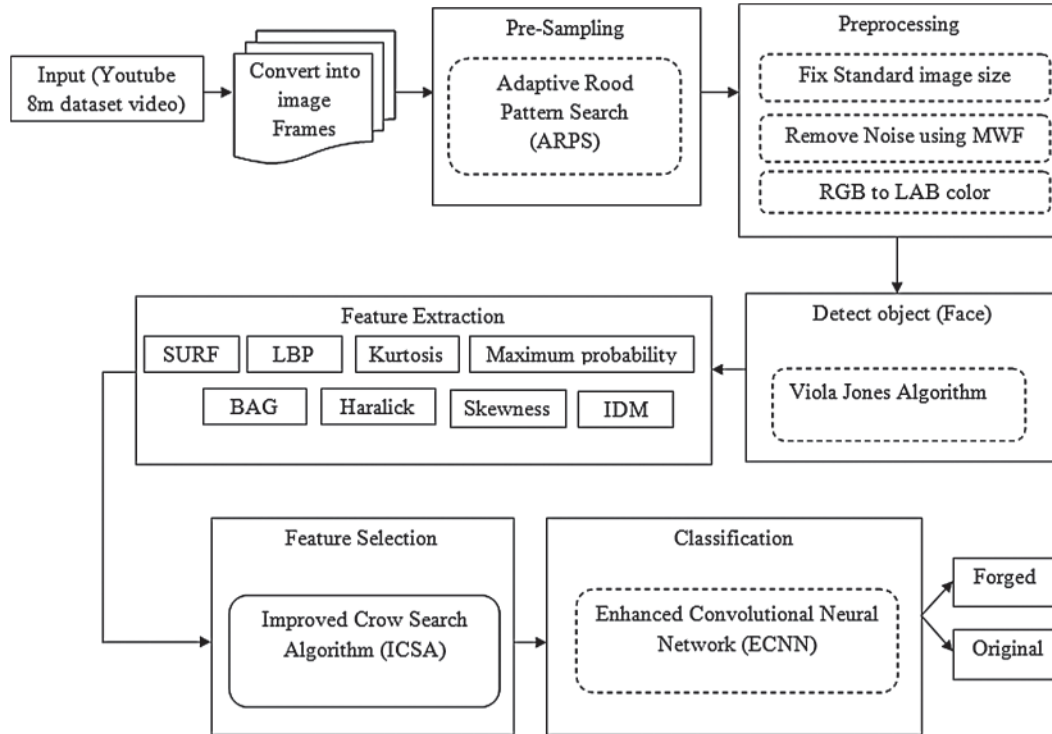


Figure 1: Workflow of the proposed detection system

3.2 Data Collection

The proposed system has collected the data from YouTube for evaluation of performance. The presented videos having a resolution bigger than 480p, which was tagged with “face,” “newscaster,” or “news program” in the youtube8m data-set was taken. YouTube-8M is an enormous scale marked video dataset that comprises of a large number of YouTube video IDs, with excellent machine-produced comments from various jargon of 3,800+ visual substances. It accompanies recomputed various media highlights from billions of edges and sound fragments, intended to fit on a solitary hard circle. This makes it conceivable to prepare a robust benchmark model on this dataset in under a day on a single GPU. Simultaneously, the dataset’s scale and decent variety can empower profound investigation of complex, broad media models that can take a long time to prepare even in a circulated manner. Fig. 2 shows the video frame original, and Fig. 3 shows the tampered video frame.

3.3 Convert Videos into Frames

The inputted video is originally converted into frames that are mathematically written as Eq. (1),

$$I = \{f_1, f_2, f_3, \dots, f_n\} \quad (1)$$

where I denotes the video frameset and f_n represents the ‘ n ’-number of frames.



Figure 2: Video frame original



Figure 3: Video frame forgery

3.4 Pre-Sampling

At this stage, the use of the ARPS reduces the number of redundant frames (useless frames). Symmetrical patterns of search refer to the shape of “rood” or “cross.” There will be ‘2’ distinct search phases called the Adaptive Rood Pattern (ARP) besides the Unity Rood Pattern (URP) that differ mainly in search points separation. Of course, the ARPS are iterative; the ARP phase is used once, until the search converges, the lightweight URP search is implemented iteratively. Fig. 4 shows the search sequence of ARPS algorithm.

3.5 Preprocessing

The resampled frames are preprocessed. The preprocessing stage involves choosing the standard image size, removal of noise and ‘RGB’ to ‘LAB’ color spaces conversion which is explained as follows.

(a) Standard Image Size

In this phase, the image is set with a fixed size. If the system gets a different size of images for performing the task, then it may produce unwanted or error results. To avoid such drawbacks, the input images are initially fixed at standard size.

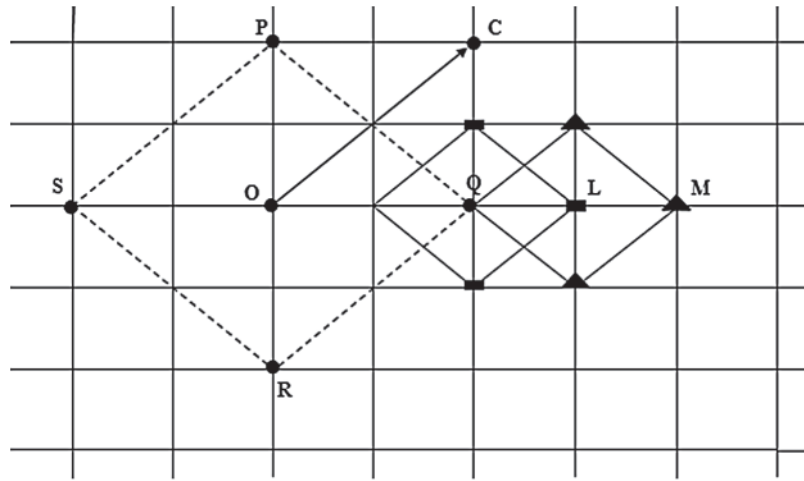


Figure 4: Search sequence for ARPS algorithm

(b) Removal of Noise

In this stage, the salt and pepper noise has been eliminated using Modified Wiener Filter (MWF), which produces a better result than the ordinary Wiener Filter (WF). It is also more effective in preserving the edges. It is a Pixel wise linear filter formed by evaluating the local mean and variance about each pixel. The image I_p value at a point (u, v) is,

$$I_E = I_p(u, v) = \eta + \frac{(\sigma^2 - r^2)}{\sigma^2} (I_i(u, v) - \eta) \tag{2}$$

Eq. (2) indicates that η is the area's mean that is under consideration, σ^2 implies the variance, r^2 is the noise variance, I_i is the image under consideration for noise removal, and I_E denotes the enhanced image that is utilized for further steps.

(c) RGB to LAB Space Conversion

After removing salt and peppers' noise from images then it transformed into $L^*a^*b^*$ color space. Therefore, the transformation is separated by two steps: (i) RGB to XYZ (tristimulus values (i.e., coordinate values of the RGB image)), and (ii) XYZ to $L^*a^*b^*$.

(i) RGB to XYZ

Assume that r, g, b are three channels of pixels, and the gamut of values is $[0, 255]$. The conversion formula is as Eq. (3):

$$\begin{cases} R = \text{gamma} \left(\frac{r}{255} \right) \\ G = \text{gamma} \left(\frac{g}{255} \right) \\ B = \text{gamma} \left(\frac{b}{255} \right) \end{cases} \tag{3}$$

The XYZ conversion is,

$$\begin{bmatrix} X \\ Y \\ Z \end{bmatrix} = A \times \begin{bmatrix} R \\ G \\ B \end{bmatrix} \quad (4)$$

In Eq. (4) A denotes the 3×3 matrix value of the gamma function of the RGB value.

(ii) XYZ to $L^*a^*b^*$

In this stage, the obtained XYZ components are converted into three components $L^*a^*b^*$ which is expressed as follows:

$$L^*a^*b^* = \begin{bmatrix} L^* = 116c_f\left(\frac{Y}{Y_n}\right) - 16 \\ a^* = 500\left[c_f\left(\frac{X}{X_n}\right) - c_f\left(\frac{Z}{Z_n}\right)\right] \\ b^* = 200\left[c_f\left(\frac{X}{X_n}\right) - c_f\left(\frac{Z}{Z_n}\right)\right] \end{bmatrix} \quad (5)$$

In Eq. (5) X_n , Y_n and Z_n denotes the tristimulus values measure light intensity based on the three primary color values (RGB), typically represented by X , Y , and Z coordinates as well as the c_f , represents the calibration function which is stated as follows,

$$c_f(t) = \begin{cases} t^{\frac{1}{3}} & \text{if } t > \eta^3 \\ \frac{t}{3\eta^2} + \frac{4}{29} & \text{otherwise} \end{cases} \quad (6)$$

Eq. (6) indicates that η value is $\frac{6}{29}$. Finally, the $L^*a^*b^*$ converted image is obtained.

3.6 Detect Objects (Face) Using Viola–Jones Algorithm

The pre-processed picture obtained from the color image of the LAB is defined by the object. In the image provided, Viola and Jones offer pace and effective ways to recognize a face. This algorithm includes the following steps in a significant way.

3.6.1 Haar Like Features

This was a rectangular digital image part that originates from its resemblance to Haar-wavelets. The two-component value of the rectangle is the variance between the sum of the pixels between the rectangular regions of '2'. The balance is determined by a three-rectangle function in the middle of the two outer rectangles that decreased from the rectangle center number. A four-rectangle component essentially tests the diagonal pairs of the variance between rectangles. The significance of rectangular features is measured as

$$V_{RF} = \left[\sum P_{A(black)} - \sum P_{A(white)} \right] \quad (7)$$

In Eq. (7) V_{RF} denotes that features value and the pixels of black and white area are denotes as $P_{A(black)}$ and $P_{A(white)}$ respectively.

3.6.2 Feature Selection and Analysis

The Viola–Jones technique used the modification of the Ada Boost algorithm created by Freund and Schapire to construct an efficacy classifier by tabbing a minimum number of critical components. The training data will include photographs for the effects of preeminence through the spectrum of lighting conditions and facial properties.

3.6.3 Integral Image

An innovative representation of images called an integral image allows evaluation of very fast features. The detection system is not directly performing with image intensities here. This method of object detection categorizes images by taking into account the meaning of basic features. The integral image is determined from a single pixel image that requires certain operations. All of these hair-like components are measured in stable time at [any] location or scale.

The integral position figure (i, j) includes the sum of the pixels above and the left part of ‘ i, j ’ including,

$$I_i(i, j) = \sum_{x' < x', y' < y'} I_E(i, j) \quad (8)$$

In Eq. (8) $I_i(i, j)$ is the main image and $I_E(i, j)$ is the real image intensity.

3.6.4 Ada Boost Algorithm

The object detection system provides an Adaboost learning algorithm for both tabbing the best feature and classifying training that uses it. This algorithm therefore generates a strong classifier as a weighted linear combination of simple weak classifiers.

$$h(x) = \text{sign} \left(\sum_{j=1}^N \beta_j h_j(x) \right) \quad (9)$$

Each weak classifier has a threshold function of feature F_j . Eq. (9) denotes that weak classifier of $h_j(x)$ having a feature F_j and limitation of threshold where indicated by θ_j and a parity that denotes the in-equality sign path:

$$h_j(x) = \begin{cases} -T_j & \text{if } F_j < \theta_j \\ T_j & \text{if otherwise} \end{cases} \quad (10)$$

Eq. (10) indicates that threshold value of $\theta_j T_j$ to ensure training and co-efficient, x and β_j where includes a 24-by-24 image sub-window.

3.6.5 Cascade Architecture

The input window evaluation is performed on the cascade’s initial classifier, and if that classifier arrives wrong, the window’s measurement is completed, and the detector arrives correct. If the classifier reappears true, however, the window will be passed to the following cascade classifier. Since most of the image windows may not look like faces, most are quickly rejected as non-faces.

3.7 Feature Extraction

In this phase, the SURF, LBP, Kurtosis, Maximum probability and BAG features are extorted as of the pre-processed image which is explained as follows:

(a) Speeded Up Robust Feature (SURF) Feature

This method uses a BLOB (Binary Large Objects) Hessian matrix detector to address the stains. This method used wave-let responses in horizontal along with vertical directions by using appropriate Gaussian weights for the assignment of feature definition and orientation. A neighbor about pivotal point is identified and divided into sub-regions, and then the wave-let responses are considered and indicated for each sub-region to obtain SURF. Eq. (11) shows that descriptor vector ' $d(y)$ ' for every sub-region.

$$SURF = d(y) = \left(\sum d_x, \sum d_y, \sum |d_x|, \sum |d_y| \right) \quad (11)$$

(b) Local Binary Pattern

The LBP is a texture centered feature that has extensive applications in image classification. The LBP feature is provided as,

$$LBP = \sum_{s=1}^n 2^s * S_f(I_N - I_C) \quad (12)$$

In Eq. (12) I_N signifies the neighboring pixel on a square window, I_C implies the center pixel in the square window, ' s ' signifies the number of neighboring pixels around a center pixel. ' S_f ' signifies specific function and $(I_N - I_C)$ is marked as the thresholds value and it is estimated by Eq. (13).

$$S_f(I_N - I_C) = \begin{cases} 1, & \text{if } I_N - I_C \geq 0 \\ 0, & \text{if } I_N - I_C < 0 \end{cases} \quad (13)$$

(c) Kurtosis

The shape of an arbitrary variable's probability distribution is delineated using the parameter called Kurtosis. For the arbitrary variable ' X ', the Kurtosis is denoted as, $K_{urt}(X)$ and it is stated as,

$$K_{urt}(X) = \left(\frac{1}{m \times n} \right) \frac{\sum (f(x,y) - M)^4}{SD^4} \quad (14)$$

In Eq. (14) SD denotes the standard deviation and M represents the mean value.

(d) Maximum Probability

Maximum probability is merely the most significant entry in the matrix as well as equivalents to the most robust response calculated by Eq. (15).

$$\text{Maximum probability} = \text{Max } \|f(x,y)\| \quad (15)$$

(e) Block Artificial Grid (BAG)

It has some visually horizontal or vertical breaks on the image. This termed BAG emerges at the border of every pixel block. This can well be utilized for resolving whether the image is

changed or not. If the entire BAGs are extracted as of a specified image, regions with BAGs with-in the block border are deliberated as forged areas. Final BAG is attained by adding two elements (image's vertical and horizontal edge) in

$$BAG = b(x, y) = b_h(x, y) + b_v(x, y) \quad (16)$$

In Eq. (16) b_v and b_h denotes the image's vertical and horizontal edge.

3.8 Feature Selection

The obligatory features are selected as of the extorted features for avoiding the execution time. The necessary features are selected using ICSA which is enlightened as follows.

3.8.1 Improved Crow Search Algorithm

The crows' intelligence activities are enthusiastic about the Crow search algorithm (CSA). The CSA has developed its potential to achieve the optimal solution for specific configurations of search spaces. Nevertheless, due to the unproductive discovery of its quest policy, its convergence is not certain. Under this situation, when faced with higher multimodal formulations, the search approach faces great challenges. This proposed method uses the ICSA to solve these difficulties. The improvement is accomplished by adding Levy's flight for random movement performance. In Lévy flights, a heavy-tailed distribution of probabilities, called the Lévy distribution, controls the phase scale. The search space is essentially discovered by the Lévy Flights relative to the uniform random distribution.

The evolutionary process of the CSA imitates the activities carried out using crows to hide and recover the additional food. As an algorithm centered on population, the size of the flock is confirmed by ' N ' individuals (crows) that are of n -dimensional with ' n ' as the problem dimension. The position ' $W_{i,k}$ ' of the crow g in the specific iteration k is illustrated in Eq. (17) and signifies a probable solution for the issue:

$$W_{i,k} = [w_{i,k}^1, w_{i,k}^2, \dots, w_{i,k}^n], \quad i = 1, 2, \dots, N; \quad k = 1, 2, \dots, \max \text{ Iter} \quad (17)$$

In Eq. (17) $\max \text{ Iter}$ is the maximum of iterations. Each (individual) crow is supposed to be capable of memorizing the better visited location $R_{i,k}$ to hide food until the present iteration in Eq. (18).

$$R_{g,k} = [r_{g,k}^1, r_{g,k}^2, \dots, r_{g,k}^n] \quad (18)$$

The position of everyone is modified as per the two behaviors such as Pursuit and evasion.

Pursuit: The crow ' h ' has follows the crow ' g ' along with specific reason to find a hidden place. Moreover crow ' g ' does not note the other crow's presence, as a result, the crow's h justification is attained.

The sort of behavior regarded by every crow g is determined y the Alertness probability (AP). So, a random value a_g uniformly distributed between '0' and '1' is sampled. Levy flights fundamentally give a random walk, the random steps of which are drawn as of a Levy distribution for significant steps:

$$a_g = Levy \sim t^{-\lambda}, \quad (1 < \lambda \leq 3) \quad (19)$$

Eq. (19) denotes that a_g is greater or equal than AP, and the behavior one is applied. Otherwise, situation two is chosen. This operation can be summarized in the subsequent model:

$$W_{g,k+1} = \begin{cases} W_{g,k} + a_g \cdot f_{g,k} \cdot (R_{h,k} - W_{g,k}) & a_i \geq AP \\ random & otherwise \end{cases} \quad (20)$$

In Eq. (20) flight length $f_{g,k}$ parameter indicates the magnitude of movement from crow $W_{g,k}$ towards the best position $W_{h,k}$ of the crow h , a_g signifies a random number having a uniform distribution on the gamut [0, 1]. The proposed ICSA algorithm's Pseudocode is exhibited in Fig. 5.

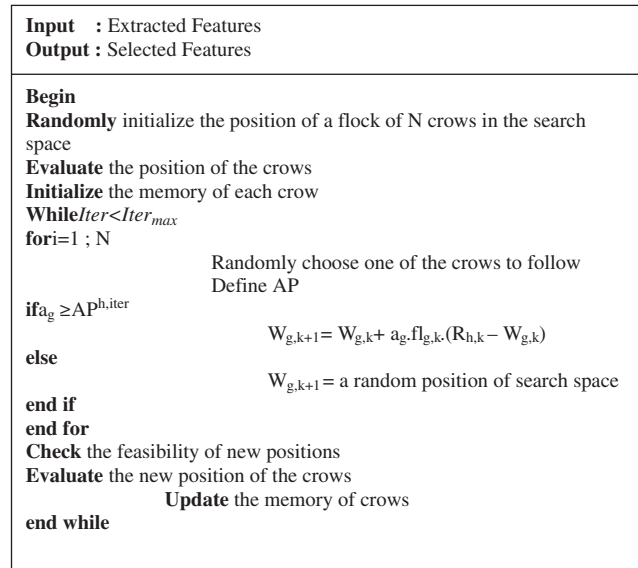


Figure 5: Pseudocode for proposed ICSA algorithm

3.9 Classification Utilizing ECNN

This section carried out the classification. The selected features are inputted to the ECNN. ECNN contains, along with local connectivity, a few conceptions called parameter sharing. Sharing parameters is the sharing of weights on a specific feature map (FM) through each neuron. Local connectivity is the concept of each neural connected only to a sub-set of the input image; this helps to reduce the total parameters of the system as a whole and makes the computation more efficient. A Visual patterns are easily detected by spotting ECNN's shared weight. In shared weight property, the ECNN model uses replicated filters that have matching weight vectors as well as have local connectivity. Taking the well-known LeNet-5, it comprises three sorts of layers, explicitly convolutional, pooling, as well as fully-connected layers. The convolutional layer intends to learn feature representations of the inputs. The architecture diagram of the ECNN is exhibited in Fig. 6.

In decipher convolution by setting up one vector, striding along with it the other vector, and processing a spot item for each walk. That spot element provides one number in the yield vector that is a section. Based on ECNNs, convolution layer is commonly made out of 3 stages. The

principal arrange includes learnable channels, parameterized each playing out a convolution in parallel. This convolution activity can be changed from the above definition in various manners, for example, the amount to walk before figuring another dab item. The subsequent stage includes a component savvy non-linearity like a completely associated layer. At long last, the third stage is called pooling. Pooling is a technique for down sampling the yield vector of the subsequent stage. One approach to do this is called max-pooling, in which the maximal component in a characterized segment of the yield is taken to speak to the whole area. To abridge, a convolutional layer attempts to discover nearby examples in the info. Each channel in the main stage is found out during preparing, so that is task explicit. As it were, the ECNN endeavors to locate the most pertinent examples that help decide how to achieve the given assignment. An identical perspective about ECNNs is by envisioning a convolutional layer just like a wholly associated layer with a limitlessly solid earlier that says loads are shared crosswise over info information passages, and a dominant part of them are zero.

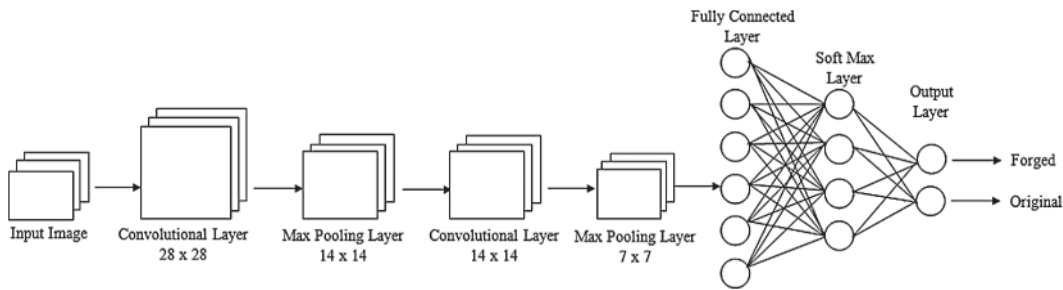


Figure 6: Architecture of ECNN

Specifically, each FM neuron is connected to the adjacent neuronal region on the other side. This neighborhood is referred to as the receptive region of the neuron on the former ground. It is possible to achieve the new FM by initially converting the input with a trained kernel and then applying an element-wise nonlinear activation function on the converted output. Using several different kernels, the entire FM is reached. Mathematically, the feature value at a location (a, b) in the k th FM of l th the layer $q_{a,b,k}^l$ is computed by:

$$q_{a,b,k}^l = w_k^l x_{a,b}^l + b_k^l \tag{21}$$

In Eq. (21) w_k^l and b_k^l signify the weight factor as well as bias term of the k th filter of the l th layer correspondingly, and $x_{a,b}^l$ implies the input patch grounded location (a, b) of the l th layer. Note that the kernel w_k^l that generates the feature map $q_{a,b,k}^l$ is shared. Such a weight sharing mechanism encompasses numerous pros; for instance, it can lessen the model intricacy and make the network easy to train. The activation function commences non-linearities to CNN that are enviable for multi-layer networks to detect non-linear features. Let $n(\cdot)$ implies the nonlinear activation function. The activation value $(n)_{a,b,k}^l$ of the convolution feature $q_{a,b,k}^l$ can well be calculated as shown in Eq. (22).

$$(n)_{a,b,k}^l = n(q_{a,b,k}^l) \tag{22}$$

Classic activation functions are tan, sigmoid, along with ReLU. The pooling layer intends to attain shift-invariance by lessening the FM resolution. It is placed usually betwixt ‘2’ convolutional layers. Every FM of a pooling layer is joined to its equivalent FM of the former convolutional layer. Implying the pooling function as $p(\cdot)$ aimed at all feature map $(n)_{a,b,k}^l$:

$$y_{a,b,k}^l = p\left((n)_{m,n,k}^l\right), \forall (m, n) \in R_{ab} \quad (23)$$

In Eq. (23) R_{ab} implies a local neighborhood about location (a, b) . The classic pooling functions are average pooling along with max pooling.

After numerous convolutional as well as pooling layers, there might be more than one fully-connected layer that intends to do higher-level reasoning. They take every neuron on the former layer and join them to each neuron of the present-layer to make universal semantic information. Take into account that the fully-connected layer is always not essential as it can be swapped by a $[1 \times 1]$ convolution layer.

The last CNN layer is the output layer. Aimed at classification, the softmax operator is generally utilized. Let ‘ θ ’ implies every CNN parameters (for instance, the weight vectors as well as bias terms). The optimal parameters intended for a specific task can well be attained by lessening a suitable loss function stated in that task. This proposed method has N desired input-output relations $\{(x^{(n)}, y^{(n)}); n \in [1, \dots, N]\}$, where $x^{(n)}$ implies the n th input data $y^{(n)}$ signifies its corresponding target label and $o^{(n)}$ is the CNN output. The loss of CNN can well be computed as follows:

$$L_f = \frac{1}{N} \sum_{n=1}^N l\left(\theta, y^{(n)}, o^{(n)}\right) \quad (24)$$

In Eq. (24) L_f denotes the loss function. Training CNN is an issue of universal optimization. Ensure whether the L_f is maximum or minimum, on the off-chance that it is minimum, then train this model. If the L_f is maximum, then the weight parameter is updated using “Adam Optimizer algorithm” again calculate the L_f Adam optimizer is explained as follows:

Adam is primarily derived as of the adaptive moment assessment. Mainly, this algorithm track the first ‘2’ uncentered moments c_t and v_t of the gradient of the objective function at every time step:

$$r_t = \nabla_{L_f} f_t\left((L_f)_{t-1}\right) \quad (25)$$

In Eq. (25) $f_t\left((L_f)_{t-1}\right)$ denotes the evaluation of the fixed loss function on the particular batch of data occurring at timestep $t - 1$, r_t indicates the gradient vector. Initially, c_t and v_t value is assigned as 0. Then the uncentered moments are estimated for each weight value.

$$c_t = \beta_1 \cdot c_{t-1} + (1 - \beta_1) \cdot r_t \quad (26)$$

$$v_t = \beta_2 \cdot v_{t-1} + (1 - \beta_2) \cdot (r_t)^2 \quad (27)$$

In Eqs. (26) and (27) $\beta_1\beta_2$ and denotes the exponential decay rates intended for the moment estimates. After calculated $c_t\nu_t$ and for each weight value c_t and ν_t will be modified by the power of the current frame index value as (Eqs. (28) and (29)).

$$\hat{c}_t = c_t / (1 - \beta_1^t) \quad (28)$$

$$\hat{\nu}_t = \nu_t / (1 - \beta_2^t) \quad (29)$$

Finally, each weight value would be updated as to its previous values \hat{c}_t and $\hat{\nu}_t$.

$$\theta_t = \theta_{t-1} - \eta \left(\hat{c}_t / \sqrt{\hat{\nu}_t} + \varepsilon \right) \quad (30)$$

In Eq. (30) θ_t denotes the updated weight value, θ_{t-1} indicates the previous weight value, η represents the learning rate, ε denotes the tolerance parameter, which is to prevent the division from zero error. For using this way, the weight parameters are updated and to diminish the L_f . By using this ECNN, the image frame is detected as the forged image frame or the original image frame.

4 Experimental Result and Discussion

This Section presents the experimental results of the proposed ECNN for the forgery detection technique in the image frames of the videos. Simulation of the proposed ECNN carried out by the MATLAB with machine configuration as Processor: Intel Core i7, OS: Windows 7, CPU speed: 3.20 GHz, RAM: 8 GB. All test successions were picked to ensure high spatial and worldly circulations. A few recordings have a higher spatial 247 action (surface), while others have higher swift action (development). The sound substance we consider to select 248 successions that had discourse, music, and encompassing sound. This assorted variety is a significant necessity while picking a video 249 database for testing altering assaults. Tab. 1 shows the common video tampering clues used in this research work.

Table 1: Common video tampering clues used in this work

Tampering clues	Copy-move	Cut-paste	Delete-fill	Localization
Composition	✗	✓	✓	✓
Cropping	✓	✓	✓	✓
Flipping	✓	✗	✓	✓
Salt and Pepper	✓	✓	✗	✓
Scaling	✗	✓	✓	✓
Rotating	✓	✓	✓	✓

4.1 Performance Analysis

Here, the proposed method's performance is done by determining a discrete number of performance parameters. The basic parameters that are calculated are 'true positive' (TP), 'true negative' (TN), 'false positive' (FP) and 'false negative' (FN) values. The proposed scheme is contrasted and evaluated centered upon the performance metrics, for instance, accuracy, specificity, and sensitivity, and F-score.

Accuracy: The accuracy refers to the closeness to the actual performance, and it is measured as follows:

$$Accuracy = \frac{TP + TN}{TP + TN + FP + FN}$$

Specificity: The specificity refers to the actual negative case forged video frame got predicated correctly.

$$Specificity = \frac{TN}{FP + TN}$$

Sensitivity: Sensitivity defines the actual positive cases forged video frame, which got predicted correctly, and it is calculated as follows:

$$Sensitivity = \frac{TP}{TP + FN}$$

F-Score: The F score, also called the F1 score or F measure, is a measure of a test's accuracy.

$$F-Score = 2 * \frac{Sensitivity * Specificity}{Sensitivity + Specificity}$$

4.2 Comparative Analysis

The proposed ECNN classifier is compared with the existing methods such as SVM and K-Nearest Neighbor (KNN), Fruitfly optimization algorithm-support vector-NN (FOA-SVNN) and Neural Network (NN) and each works is discussed in detail as follows:

SVM: SVM is a binary classifier. It attempts to find a hyperplane that can separate two class of data by the most significant margin.

K-Nearest Neighbor (KNN): The k-NN method accepts that an unclassified thing can be characterized by taking a looking at k of its effectively ordered, closest neighbors and discovering which class the most significant number of them fall into.

Fruitfly optimization algorithm-support vector-NN (FOA-SVNN) can adaptively determine the two critical hyper-parameters for SVM.

Neural Network (NN): A neural network can be used for many different tasks. One of these tasks is classification.

The performance analysis value of the proposed forgery detection system using ECNN and existing techniques, for instance, SVM and K-Nearest Neighbor (KNN), Fruitfly optimization algorithm-support vector-NN (FOA-SVNN) and Neural Network (NN) for different metrics comparison are shown in below [Tab. 2](#).

The preceding [Tab. 2](#) displays the comparison of the proposed ECNN forgery detection technique with the existent techniques in respects of accuracy, specificity, sensitivity. From [Tab. 2](#), it is clear that the existing NN method has provided the bad performance than the other existent methods. Next, existing KNN is a lot better than the NN in the forgery detection system. ECNNs are generally excellent feature extractors. This implies you can remove helpful characteristics from a previously prepared ECNN with its prepared loads by nourishing your information on each level and tune the ECNN a piece for the particular errand. ECNNs are exceptionally useful in such a task contrasted with NNs. Another favorable position of this pre-preparing is that we

abstain from preparing of ECNN and spare memory, time. The main thing you need to prepare is the classifier toward the end for your labels. From overall observation based on the table value, it proves that the proposed ECNN forgery detection system provides better performance than the other existing methods.

Table 2: Demonstrate the performance of the proposed ECNN with the existing FOA-SVNN, SVM, KNN and NN

Performance metrics	ECNN	FOA-SVNN	SVM	KNN	NN
Accuracy	97.21	94	87.04	79.79	87.84
Specificity	98.56	95.83	94	94.67	94
Sensitivity	95.67	94	67.01	55.88	68.97

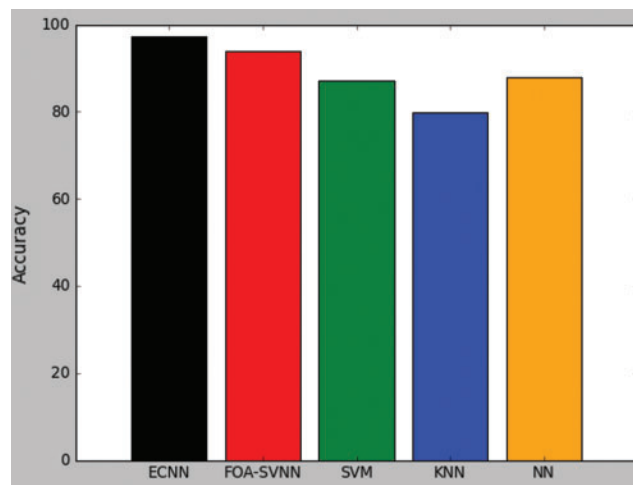


Figure 7: Accuracy performance comparison for ECNN with existing methods

Fig. 7 shows the performance of the proposed ECNN with the existing SVM, FOA-SVNN, KNN, and NN based on accuracy metric. The proposed ECNN achieves 97.21 accuracy, but the existing FOA-SVNN achieves 94 accuracy, which is 32.1 lesser than the proposed technique. Also, the other existing methods, namely SVM, KNN, as well as NN, have 94, 94.67, and 94 accuracy. This discussion exhibits that the ECNN encompass better performance when weighted against the existent methods.

Fig. 8 exhibits the comparison graph for the proposed ECNN with the existing techniques based on specificity measure. The proposed method's specificity is 98.56. The existing systems FOA-SVNN, SVM, KNN, and NN, have 95.83, 94, 94.67, and 94, respectively. Hence it proves that the specificity value is high for the proposed work than the existing systems. k-NN is straightforward and requires tuning only one hyperparameter (the estimation of k), while neural network preparing includes numerous hyperparameters controlling the size and structure of the system and the enhancement methodology, so neural network provides high specificity than KNN algorithm. The excellence of the ECNN lies in utilizing the preparing power accessible to let the model gain proficiency with all the bit qualities to accomplish the last focus of the model,

which could be a necessary arrangement. At the point when you take a look at the halfway pictures during derivation, you will perceive how the various hubs are distinguishing various edges, shading, and so on, in the first convolution layers only like PC vision channels. Be that as it may, the expansion of this separating prompts distinguishing progressively complex examples in resulting Convolution layers. The proposed ECNN performed better with the value for specificity as 98.56.

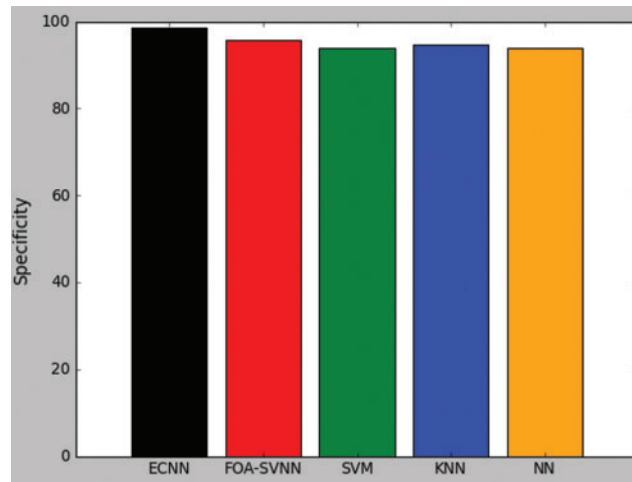


Figure 8: Demonstrate the performance of the proposed ECNN with existing detection methods in terms of specificity

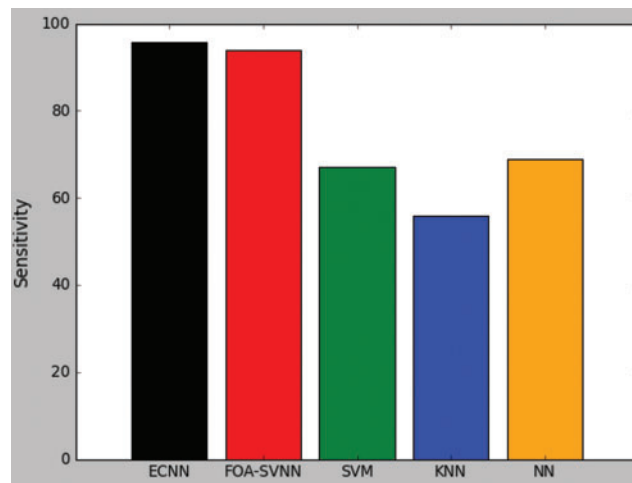


Figure 9: Sensitivity comparison graph for the proposed ECNN technique with existing techniques

Fig. 9 compared the performance of the ECNN with the existing forgery detection techniques based on the sensitivity metric. ECNN achieves 95.67 sensitivity, existing FOA-SVNN obtain 94 sensitivity, SVM has 67.01, KNN achieves 55.88, and the NN has 68.97. It exhibits that the ECNN system has offered better performance when weighted against the existent methods.

Tab. 3 shows the F-score value of proposed ECNN with the existing FOA-SVNN, SVM, KNN, and NN.

Table 3: Demonstrate the F-score of the proposed ECNN with the existing FOA-SVNN, SVM, KNN and NN

Performance metrics	ECNN	FOA-SVNN	SVM	KNN	NN
F-Score	97.09349946	94.90617921	78.24284206	70.27777615	79.56286433

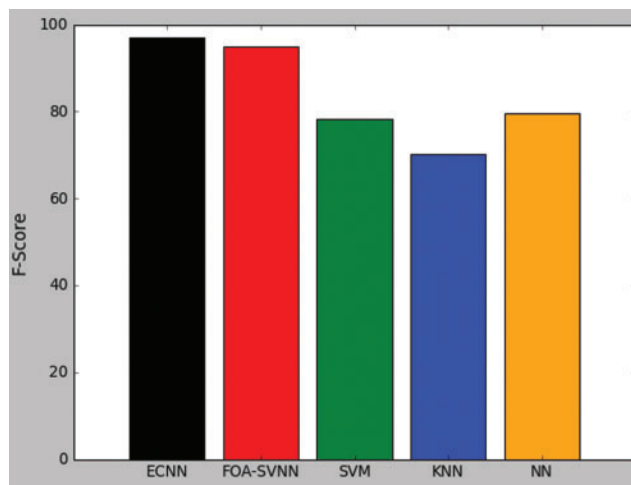


Figure 10: F-score comparison graph for the proposed ECNN technique with existing techniques

F Score is the weighted normal of sensitivity and specificity. Like this, this score considers both bogus positives and false negatives. Naturally, it is not as straightforward as exactness. However, F is generally more valuable than precision, particularly on the off chance that you have a lopsided class circulation. From Fig. 10, we can understand that ECNN provides a better F score than the Existing method.

5 Conclusion

Nowadays, many multimedia tools and applications are available that utilized to edit or temper medical files. Most of current detection methods are not performed well in the accuracy level. Here, the forgery detection image frames of the videos are done using ECNN proves the performance. The input video is transmuted into frames, next the frames are pre-sampled. Then, perform the preprocessing process for ameliorating the image frames. After that, select the features from the pre-processed images. Then, select the necessary features as of the extorted features using the ICSA algorithm, in the final stage, the image is classified centered on the preferred features using ECNN. The proposed classification technique's performance is weighed against that of the existent techniques. The proposed ECNN performance is compared with the existent FOA-SVNN, SVM, KNN, as well as NN in terms of sensitivity, accuracy, and also specificity. The Experimental outcomes exhibited that the proposed ECNN classifies the objects more accurately than the existent methods. The proposed method has achieved high F-Score of 97.09 compare to

other existing work. In the future, this proposed work can extend by using different optimization techniques to achieve more accuracy.

Funding Statement: This work does not receive any funding or financial support from any agencies.

Conflicts of Interest: Authors declare that there is no conflict of interest.

References

1. Birajdar, G. K., Mankar, V. H. (2013). Digital image forgery detection using passive techniques: a survey. *Digital Investigation*, 10(3), 226–245. DOI 10.1016/j.diin.2013.04.007.
2. Snigdha Mankar, K., AjayGurjar, A. (2015). Image forgery types and their detection: a review. *International Journal of Advanced Research in Computer Science and Software Engineering*, 5(4), 60–68.
3. Abdalla, Y. E., Iqbal, M. T., Shehata, M. (2018). Fusion approaches system of copy-move forgery detection. *American Journal of Computer Science and Engineering Survey*, 6(1), 1–12.
4. Kaur, A., Vats, I. (2017). Authentication based image forgery detection using optimized features in JPEG images. *International Journal of Advanced Research in Computer Science*, 8(7), 616–621. DOI 10.26483/ijarcs.v8i7.4316.
5. Sharma, V., Jha, S., Bharti, R. K. (2016). Image forgery and its detection technique: a review. *International Research Journal of Engineering and Technology*, 3(3), 756–762.
6. Zhang, Y., Zhao, C., Pi, Y., Li, S. (2012). Revealing image splicing forgery using local binary patterns of DCT coefficients. *Communications, Signal Processing and Systems*, USA, 181–189.
7. Lad, M., Patel, N. (2016). Passive digital image forgery detection techniques and implementation. *International Journal of Innovative Research in Electrical, Electronics, Instrumentation and Control Engineering*, 4(5), 417–424.
8. Bianchi, T., Piva, A. (2012). Image forgery localization via block-grained analysis of JPEG artifacts. *IEEE Transactions on Information Forensics and Security*, 7(3), 1003–1017. DOI 10.1109/TIFS.2012.2187516.
9. Kang, X., Stamm, M. C., Peng, A., Liu, K. J. R. (2013). Robust median filtering forensics using an autoregressive model. *IEEE Transactions on Information Forensics and Security*, 8(9), 1456–1468. DOI 10.1109/TIFS.2013.2273394.
10. Muhammad, G., Al-Hammadi, M. H., Hussain, M., Bebis, G. (2014). Image forgery detection using steerable pyramid transform and local binary pattern. *Machine Vision and Applications*, 25(4), 985–995. DOI 10.1007/s00138-013-0547-4.
11. Li, J., Li, X., Yang, B., Sun, X. (2014). Segmentation-based image copy-move forgery detection scheme. *IEEE Transactions on Information Forensics and Security*, 10(3), 507–518.
12. Prakash, C. S., Kumar, A., Maheshkar, S., Maheshkar, V. (2018). An integrated method of copy-move and splicing for image forgery detection. *Multimedia Tools and Applications*, 77(20), 26939–26963.
13. Hu, W. C., Chen, W. H., Huang, D. Y., Yang, C. Y. (2016). Effective image forgery detection of tampered foreground or background image based on image watermarking and alpha mattes. *Multimedia Tools and Applications*, 75(6), 3495–3516. DOI 10.1007/s11042-015-2449-0.
14. Bhartiya, G., Jalal, A. S. (2017). Forgery detection using feature-clustering in recompressed JPEG images. *Multimedia Tools and Applications*, 76(20), 20799–20814. DOI 10.1007/s11042-016-3964-3.
15. Mahmood, T., Mehmood, Z., Shah, M., Saba, T. (2018). A robust technique for copy-move forgery detection and localization in digital images via stationary wavelet and discrete cosine transform. *Journal of Visual Communication and Image Representation*, 53, 202–214. DOI 10.1016/j.jvcir.2018.03.015.
16. Elsharkawy, Z. F., Abdelwahab, S. A. S., Abd El-Samie, F. E., Dessouky, M., Elaraby, S. (2019). New and efficient blind detection algorithm for digital image forgery using homomorphic image processing. *Multimedia Tools and Applications*, 78(15), 21585–21611. DOI 10.1007/s11042-019-7206-3.

17. Oommen, R. S., Jayamohan, M., Sruthy, S. (2016). Using fractal dimension and singular values for image forgery detection and localization. *Procedia Technology*, 24, 1452–1459. DOI 10.1016/j.protcy.2016.05.176.
18. Youseph, S., Cherian, R. R. (2015). Pixel and edge based illuminant color estimation for image forgery detection. *Procedia Computer Science*, 46, 1635–1642. DOI 10.1016/j.procs.2015.02.099.
19. Pun, C. M., Yuan, X. C., Bi, X. L. (2015). Image forgery detection using adaptive over segmentation and feature point matching. *IEEE Transactions on Information Forensics and Security*, 10(8), 1705–1716. DOI 10.1109/TIFS.2015.2423261.
20. Zhong, J., Gan, Y., Young, J., Huang, L., Lin, P. (2017). A new block-based method for copy move forgery detection under image geometric transforms. *Multimedia Tools and Applications*, 76(13), 14887–14903. DOI 10.1007/s11042-016-4201-9.
21. Barani, M. J., Valandar, M. Y., Ayubi, P. (2019). A new digital image tamper detection algorithm based on integer wavelet transform and secured by encrypted authentication sequence with 3D quantum map. *Optik*, 187, 205–222. DOI 10.1016/j.ijleo.2019.04.074.
22. Johnston, P., Elyan, E. (2019). A review of digital video tampering: from simple editing to full synthesis. *Digital Investigation*, 29, 67–81. DOI 10.1016/j.diin.2019.03.006.
23. Hong, J. H., Yang, Y., Oh, B. T. (2019). Detection of frame deletion in HEVC-coded video in the compressed domain. *Digital Investigation*, 30, 23–31. DOI 10.1016/j.diin.2019.06.002.
24. Uliyan, D. M., Sadeghi, S., Jalab, H. A. (2019). Anti-spoofing method for fingerprint recognition using patch based deep learning machine. *Engineering Science and Technology*, 23(2), 264–273.
25. Bi, X., Pun, C. M. (2018). Fast copy-move forgery detection using local bidirectional coherency error refinement. *Pattern Recognition*, 81, 161–175. DOI 10.1016/j.patcog.2018.03.028.
26. Velliangiri, S. (2020). An enhanced multimedia video surveillance security using wavelet encryption framework. *Journal of Mobile Multimedia*, 15(3), 239–254.

Finite element analysis and design of cold-formed steel built-up closed columns with flange and web intermediate stiffeners

August 2020 · *Canadian Journal of Civil Engineering* 47(07):1-13
DOI:10.1139/cjce-2019-0063

Authors:



Aruna Govindan
BMS Institute of Technology and Manage...



Karthika Velayutham
Jay Shriram Group of Institutions



S. Sukumar
Paavai Group of Institutions

[Download citation](#)

[Copy link](#)

[Citations \(5\)](#)

[References \(19\)](#)

Abstract

This paper describes a finite element analysis (FEA) and design of cold-formed steel built-up closed sections with intermediate stiffeners in the flange and web under axial compression. A finite element model (FEM) was developed and validated using the available experimental results. The validated FEM can be used for further parametric study on strength of built-up closed columns. The results obtained from the parametric study are compared with the current direct strength method (DSM) in the North



[Request full-text PDF](#)

To read the full-text of this research, you can request a copy directly from the authors.

ResearchGate

Discover the world's research

- 25+ million members
- 160+ million publication pages

Article [Publisher preview available](#)

Development of novel Bi1-xSmxFeO3 based polymer-ceramic nanocomposite for microwave application

January 2020 · *Journal of Materials Science: Materials in Electronics* 31(1)
DOI:10.1007/s10854-019-02526-z

Authors:



Anlin Golda
Mepco Schlenk Engineering College



Arumugam Marikani
Mepco Schlenk Engineering College



E. John Alex

[Download citation](#)

[Copy link](#)

[Citations \(7\)](#) [References \(32\)](#) [Figures \(13\)](#)

Abstract and Figures

Bismuth ferrite (BiFeO₃) is a widely explored magneto electric ceramic whose properties can be enhanced through doping with a rare earth metal like samarium. Methoxy assisted sol-gel technique was used in the synthesis of pure phase bismuth ferrite and various concentrations of samarium doped bismuth ferrite Bi_{1-x}Sm_xFeO₃ where x = 0.05 and x = 0.1 (Bi_{0.95}Sm_{0.05}FeO₃, Bi_{0.9}Sm_{0.1}FeO₃) nanoparticles. The synthesized nanoparticles were characterized for their structural, morphological, and electrical behavior. The synthesized nanoparticles were used in the making of polymer-ceramic nanocomposite films by homogeneous dispersion of the nanoparticles into the

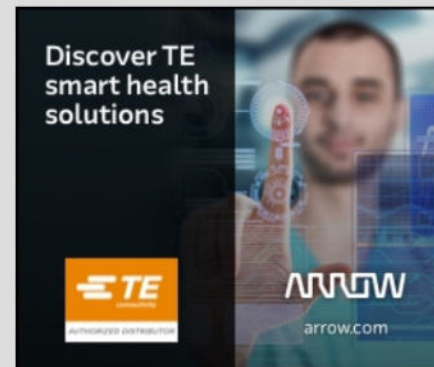


[Read publisher preview](#)

[Request full-text PDF](#)

To read the full-text of this research, you can request a copy directly from the authors.

Advertisement



ResearchGate

Discover the world's research

- 25+ million members
- 160+ million publication pages
- 2.3+ billion citations





Recent Advances in Computer Science and Communications

Editor-in-Chief >>

ISSN (Print): 2666-2558
ISSN (Online): 2666-2566

Back Journal Subscribe

Research Article

Combinatorial Double Auction Based Meta-scheduler for Medical Image Analysis Application in Grid Environment

Author(s): Karthikeyan Periyasami*, Arul Xavier Viswanathan Mariammal, Iwin Thanakumar Joseph and Velliangiri Sarveshwaran

Volume 13, Issue 5, 2020

Page: [999 - 1007]

Pages: 9

DOI: [10.2174/2213275911666190320161934](https://doi.org/10.2174/2213275911666190320161934)

Price: \$65



Become An Editorial Board Member Register Here

Become a Reviewer Register Here

Call for Editors Register Here

Abstract

Background: Medical image analysis application has complex resource requirement. Scheduling Medical image analysis application is the complex task to the grid resources. It is necessary to develop a new model to improve the breast cancer screening process. Proposed novel Meta scheduler algorithm allocate the image analyse applications to the local schedulers and local scheduler submit the job to the grid node which analyses the medical image and generates the result sent back to Meta scheduler. Meta schedulers are distinct from the local scheduler. Meta scheduler and local scheduler have the aim at resource allocation and management.

Article Metrics PDF 3

	2	Total citations
	0	Recent citations
	1.05	Field Citation Ratio
	n/a	Relative Citation Ratio

Crystal structure of Samarium based orthoferrites for Solid Oxide Fuel Cells

Padigela Srinivas Reddy, Prashanth Kumar Vaidya, Suresh Sripada

[PDF](#)

Abstract

Synthesis and crystal structure of $\text{Sm}_{1-x}\text{Sr}_x\text{FeO}_3$ materials are studied. Single phase perovskite-based rare earth orthoferrites are synthesized using sol-gel method. The samples are formed in Single-phase solid solution of orthorhombic perovskite composition. Structural aspects of the distorted perovskite ABO_3 phase are confirmed by powder XRD. The lattice parameters are resolute at normal room temperature (nearly 30oC) by XRD. Lattice parameters and volume are increased with growing Sr material. The diffraction records exposed no indication for order of Samarium and Strontium at the A site, nor for oxygen situation ordering at O sites for greatly condensed samples.

Issue

[Vol. 63 No. 6 \(2020\)](#)

Section

Articles



0.3 2019 CiteScore

9th percentile

Powered by Scopus

[Make a Submission](#)

Downloads

[Copyright Transfer Form](#)

[Paper Template](#)

Important Links

[Home](#)

[Aims and Scope](#)

[Paper Topics](#)

[Call for Papers](#)

[Instructions for Authors](#)

[Archive](#)

[Download](#)

[Ethics & Policies](#)

[Publication Ethics and Publication](#)

Image Creator from Designer

Microstructure of Ca doped Neodymium based perovskites for SOFC

N.Maramu, Padigela Srinivas Reddy, N.Arundhathi, Y.S. Reddy, Prashanth Kumar Vaidya

Abstract

The materials $Nd_{1-x}Ca_xCoO_3$ ($0 \leq x \leq 0.4$) are prepared using sol-gel technique. These compounds are formed clearly in the temperature ranges of 600-7000C. The powders are pelletized in different shapes and finally sintered at 12000C for 4 hours. The microstructure of samples is studied using Scanning Electron Microscopy (SEM). SEM measurements show that the porosity is 3-15% and materials are closely packed with small voids

PDF

Issue

[Vol. 63 No. 6 \(2020\)](#)

Section

Articles



0.3 2019 CiteScore

9th percentile

Powered by Scopus

Make a Submission

Downloads

[Copyright Transfer Form](#)

[Paper Template](#)

Important Links

[Home](#)

[Aims and Scope](#)

[Paper Topics](#)

[Call for Papers](#)

[Instructions for Authors](#)

[Archive](#)

[Download](#)

[Ethics & Policies](#)

[Publication Ethics and Publication](#)

^{57}Fe Mossbauer and electrical studies of Mn doped YFeO_3 prepared via sol-gel technique

G Padmasree¹, S Shravan Kumar Reddy², J Ramesh³, P Yadagiri Reddy⁴ and Ch Gopal Reddy⁴ 

Published 27 November 2020 • © 2020 The Author(s). Published by IOP Publishing Ltd

[Materials Research Express](#), Volume 7, Number 11

Citation G Padmasree *et al* 2020 *Mater. Res. Express* 7 116103

DOI [10.1088/2053-1591/abcc2c](https://doi.org/10.1088/2053-1591/abcc2c)



Figures ▾ References ▾

[+ Article and author information](#)

Abstract

Polycrystalline $\text{YFe}_{1-x}\text{Mn}_x\text{O}_3$ ($x = 0, 0.1, 0.2, 0.3, 0.4$ and 0.5) samples are prepared via sol-gel method. Structural characterization of these samples is done by x-ray diffraction (XRD) technique and Raman spectroscopic method. Intense peaks in XRD graphs show that the sample is crystalline in nature and Reitveld refined XRD data shows that the samples are formed in single phase. Raman spectroscopic study confirms the structure and phase purity of the samples. Room temperature ^{57}Fe Mossbauer studies confirm that Fe ion exists in ferric state. The hyperfine field (B_{hf}) values are found to decrease with increase in manganese (Mn) concentration. This decrease in B_{hf} value indicates the increase in antiferromagnetic nature of the samples, which arises due to the weakening of magnetic interactions between the Fe ions. From room temperature leakage current density (J-E) measurements, it is

This site uses cookies. By continuing to use this site you agree to our use of cookies. To find out more, see our [Privacy and Cookies](#) policy.

682 Total downloads



Submit

[Submit to this Journal](#)

MathJax

[Turn on MathJax](#)

Share this article



Abstract

- [1. Introduction](#)
- [2. Experimental](#)
- [3. Results and discussion](#)
- [4. Conclusions](#)

[Acknowledgments](#)

[References](#)

[↑ Back to top](#)

You may also like

JOURNAL ARTICLES

Local electronic and magnetic properties of pure and Mn-containing magnetocaloric $\text{LaFe}_{13-x}\text{Si}_x$ compounds inferred from Mössbauer spectroscopy and magnetometry

The effect of hybridization on local magnetic interactions at highly diluted Ce ions in tetragonal intermetallic compounds RERh_2Si_2 (RE=Ce, Pr, Nd, Gd, Tb, Dy)

A TDPAC study of static and dynamic magnetic behaviour

Oxidation states and the quality of lower interfaces in magnetic tunnel junctions: oxygen effect on crystallization of interfaces

Mössbauer spectroscopic study of spin reorientation in Mn-substituted yttrium orthoferrite

Interplay of 4f-3d magnetism and ferroelectricity in DyFeO_3

PDF

Help

An Enhanced Multimedia Video Surveillance Security Using Wavelet Encryption Framework

May 2020 · *Journal of Mobile Multimedia* 15(3):239-254


DOI:10.13052/jmm1550-4646.1534

Authors:



Velliangiri Sarveshwaran

SRM Institute of Science and Technology



Download full-text PDF

Read full-text

Download citation

Copy link

Citations (5) References (19) Figures (3)

Abstract and Figures

Multimedia digital data include medical record and financial documents, which are not guaranteed with security. The concerns for security of multi-media digital data is been a widespread issue in the field of cybernetics. With increasing malwares in video payloads, the proposed study aims to reduce the embedding of malwares using Pseudo Arbitrary Permutation based Cellular Automata Encryption (PAP-CAE) System in video payloads. This method reduces the malware attacks and distortion rate by permuting the secret keys with Pseudo arbitrary permutation. Before the application of PAP-CAE, 2D wavelet transform is applied on the multimedia files that compresses the complex files into different scales and position to be transmitted via a network with reduced size. Simultaneously, it performs the process of decryption and decompression to retrieve the original files. The proposed method is evaluated against existing methods to test its efficacy in terms of detection accuracy, detection time of malwares and false positive rate. The result shows that the proposed method is effective against the detection of malwares in multimedia video files.

ResearchGate

Discover the world's research

- 25+ million members
- 160+ million publication pages
- 2.3+ billion citations

Join for free

Advertisement

Ads by Google

Send feedback Why this ad? ⓘ

Document details - Investigation of deep learning methodologies in intelligent green transportation system

1 of 1

Export Download More... >

Journal of Green Engineering

Volume 10, Issue 3, March 2020, Pages 931-950

Investigation of deep learning methodologies in intelligent green transportation system(Article)

Joseph, S.I.T., Velliangiri, S., Devadass, C.S.C. 🔍

^aDepartment of Computer Science and Engineering, Karunya Institute of Technology and Sciences, Coimbatore, Tamilnadu, India

^bDepartment of Computer Science and Engineering, CMR Institute of Technology, Hyderabad, India

^cDepartment of Civil Engineering, Samskruti College of Engineering and Technology, Hyderabad, India

Abstract

Due to the advancement of technologies in the past few years, huge amount of data especially in the transportation domain received through devices such as road sensors, CCTV, probes, GPS etc. It is quite challenge to build a consistent and robust prediction models using traditional machine learning models in these complicated scenarios. On demand information about traffic is highly essential for the intelligent green transportation system. Now a day's deep learning shows promising significance in every aspect of research as well as industrial applications. This research article reviews the various deep learning methodologies in intelligent green transportation system by means of automatic vehicle detection, traffic flow forecasting, transportation network representation, prediction etc. © 2020 Alpha Publishers.

Cited by 4 documents

Jose, V.S. , Sandhya, H. , Varghese, B.

Artificial intelligence towards smart green transportation: A path towards sustainability

(2023) *Achieving Economic Growth and Welfare Through Green Consumerism*

Li, Y. , Niu, W. , Tian, Y.

Multiagent Reinforcement Learning-Based Signal Planning for Resisting Congestion Attack in Green Transportation

(2022) *IEEE Transactions on Green Communications and Networking*

Srivastava, T. , Virk, S. , Ganguli, S.

An overview of the intelligent green technologies for sustainable smart cities

(2022) *Intelligent Green Technologies for Sustainable Smart Cities*

Sustainable Effects of Crimped White Polypropylene Fibre with Fly Ash and SBR Latex to Act as Green Building Materials in Modified Concrete

February 2020 · *Journal of Green Engineering* 10(2):327-341

Authors:



Sounthararajaan V.M Dr.



Sivasankar Sandrasekaran
Sree Buddha College of Engineering Pat...



A Rajarajeswari



L Ponraj Sankar

Download citation

Copy link

Citations (2)

References (14)

Figures (7)

Abstract and Figures

This paper deals with the sustainable effect of styrene-butadiene rubber (SBR) latex with crimped PP (polypropylene) fibre 0.1% and 0.3% (aspect ratio-80) used for high-performance concrete (HPC) on mechanical behaviour. However, the constant dosage percentage of SBR latex (7%) of polymer mixes proportion with w/c-0.3. The laboratory test has performed the crushing and flexural rigidity of polymer-modified (PM) concrete exhibit HS (higher strength) than compared to control concrete (CC). Also, SBR latex without fibre concrete exhibits an improved crushing strength of 16.31% than that of



Download full-text PDF

Read full-text

ResearchGate

Discover the world's research

- 25+ million members
- 160+ million publication pages
- 2.3+ billion citations

Advertisement

Khazana Jewelry

Khazana Jewellery

Open

Document details - An Efficient Optimal Neural Network-Based Moving Vehicle Detection in Traffic Video Surveillance System


1 of 1

Export Download More... >

Circuits, Systems, and Signal Processing

Volume 39, Issue 2, 1 February 2020, Pages 734-756

An Efficient Optimal Neural Network-Based Moving Vehicle Detection in Traffic Video Surveillance System(Article)

Appathurai, A., Sundarasekar, R., Raja, C., Alex, E.J., Palagan, C.A., Nithya, A. 

^aInfant Jesus College of Engineering, Tuticorin, Tamil Nadu, India

^bAnna University, Chennai, Tamil Nadu, India

^cKoneru Lakshmaiah Education Foundation, Vaddeswaram, AP, India

[View additional affiliations](#) 

Abstract

This paper presents an effective traffic video surveillance system for detecting moving vehicles in traffic scenes. Moving vehicle identification process on streets is utilized for vehicle tracking, counts, normal speed of every individual vehicle, movement examination, and vehicle classifying targets and might be executed under various situations. In this paper, we develop a novel hybridization of artificial neural network (ANN) and oppositional gravitational search optimization algorithm (ANN-OGSA)-based moving vehicle detection (MVD) system. The proposed system consists of two main

Cited by 45 documents

Saikrishnan, V. , Karthikeyan, M.

Mayfly Optimization with Deep Learning-based Robust Object Detection and Classification on Surveillance Videos

(2023) Engineering, Technology and Applied Science Research

Mohammaed, A.H. , Mahmood, Z.S. , Nasret, A.N.

A New Method to Road Traffic Monitoring Using Artificial Systems

(2023) AIP Conference Proceedings

Luo, K. , Kong, X. , Zhang, J.

Computer Vision-Based Bridge Inspection and Monitoring: A Review

(2023) Sensors

[View details of all 45 citations](#)

Document details - Characterisation on toughness property of self-compacting fibre reinforced concrete

1 of 1

Export Download More...>

Journal of Environmental Protection and Ecology

Volume 21, Issue 6, 2020, Pages 2153-2163

Characterisation on toughness property of self-compacting fibre reinforced concrete(Article)

Gopalakrishnan, R., Mohan, A., Ponrajsankar, L., Vijayan, D.S.

^aDepartment of Civil Engineering, SRM Easwari Engineering College, Chennai, India

^bCivil Engineering Department, CMR Institute of Technology, Hyderabad, India

^cCivil Engineering Department, Aarupadai Veedu Institute of Technology, Vinayaka Missions Research Foundation (VMRF), TN, India

Abstract

This study deals with the toughness property of the fibre reinforced self-compacting concrete (FRSCC) and mechanical properties of polypropylene fibre reinforced self-compacting concrete through experimental studies. To achieve the objectives the laboratory testing has been performed with different percentage of steel fibres (1.5, 2.0, 2.5, and 3%) are added with additional 1.0 to 2.0% of polypropylene by weight of cementitious material. With the addition of different types of fibres, the toughness increases with change of increase in percentage of fibres up to 2.5%. But beyond 1.5% addition of fibre types resulted in lower toughness for the steel fibres. And observed that, the limitation for steel fibre in self-compacting concrete changes the toughness up to 2.5% of volume of concrete. Finally, this research gives comparative study for characteristic properties of polypropylene

Cited by 42 documents

Mohan, A., Dinesh Kumar, R., Satchidanandam, J.

Simulation for Modified Bitumen Incorporated with Crumb Rubber Waste for Flexible Pavement

(2023) *International Journal of Intelligent Systems and Applications in Engineering*

Prabha, G., Mohan, A., Kumar, R.D.

Computational Analogies of Polyvinyl Alcohol Fibres Processed Intelligent Systems with Ferrocement Slabs

(2023) *International Journal of Intelligent Systems and Applications in Engineering*

Mohan, A., Sudhan, K.

Computational Technologies in Geopolymer Concrete by Partial Replacement of C&D Waste

Document details - Dynamic crushing and energy absorption performance of newly designed multitubular structures

1 of 1

Export Download More... >

Materials Today: Proceedings

Volume 27, Issue 2, 2020, Pages 1928-1933

1st International Conference on Advanced Light-Weight Materials and Structures, ICALMS 2020; Hyderabad; India; 6 March 2020 through 7 March 2020; Code 161490

Dynamic crushing and energy absorption performance of newly designed multitubular structures(Conference Paper)

Nagarjun, J., Praveen Kumar, A., Yamini Reddy, K., Ponraj Sankar, L. 

^aDepartment of Mechanical Engineering, CMR Technical Campus, Hyderabad, India

^bDepartment of Civil Engineering, CMR Institute of Technology, Hyderabad, India

Abstract

Thin-walled shells like square, conical and polygonal sections are preferred in structural applications requiring high performance under impact loadings for their less weight, and excellent energy dissipating ability. In the current research article, Finite element simulations on the buckling behaviour and crashworthiness performance indicators of multitubular structures were executed. The axial impact crushing behaviour of the proposed multitubular tubes was compared with the traditional simple geometrical tubes and the outcomes revealed that multitubular structures

Cited by 12 documents

Praveen Kumar, A. , Vetrivel Sezhian, M.
Influence of curvy stiffeners on the axial crushing response of 3D-printed polymer composite cylindrical tubular structures

(2023) *Proceedings of the Institution of Mechanical Engineers, Part L: Journal of Materials: Design and Applications*

Tian, L. , Zhou, Y. , Sun, Y.
Energy absorption performance of multicellular thin-walled energy-absorbing components of anti-shock support columns | 防冲支架立柱多胞薄壁吸能构件能量吸收性能

(2023) *Meitan Xuebao/Journal of the China Coal Society*

Zhu, T. , Jiang, G.
Investigation of the Effect of Cross-Section Structure of Thin-Walled Aluminium Tubes

Document details - A monotonic optimization approach for solving strictly quasiconvex multiobjective programming problems


1 of 1

Export Download More... >

Journal of Intelligent and Fuzzy Systems

Volume 38, Issue 5, 2020, Pages 6053-6063

A monotonic optimization approach for solving strictly quasiconvex multiobjective programming problems(Conference Paper)([Open Access](#))

Thang, T.N., Solanki, V.K., Dao, T.A., Thi Ngoc Anh, N., Van Hai, P. 

^aSchool of Applied Mathematics and Informatics, Hanoi University of Science and Technology, Hanoi, Viet Nam

^bDepartment of Computer Science and Engineering, CMR Institute of Technology, Hyderabad, TS, India

^cDepartment of Information Technology, Uppsala University, Uppsala, Sweden

[View additional affiliations](#) ▾

Abstract

In this article, we use a monotonic optimization approach to propose an outcome-space outer approximation by copolyblocks for solving strictly quasiconvex multiobjective programming problems which include many classes of captivating problems, for example when the criterion functions are nonlinear fractional. After the algorithm is terminated, with any given tolerance, an approximation of the weakly efficient solution set is obtained containing the whole weakly efficient solution set of the problem. The algorithm is proved to be convergent and it is suitable to be implemented in

Cited by 6 documents

Tuan, T.A. , Hoang, L.P. , Le, D.D.

A framework for controllable Pareto front learning with completed scalarization functions and its applications

(2024) *Neural Networks*

Hoang, L.P. , Le, D.D. , Tuan, T.A.

Improving Pareto Front Learning via Multi-Sample Hypernetworks

(2023) *Proceedings of the 37th AAAI Conference on Artificial Intelligence, AAAI 2023*

Thanh, B.T. , Van Tuan, D. , Chi, T.A.

Multiobjective Logistics Optimization for Automated ATM Cash Replenishment Process

(2023) *Lecture Notes on Data Engineering and Communications Technologies*

Document details - Using MLPA for smart mushroom farm monitoring system based on IoT

1 of 1

Export Download More... >

International Journal of Networking and Virtual Organisations

Volume 22, Issue 4, 2020, Pages 334-346

Using MLPA for smart mushroom farm monitoring system based on IoT(Article)

Velliangiri, S., Sekar, R., Anbhazhagan, P.

^aDepartment of Computer Science and Engineering, CMR Institute of Technology, Hyderabad, Telangana, 501401, India

^bDepartment of ECE, Koneru Lakshmaiah Education Foundation, Vijayawada, Andhra Pradesh, India

^cDepartment of Information Technology, Gayatri Vidya Parishad College of Engineering (A), Visakhapatnam, Andhra Pradesh, 530048, India

Abstract

Mushroom has turned out to be a standout amongst the most fundamental consumable items in our everyday life. To increase mushroom production and to reduce manual work smart mushroom monitoring has been proposed with the assistance of internet of things (IoT) and machine learning (ML) algorithms called machine learning with prediction analysis (MLPA) technique. In this proposed MLPA technique, sensors mounted in the mushroom farm collect moisture, temperature and humidity data from soil and air, which is used to predict disease for mushroom from past history data. Based on the sensor value and prediction by ML algorithm, the farmer can predict weekly irrigation plan. The sensors are connected to IoT device which sends collected data for analysis using ML algorithms. Three main tasks of ML algorithms are regression, classification and

Cited by 14 documents

Ahlawat, C. , Krishnamurthi, R.

Towards smart technologies with integration of the internet of things, cloud computing, and fog computing

(2023) *International Journal of Networking and Virtual Organisations*

Guo, J.

Evaluation and analysis of classroom teaching quality of art design specialty based on DBT-SVM

(2023) *International Journal of Networking and Virtual Organisations*

Dipali, D. , Subramanian, T. , Kumaran, G.S.

A smart oyster mushroom cultivation using automatic fuzzy logic controller

(2023) *Journal of Discrete Mathematical*

Document details - Compact multiband printed antenna design and analysis

1 of 1

Export Download More... >

International Journal of Control and Automation
Volume 13, Issue 3, 2020, Pages 58-63

Compact multiband printed antenna design and analysis(Article)

Praveen Kumar, K., Amulya, B., Venkateshwar Rao, B.

^aDept. of ECE, CMR Institute of Technology, Hyderabad, Telangana, India
^bDept. of ECE, CMR College of Engineering & Technology, Hyderabad, Telangana, India

Abstract

Current article, presents the elliptical slot antenna design procedure for multiband applications. The suggested antenna covers L-band, WIMAX, WLAN and X band. By placing inverted T-shaped stub and three reverse U-shape stubs, the resonating characteristics of the antenna are observed. The resonating frequencies are 1.95, 4.14, 5.05, 5.89 and 9.15 GHz respectively. Proposed structure depicting better return loss ($S_{11} < -10\text{dB}$) with compact size. Peak gain of 3.35 dB, antenna efficiency of 82% was achieved at all operating bands. Omni-directional radiation pattern along H-plane and bi-directional radiation pattern along E-plane are achieved. © 2020 SERSC.

Author keywords

- Microstrip Antenna
- Multi band
- T-slot
- U-slot

Cited by 0 documents

Inform me when this document is cited in Scopus:
Set citation alert > Set citation feed >

Related documents
Find more related documents in Scopus based on:
Authors > Keywords >

Document details - Machine learning approaches for healthcare data analysis

1 of 1

Export Download More... >

Journal of Critical Reviews

Volume 7, Issue 4, 2020, Pages 806-811

Machine learning approaches for healthcare data analysis(Review)

Eedi, H., Kolla, M.

^aJNTUH College of Engineering Hyderabad, Department of CSE, Hyderabad, India

^bCMR Institute of Technology, Department of CSE, Hyderabad, India

Abstract

Breast cancer is the most common cancer in women worldwide and it remains the most common cause of cancer-related death in woman globally. Machine Learning techniques have been proven to be of great help in prognosis and diagnosis of various health related issues. This work constitutes a comparison of five machine learning (ML) algorithms: Logistic Regression (LR), K-Nearest Neighbor (KNN), Naive-Bayes (NB), Decision Tree (DT), Random Forest (RF) on the Breast Cancer Wisconsin Diagnostic (BCWD) dataset. Features were extracted from the digitized images of FNA tests on a breast mass. Results show that Random Forests performs better among all the models across different classification metrics such as accuracy, precision, recall, and f1-score. © 2019 by Advance Scientific Research.

Author keywords

Breast cancer Decision Tree K-Nearest Neighbor Logistic Regression Machine Learning Naive-Bayes Random Forest

Cited by 4 documents

Tembely, M. , Vadillo, D.C. , Dolatabadi, A.

A Machine Learning Approach for Predicting the Maximum Spreading Factor of Droplets upon Impact on Surfaces with Various Wettabilities

(2022) *Processes*

Rahman, L.A. , Marikannan Booma, P.

The Early Detection of Autism Within Children Through Facial Recognition; A Deep Transfer Learning Approach

(2022) *2nd IEEE International Conference on New Technologies of Information and Communication, NTIC 2022 - Proceeding*

Javaid, M. , Haleem, A. , Pratap Singh, R.

Significance of machine learning in healthcare: Features, pillars and applications

(2022) *International Journal of Intelligent Networks*

View details of all 4 citations

Document details - Development of novel $\text{Bi}_{1-x}\text{Sm}_x\text{FeO}_3$ based polymer-ceramic nanocomposite for microwave application

1 of 1

Export Download More... >

Journal of Materials Science: Materials in Electronics

Volume 31, Issue 1, 1 January 2020, Pages 324-336

Development of novel $\text{Bi}_{1-x}\text{Sm}_x\text{FeO}_3$ based polymer-ceramic nanocomposite for microwave application(Article)

Golda, R.A., Marikani, A., Alex, E.J. 

^aDepartment of Electronics and Communication Engineering, JACSI College of Engineering, Nazareth, Tamil Nadu, India

^bDepartment of Physics, Mepco Schlenk Engineering College, Sivakasi, Tamil Nadu, India

^cDepartment of Electronics and Communication Engineering, CMR Institute of Technology, Hyderabad, Telangana, India

Abstract

Bismuth ferrite (BiFeO_3) is a widely explored magneto electric ceramic whose properties can be enhanced through doping with a rare earth metal like samarium. Methoxy assisted sol-gel technique was used in the synthesis of pure phase bismuth ferrite and various concentrations of samarium doped bismuth ferrite $\text{Bi}_{1-x}\text{Sm}_x\text{FeO}_3$ where $x = 0.05$ and $x = 0.1$ ($\text{Bi}_{0.95}\text{Sm}_{0.05}\text{FeO}_3$, $\text{Bi}_{0.9}\text{Sm}_{0.1}\text{FeO}_3$) nanoparticles. The synthesized nanoparticles were

Cited by 7 documents

Ikhsan, F.H. , Yee, S.K. , Esa, F.

Magneto-dielectric properties of $\text{Ni}_{0.25}\text{Cu}$... and its application as substrate of microstrip patch antennas

(2023) *Journal of Materials Science: Materials in Electronics*

Othman, M. , Mallek-Zouari, I. , Akrou, H.

Synthesis and properties of ultra-small BiFeO_3 nanoparticles doped with cobalt

(2023) *Ceramics International*

Ullah, F. , Mir, F.A.

Dielectric and Magnetic Studies of LaFeO_3 -Polyvinyl Alcohol Composite Films and Their Subsequent Use in Microwave Antennas

Document details - Integrating employee value model with churn prediction


1 of 1

Export Download More... >

International Journal of Sensors, Wireless Communications and Control

Volume 10, Issue 4, 2020, Pages 484-493


Integrating employee value model with churn prediction(Article)

Anh, N.T.N., Tu, N.D., Solanki, V.K., Giang, N.L., Thu, V.H., Son, L.N., Loc, N.D., Nam, V.T. 

^aApplied Mathematics Department, School of Applied Mathematics and Informatics, Hanoi University of Science and Technology, Hanoi, Viet Nam

^bMathematics for Informatics Department, School of Applied Mathematics and Informatics, Hanoi University of Science and Technology, Hanoi, Viet Nam

^cCommunication and Computer Networks Department, School of Information and Communication Technology, Hanoi University of Science and Technology, Hanoi, Viet Nam

[View additional affiliations](#) 

Abstract

Background: In recent years, human resource management is a crucial role in every companies or organization's operation. Loyalty employee or Churn employee influence the operation of the organization. The impact of Churn employees is difference because of their role in organization.

Objective: Thus, we define two Employee Value Models (EVMs) of organizations or companies based on employee features that are popular of almost companies. **Methods:** Meanwhile, with the development of Artificial intelligent, machine learning is possible to give predict data-based models having high accuracy. Thus, integrating Churn prediction, EVM and machine learning such as support vector machine, logistic regression, random forest is proposed in this paper. The strong points of each model are used and weak points are reduced to help the companies or organizations avoid

Cited by 5 documents

Mahalakshmi, V. , Chitra, D. , Isravel, Y.A.D.

Healthcare Operational Intellectual Ability in Analysing the Factors Affecting Employee Churn

(2023) *EAI/Springer Innovations in Communication and Computing*

Nosratabadi, S. , Zahed, R.K. , Ponkratov, V.V.

Artificial Intelligence Models and Employee Lifecycle Management: A Systematic Literature Review

(2022) *Organizacija*

Chaudhary, M. , Gaur, L. , Chakrabarti, A.

Comparative Analysis of Entropy Weight Method and C5 Classifier for Predicting Employee Churn

(2022) *Proceedings of 3rd International Conference on Intelligent Engineering and Management, ICIEM 2022*



INTERNATIONAL JOURNAL OF CREATIVE RESEARCH THOUGHTS (IJCRT)

An International Open Access, Peer-reviewed, Refereed Journal

Implications of Knowledge Management on the Financial Performance and Efficiency of Selected Indian companies

*Umamaheswararao Gobbilla

Associate Professor

CMR Institute of Technology
Hyderabad

** Dr. Bhavani Shree A

Associate Professor

Vidyavardhaka College of Engineering
Mysore

Abstract

Knowledge management (KM) came into existence in India at the beginning of 2000 but to date, the extent of KM implementation differs widely across industries. Some companies have successfully implemented knowledge management but there are others that practice KM in bits and pieces. Empirical evidence to some extent supports that KM has a positive impact on operational performance including financial performance. The purpose of this study is to confirm these findings in selected Indian organizations via an awareness study of the employees. The sample for the study is companies listed in Indian stock exchanges with 200 respondents across different sectors and with different levels in the organization. KM practices in these organizations vary from moderate to high. Data for the study was collected between 2019-2020. The findings of the study indicate that most of the organizations which claim that they have implemented KM but are not deriving the results out of it may not be aware of the term "effective KM". Effective KM does not mean 'more the learning the better' or 'the more knowledge the better' rather it means relevant knowledge. The results of the study indicate a proclivity towards better financial performance for companies that are practicing effective KM. This study thus rejects the findings of some previous studies which state that KM does not have an impact on financial performance limitation of the study is that it is focused on a few sectors and based on the perception of the employees.

Key Words: Efficiency, Financial Performance, Knowledge Management, Listed Companies.

1. Introduction to Knowledge management (KM)

The rapid growth of technology has resulted in the formation of a knowledge-based business environment. If one was to think of the way businesses have evolved over the years, they moved from a position where capital was the prime requirement to set up a business, moving on to mass production becoming the criterion for a successful business and later to the business idea or knowledge insight being the center for good business growth (Drucker, 1995). This development happened somewhere in the early nineties where it was realized that knowledge management is not a trend but a necessity and needs to be adopted as a discipline.

2. Review of Literature

The literature on KM indicates that knowledge does cause a change in organizational performance (Tippins and Sohi, 2003; Kalling, 2003; Darroch, 2005; Kridan and Goulding, 2006; Marque's and Simon, 2006; Sigala and Chalkiti, 2007; Bogner and Bansal, 2007; King et al., 2008; Pillania, 2008).

However not all the studies support that the change is a positive one. Kalling (2003) in his study linking KM to the performance observed that the link between KM and performance might not always exist and that the relationship may stop at representations of profit but not profit itself.

Darroch (2005) testing the impact of KM on innovation and firm's performance debated that of all the KM processes, only responsiveness to knowledge had an impact on financial performance.

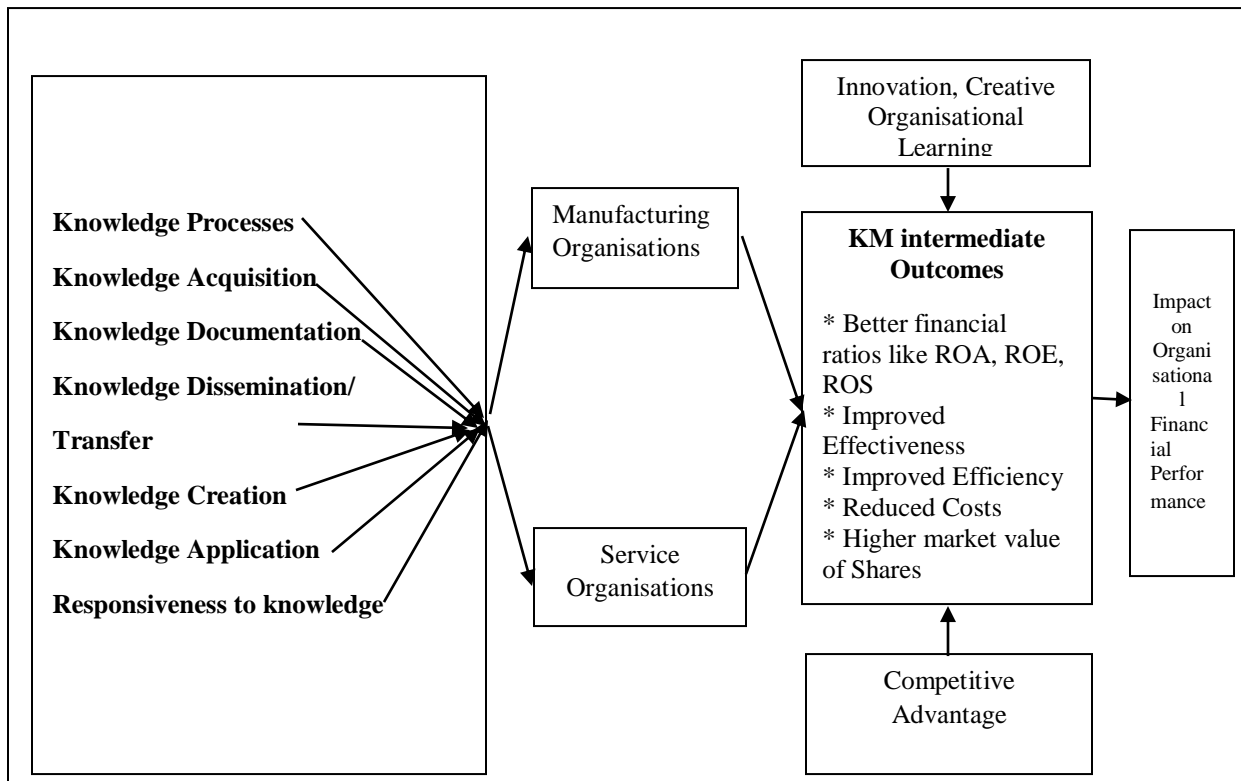
Seleim (2011) in his study KM and OP in Egyptian software firms concludes that only knowledge application influences organization performance.

Marque's & Simon (2006), in their study, observed that The effect of KM on firm performance has suggested that the relationship could exist but it can be tested by conducting a longitudinal study and the results could be clearer. Authors, however, believe that KM has various financial and non-financial benefits which have a bearing on the organizational performance like 'better decision making, flatter teamwork, improved learning, better communication, enhanced employee skills, higher employee satisfaction, enhanced flexibility, better customer relations, better service quality, improved customer satisfaction' (Singh et.al, 2006; Dalkir, 2005; Chase, 1997); increased employee empowerment, employee loyalty, and business continuity, developing core competencies, improved business processes, risk reduction (Anantatmula & Kanungo, 2006; Beijerse,1999); sharing best practices (Davenport, 1998); developing new business opportunities (KPMG, 2000); innovation (Darroch, 2005; Davenport, 1998; Dalkir, 2005); efficient management of intellectual capital (Demarest, 1997); improved labor productivity (Pham & Hara, 2011).

The listing is important for knowing which benefits are directly impacting financial performance and which have an indirect impact. Under financial benefits, KM is known to have resulted in higher sales/profits; increased operational efficiency by cycle time reduction; improved revenues through licensing of patents (Singh et. al, 2006, Anantatmula & Kanungo, 2006; Chase, 1997), reduced costs (Feng et. al, 2004); Higher ROA and ROS (Vidovia, 2010).

Based on the literature review, a model has been developed for the study:

Knowledge Management and Organisational Performance Model



3. Objectives of the Study:

- To identify whether the employees of the organizations are aware of the KM practices which the organization is pursuing.
- To study the perception of the employees about KM and its benefits.
- To relate to the financial performance to assess the tangible benefits of KM.

4. Methodology

Sample Selection

The study is an awareness-based study and stratified random sampling has been used. The sample for the study is companies listed on the National Stock Exchange(S&P Nifty50). The companies were arranged in descending order based on their turnover. S&P Nifty50 companies were selected as samples and were contacted for the survey. Out of 50, 20 companies agreed to respond to the survey giving a response rate of 40%. A structured questionnaire comprising 40 questions was sent to these company employees which included all the levels – senior, middle, and executives. The employees were contacted via email or personal meetings to collect the responses. The completed questionnaire responses were received from Five companies only which were used for the analysis. A total of 200 responses were collected across these companies.

The instrument for the study was an adopted one from a study conducted in Egypt in 2007 but since this study was conducted on the Egyptian software firms, the questionnaire needed modifications to make it suitable for the Indian scenario and covering questions on all kinds of industries. The modified instrument was tested by conducting a pilot study in a banking & finance company at its multiple locations. Based on the pilot study, changes were made in the instrument before it was sent to other companies for their responses. The instrument was tested for reliability which was 0.95 and considered to be very good (Nunally,1967).

Tool for the Study

The research in the discussion is part of the broader study on knowledge management which is being conducted to see if KM has an impact on the financial performance of the companies. This tool was designed to assess the level of KM in the organizations and if it had an impact on financial performance. The study is being conducted in two broad sectors being manufacturing and service. In each of these sectors, different organizations were contacted to participate in the survey. The companies include a wide range of sectors like – banking and finance, Information technology, infrastructure, automobile, steel, telecom, aviation, and pharmaceuticals. The questionnaire is based on a five-point Likert scale from 1 to 5 where 1 denotes complete disagreement and 5 denotes complete agreement to a practice/ condition. There were 40 questions in all focusing on various KM aspects/practices like knowledge acquisition, knowledge documentation, knowledge transfer, knowledge creation, knowledge application, responsiveness to knowledge, and KM related performance. The demographics which are an important part of this study have been discussed in the next section. Data for the study was collected between 2019-2020.

5. Data Analysis and Findings

Demographics of the Study

Five companies were taken for the study with an equal representation of four industries each from both the manufacturing and service sector. The number of respondents was 200 but the number varied from organization to organization. The respondent details are given below in the following figures.

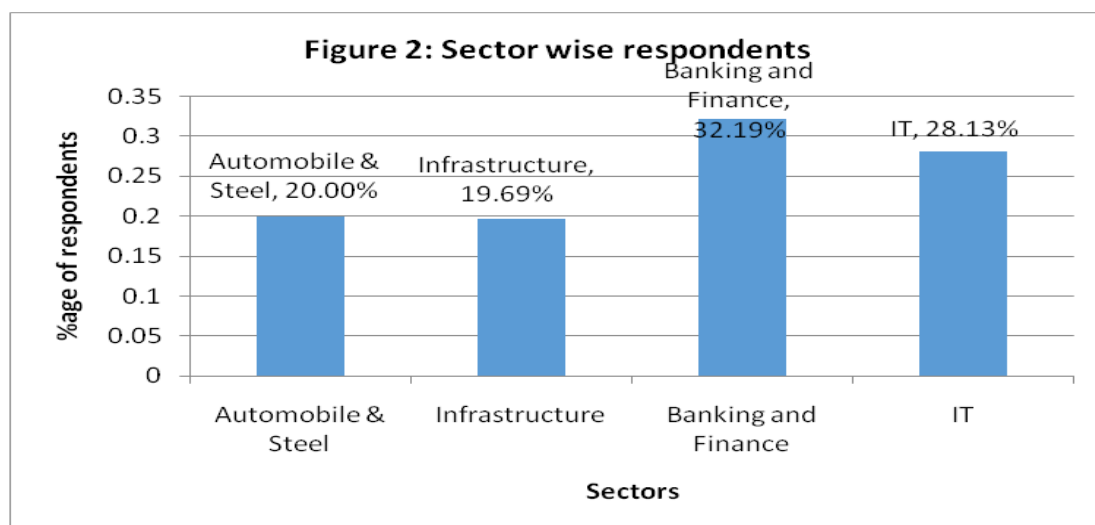


Figure 3: Gender

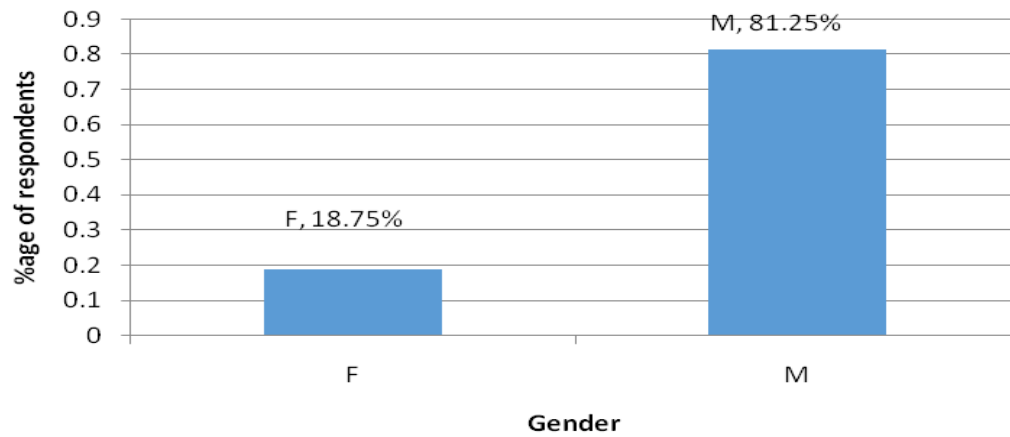


Figure 4: Experience in years

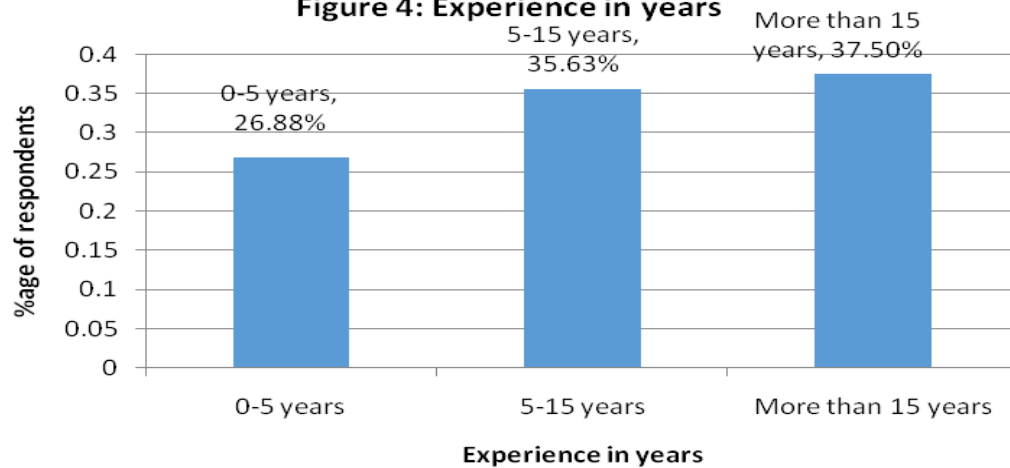


Figure 5: Age

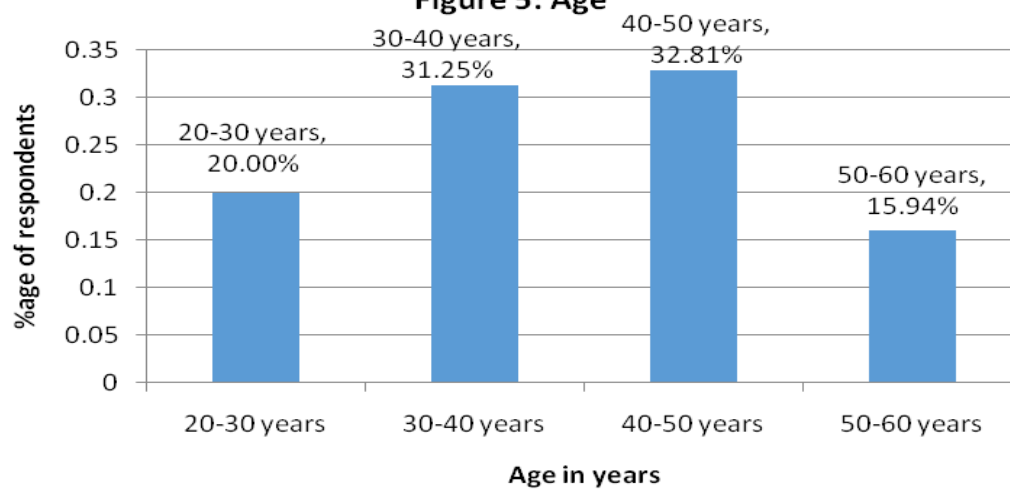
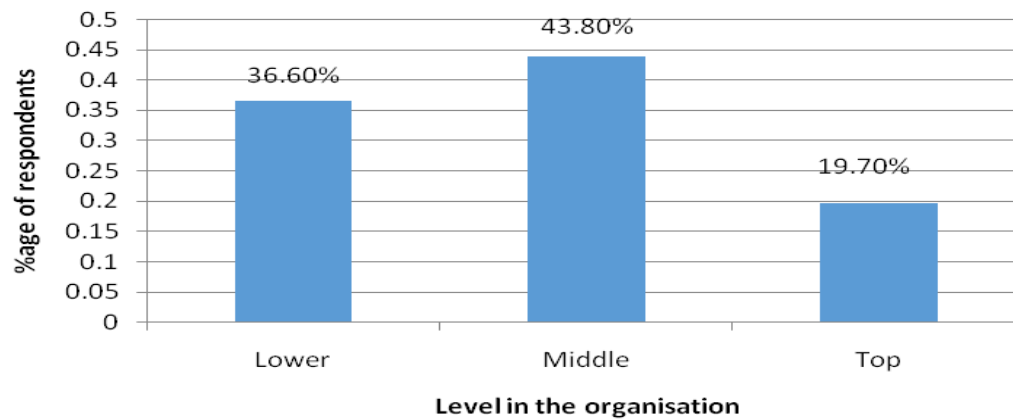


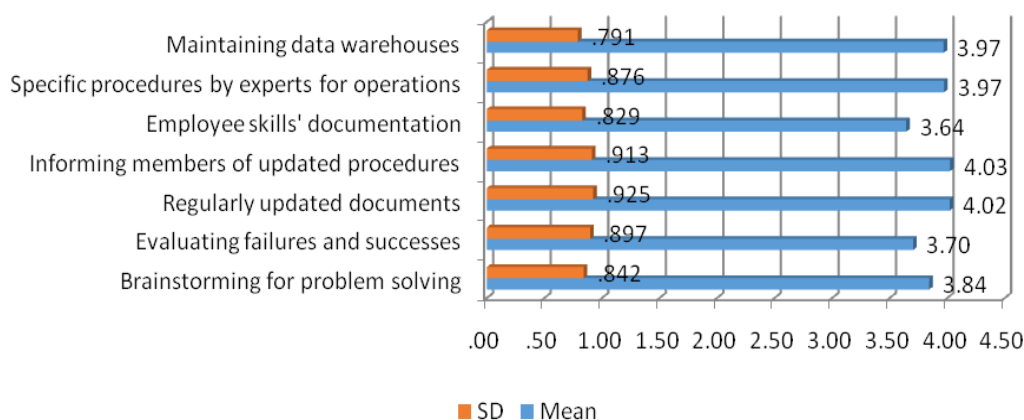
Figure 6: Level of respondents

Initiatives for Knowledge Acquisition (KA)

Knowledge acquisition practice as a construct had eight items. The responses show that the most highly observed practice in KA for organizations is recording the needs of customers i.e. regularly collecting information about the needs of customers with a mean score of 4.11. This was followed by conducting regular training with a mean score of 4.01 wherein employees in the firm regularly attend courses, seminars, or other training programs to remain informed.

Initiatives for Knowledge Documentation (KD)

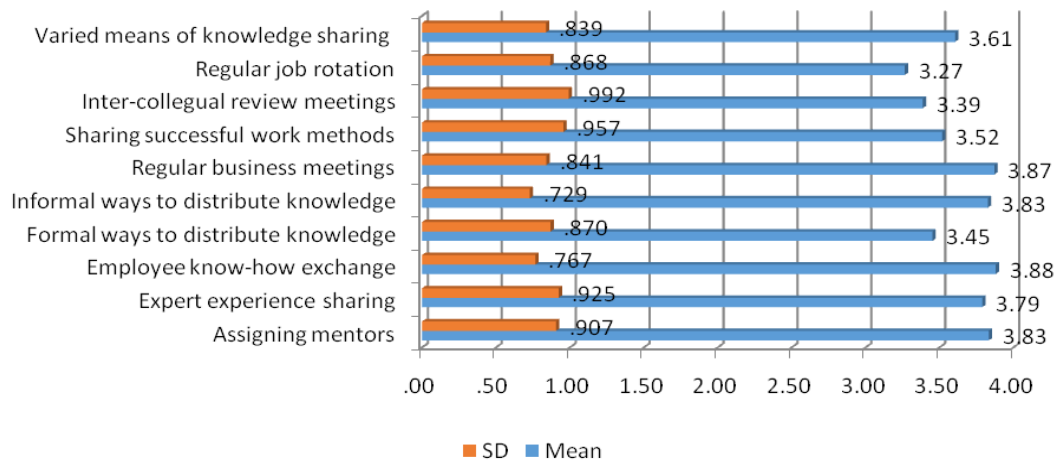
The mean score in knowledge documentation is lower than the highest mean score in the KA practice. While for KA practices, it was 4.11, here it is only at 4.03 which is for informing members for updated procedures which means that the firm informs its members from time to time of changes in procedures, handbook, etc.

Figure 8 : Initiatives for Knowledge Documentation

Initiatives for Knowledge Transfer (KT)

Compared to KD and KA, the mean scores for this practice are much lower. The highest score in this category if were 3.88; for employee know-how exchange i.e. the extent to which employees share with colleagues and others their knowledge/know how.

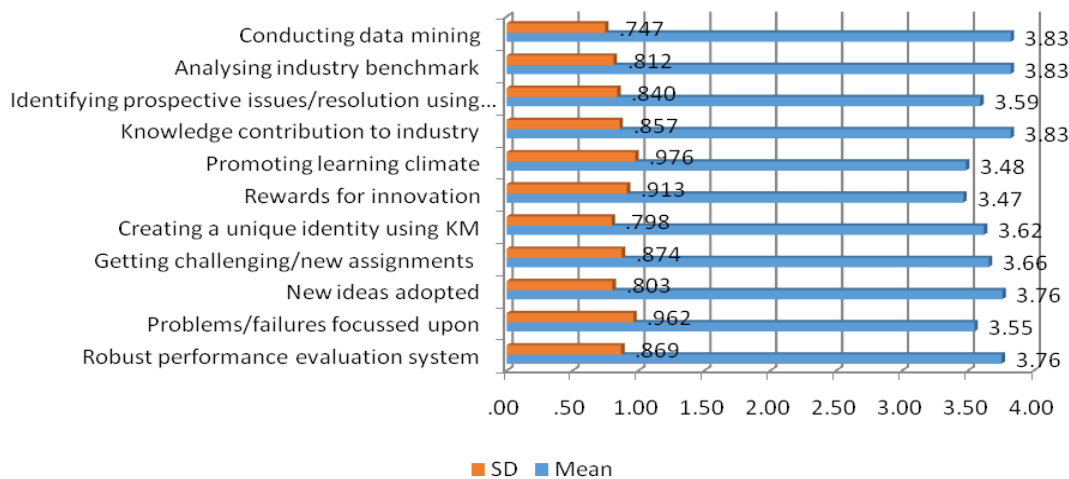
Figure 9 : Initiatives for Knowledge Transfer



Initiatives for Knowledge Creation (KC)

The mean scores for the responses for knowledge creation showed that most of these were in the category of agreeing rather than strongly agree. Three practices being – conducting data mining to discover new knowledge and insights, analyzing benchmark at the industry level, and contributing to the development of the important ideas and knowledge in the industry had a mean score of 3.83.

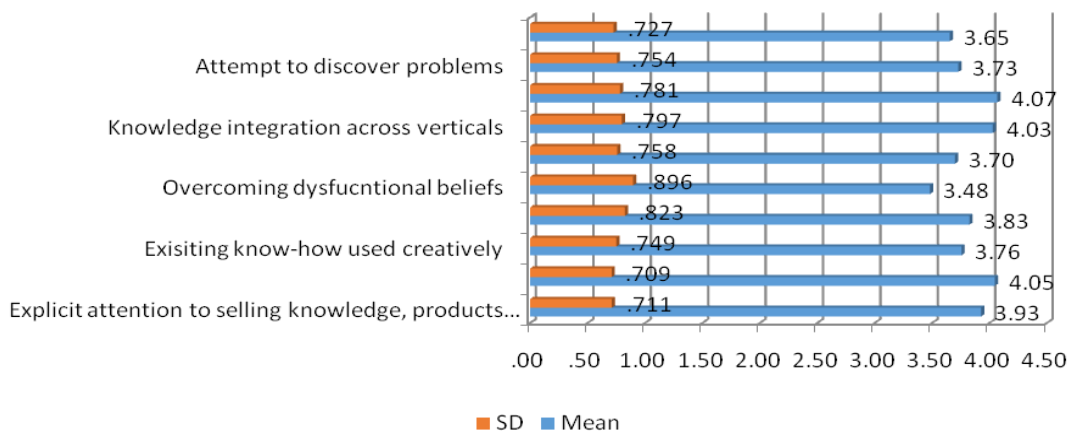
Figure 10: Initiatives for Knowledge Creation



Initiatives for Knowledge Application (KAp)

The highest score in this category was 4.07 for maximizing knowledge use which implies that the firm maximizes knowledge to use through its organizational structure, management systems, and practices.

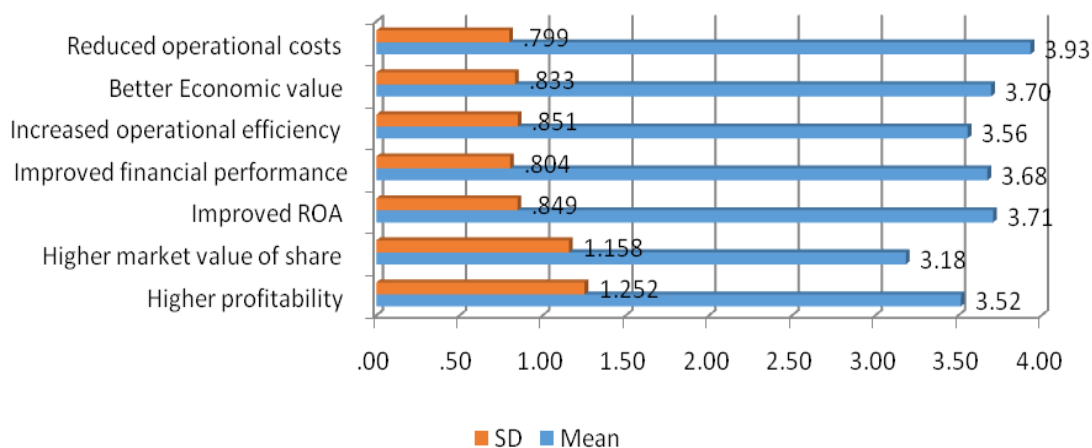
Figure 11: Initiatives for Knowledge Application



Impact on Financial Performance

The next part of the tool was aimed at ascertaining whether the respondents felt that knowledge management had an impact on the financial performance of their organization. The responses here were in the range of neutral to somewhat agree. The highest mean score was 3.93 for the reduced operational cost which implied that KM implementation helped in reducing operational costs. The respondents also felt that their Return on Assets improved due to KM and rated it at 3.71. The third important aspect was that KM resulted in a better Economic value for the organization with a score of 3.70. A mean score of 3.68 was given to better financial performance as respondents felt that post-KM implementation, their financial performance has been better than before. Increased operational efficiency and better profitability were two more benefits of KM with a mean score of 3.56 and 3.52 respectively. The respondents felt that the day to day operations had improved due to the existence of knowledge documents, data warehouses, and a lot of time could be saved not hunting for information which was the case before KM being implemented. Since the cost was being saved and operational efficiency had improved, the impact on profitability was direct. However, it was not clear as to what percentage of increase was attributable to the KM efforts.

Figure 12: Impact on financial performance



KM and Increased Efficiency

By adjudging the scores on how responsive the company was to the acquired knowledge, the impact on efficiency was ascertained. The highest mean score was 4.27 for a prompt response to customer complaints/concerns/ queries. The respondents agreed that their firm was quick in resolving customer complaints as their staff was trained and sufficiently aware to handle the situation. The second prevalent practice in this category was a well-developed marketing function resulting in marketing plans being implemented effectively. The third was the organization being flexible and pro-active in implementing strategies with a mean score of 3.86. Information about new technological developments affecting business being circulated quickly in the organization had a score of 3.85. The lowest score of 3.74 was for competitors' strategic actions quickly circulated in the organization. Though this score is low compared to the other scores in this category but standalone even this figure is implying that respondents agree to it.

6. Conclusion

Out of the different practices which were evaluated amongst the employees, the initiatives for knowledge acquisition, documentation, and application were found to be more popular than knowledge transfer and sharing. Employees felt that KM has an impact on the financial performance but they did not rate it very high in their responses. A possible reason could be that either the employees felt that their organization could do even better or they were not sufficiently aware of all the financial benefits which were accruing to the business. The latter could be true with employees at the entry-level or with lesser years of experience who may not understand the financial implications fully. Nevertheless, personal interviews with senior-level managers revealed that they were optimistic about KM bringing a positive impact on their financial performance. Almost all the respondents were optimistic about KM and its impact on efficiency. They felt that operational issues like resolving customer queries, robust marketing functions, introducing new technological developments, agility to change, and fighting competition were all possible due to KM. Firms use KM to improve their financial performance, keep ahead of the competition by introducing new products/technologies, and keep innovating using the existing knowledge for long term sustainability. The study rejects the findings of previous researchers who suggested that KM does not have an impact on financial performance. The study can be extended by mapping the financials of these companies and seeing if the results converge or diverge with the perception study.

7. Limitations of the Study

The study has been done in India and covers selective sectors. The results could vary if bigger sample size is taken.

References:

- Anand, A., & Singh, M. D. (2011). Understanding knowledge management. *International Journal of Engineering Science and Technology*, 3(2), 926-939.
- Arora, R. (2002). Implementing KM-a balanced score card approach. *Journal of knowledge management*, 6(3), 240-249.
- Bagorogoza, J. K., de Waal, A. A., van den Herik, H. J., & van de Walle, B. A. (2011). *Improving organisational performance through knowledge management: The case of financial institutions in Uganda* (No. 2011/18).
- Bogner, W. C., & Bansal, P. (2007). Knowledge management as the basis of sustained high performance. *Journal of Management Studies*, 44(1), 165-188.
- Chase, R. L. (1997). The knowledge-based organization: an international survey. *Journal of Knowledge Management*, 1(1), 38-49.
- Courtney, J. F. (2001). Decision making and knowledge management in inquiring organizations: toward a new decision-making paradigm for DSS. *Decision support systems*, 31(1), 17-38.
- Darroch, J. (2005). Knowledge management, innovation and firm performance. *Journal of knowledge management*, 9(3), 101-115.
- Davenport, T. H., De Long, D. W., & Beers, M. C. (1998). Successful knowledge management projects. *MIT Sloan Management Review*, 39(2), 43.
- Demarest, M. (1997). Understanding Knowledge Management. *Journal of Long Range Planning*, 30(3), 374-84.
- Fowler, A. (2000). The role of AI-based technology in support of the knowledge management value activity cycle. *The Journal of Strategic Information Systems*, 9(2), 107-128.
- Holsapple, C. W. and Joshi, K. D. (1999, January): Description and analysis of existing knowledge management frameworks, In Systems Sciences, 1999. HICSS-32. Proceedings of the 32nd Annual Hawaii International Conference, p. 15-IEEE.
- King, W. R., Chung, T. R., & Haney, M. H. (2008). Knowledge management and organizational learning. *Omega*, 36(2), 167-172.
- KPMG, Knowledge Management Research Report 2000, KPMG Consulting (ed.), Retrieved June 22, 2010 from www.insite.cz/data/kpmg_Knowledge_Management_report2000.pdf (accessed on December 20, 2014).
- Liao, S. H. (2003). Knowledge management technologies and applications—literature review from 1995 to 2002. *Expert systems with applications*, 25(2), 155-164.
- Liebowitz, J. (2001). Knowledge management and its link to artificial intelligence. *Expert systems with applications*, 20(1), 1-6.
- Palacios Marqués, D., & José Garrigós Simón, F. (2006). The effect of knowledge management practices on firm performance. *Journal of Knowledge Management*, 10(3), 143-156.
- McAdam, R., & Reid, R. (2001). SME and large organization perceptions of knowledge management: comparisons and contrasts. *Journal of knowledge management*, 5(3), 231-241.

- Moustaghfir, K. (2008). The dynamics of knowledge assets and their link with firm performance. *Measuring Business Excellence*, 12(2), 10-24.
- Nonaka, I., & Takeuchi, H. (1995). *The knowledge-creating company: How Japanese companies create the dynamics of innovation*. Oxford university press.
- Nunnally, J. C., Bernstein, I. H., & Berge, J. M. T. (1967). *Psychometric theory* (Vol. 226). New York: McGraw-Hill.
- Pham, Q. T., & Hara, Y. (2012). KM Approach for Improving the Labor Productivity of Vietnamese Enterprise. *Dynamic Models for Knowledge-Driven Organizations*, 206.
- Pillania, R. K. (2008). Strategic issues in knowledge management in small and medium enterprises. *Knowledge Management Research & Practice*, 6(4), 334-338.
- Rubenstein-Montano, B., Liebowitz, J., Buchwalter, J., McCaw, D., Newman, B., Rebeck, K., & Team, T. K. M. M. (2001). A systems thinking framework for knowledge management. *Decision support systems*, 31(1), 5-16.
- Ruiz-Mercader, J., MeroñO-Cerdan, A. L., & Sabater- SÁNchez, R. (2006). Information technology and learning: Their relationship and impact on organisational performance in small businesses. *International Journal of Information Management*, 26(1), 16-29.
- Seleim, A., & Khalil, O. (2007). Knowledge management and organizational performance in the Egyptian software firms. *International Journal of Knowledge Management (IJKM)*, 3(4), 37-66.
- Sharma, K. (2013). Knowledge Management and its Impact on Organisations: An Assessment of Initiatives in the Industry. *Journal of Technology Management for Growing Economies*, 4(2).
- Tippins, M. J., & Sohi, R. S. (2003). IT competency and firm performance: is organizational learning a missing link?. *Strategic management journal*, 24(8), 745-761.
- Vidoviæ, M. (2010). The link between the quality of knowledge management and financial performance– The case of Croatia. *EFZG Working Paper Series/ EFZG Serija èlanaka u nastajanju*, (03), 1-15.
- Wiig, K. M. (1994). *Knowledge Management Foundations: Thinking about Thinking-how People and Organizations Represent, Create, and Use Knowledge*. Schema Press, Limited.
- Yew Wong, K., & Aspinwall, E. (2005). An empirical study of the important factors for knowledge management adoption in the SME sector. *Journal of knowledge management*, 9(3), 64-82.
- Zack, M. H. (2002). Developing a knowledge strategy. *The strategic management of intellectual capital and organizational knowledge*, 255-76.

JOB STRESS AND ITS EFFECT ON EMPLOYEE PRODUCTIVITY AND ORGANIZATIONAL COMMITMENT

Dr. Bhavani Shree¹, Dr. Lakshmi.P² Dr. Bharthi³ Umamaheswararao Gobbilla⁴

Associate Professor^{1, 2, 4} Assistant Professor³

Department of Business Administration^{1, 2}

Vidyavardhaka College of Engineering, Mysore, India ^{1, 2}

Dr. NSAM First Grade College ³ CMRIT Hyderabad ⁴

Orcid No. orcid.org/0000-0002-0911-769X¹ [orcid-org/0000-0001-8084-3005](https://orcid.org/0000-0001-8084-3005)²

ABSTRACT:

The concept of Job stress has been considered as the mental distractions and imbalance between the emotional and mental levels of an individual. Stress is a universal element and these days it is been seen in almost all occupations and almost all employees. The study aims to investigate the impact of job stress on employees' productivity and commitment among the employees of manufacturing units in Mysuru. The sample size taken for the study is 41 units in the Mysuru district. The sample was taken for the 250 employees from these units at the middle level. Many factors contribute to job stress but when there are good management practices and when management understands employee's grievance and expectations there are chances of lowering stress in employees. This leads to increased productivity and a higher level of commitments when there is a good rapport between management and employees. Sometimes stress may be positive and most of the time it is negative. To the results reveal that there is an effect of stress on job productivity and commitment levels of employees in these units

1. Introduction

Stress is an imbalance between the mental and emotional levels of an individual. An increase in speed, efficiency, and competition in organizations these days is one of the causes of stress. The positive dimension of stress is called stress. High workload, lack of skills, discrimination among employees in the workplace, the work environment may cause stress. Sometimes stress may be positive and most of the time tends to be negative. Stress is one of the common things that is been seen in almost all employees during the current period.

One of the stresses related to the job is industrial stress known as occupational. Stress occurs when there are unforeseen odd jobs. Stress is usually uncertain it can't be predicted and employees or any other person will not know when stress occurs and why stress occurs.

Stress can be physical stress or it can be mental stress. Stress is derived from many sources. It can be pressure from boss or superior, family interaction, irritating colleagues, angry customers, and hazardous conditions. Long hours of work may be one of the reasons for stress. When you can't cope up with co-workers or colleagues or any other employees around the work environment stress will increase. Physical exercise, positive thinking, and time management may reduce stress. Stress majorly affects emotionally. Stress can lead to the worst health conditions.

Productivity tells about how efficient an employee is in his work. A productivity measure is expressed in terms of the ratio of output per unit of input. Productivity increase results in greater outcomes and with the same quantity of input. Productivity can be company productivity, team productivity, and personal productivity.

Company productivity depends upon relations in the company environment of the company and management of the company. Team productivity involves relations with the team member's quality of the teams and team management. Personal productivity depends on personal relations personal quality and personal management.

Organizational commitment is the relationship of employees with the organization. It is the bond employees experience with their organization. Employee commitment refers to the equivalence between the goals of the person and the organization whereby the individual identifies with and extends effort on behalf of the general goals of the organization. The developed trust will increase the commitment of the employees.

2. Literature Review

Word related pressure is a significant reason for non-attendance, expanding turnover expectations, lower efficiency, and modern mishaps. One-fourth of the activity related pressure experienced by colleague's claims to strenuous working conditions **Ryland and Greenfield (1991)**.

Wiener (1982), action happiness is a manner toward business-related conditions, highlights, or parts of the movement. Along these lines, duty suggests a progressively unmistakable proportion of a relationship with the utilizing association as opposed to express assignments, common components, and the region where the commitments are performed.

Bickford, 2005-Work overload is often associated with the imposition of unrealistic deadline timeframes for completion of tasks. If the volume of work mismatches or surpasses the skills, knowledge, and abilities of the worker, these cause stress.

According to **(Rose,2003)** delegates have an inclination towards an abnormal state of worry as for time, working for longer hours which decreases specialist's request performing better. The officials hold up helps in dropping or assembles stress in delegates, apparent definitive help, the board reinforces determinedly in lessening business associated stress in specialists. There are a lot of reasons causing weight work-family conflict work overweight one reason identified by Stamper &Johlke is that if the affiliation or the administrators don't value delegates for

persevering work, responsibility towards affiliation makes weight and generally makes expect to go away.

Mathis and Jackson (2000) pointed out that absenteeism epitomizes the form of withdrawal behavior from an extremely stressful occupation. Presentism: That laborer's coming to work yet not working up to their abilities at work. In a check, 60 % of the laborer's announced losing effectiveness because of stress while at the job.

Mowday et al. (2000) characterized authoritative responsibility as being faithful to the organization, and the organization being faithful to the representative, clearly downplays the multifaceted nature associated with an individual's demeanor toward and conduct inside his or her utilizing association.

3. Objectives

1. To analyze the influence of job stress on productivity.
2. To investigate the effect on job stress on employee commitment.
3. To identify factors responsible for job stress.

4. Research Design

The type of research used is Descriptive. The sampling technique used is Non Probability sampling and the sampling method used here is simple random sampling. The 41 manufacturing units in Mysuru district, Karnataka State are taken as sampling units for the study. The data collected using Primary data sources with the help of questionnaires. The 250 respondents are taken as the sample size for the study. The proposed statistical tests being used are Regression, Anova, and Correlation.

5. Analysis and Interpretation

From the reliability test, it is found that the Cronbach's Alpha value for 36 items is 0.815 which is more than 0.7 hence the researcher can rely upon the sample for further research. The Correlation test is found that there exists a negative relationship between Job Stress (JS) and Productivity (PR). The value is found to be -0.203. Correlation test it is found that there exists a positive relationship between job stress and Organizational Commitment (OC). The value is found to be 0.639. From the Regression test, it is found that there is a 4.1% impact of job stress on productivity. From Regression test, it is resulting in a 40.8% influence of job stress on

commitment. Regression test it is found that there are a 0.4% impact of Resource Constraint (RC) impacts on productivity, 0.1% impact of Work-life Balance (WLB) impacts on Productivity, 1.32% impact of Job Security (JS) impacts on Productivity, 0.8% impact of Job Involvement (JI) impacts on Productivity. One way ANOVA test is found that the significant impact of education on organizational commitment and no significant impact of education on productivity, there is no significant impact of experience on organizational commitment and productivity, there is a significant impact of income on organizational commitment and productivity.

To analyze the Relationship between Employee Job Stress and Productivity

As per table1, the consequences of the equivalent uncover that there is a higher negative relationship between workers' activity stress and their productivity at -0.203, This outcome is predictable with a large portion of the examinations that have been led in India and different nations.

To analyze the relationship between Employee Job Stress and their Commitment

As per table 1, the results of the same reveal that there is a positive correlation between employees' job stress and organizational commitment at 0.639, which is significant statistically at a 1% level. It indicates that even when employees are stressed at work, they will be committed to their work and organization. This result is consistent with most of the studies that have been conducted in India and other countries.

Impact of Job Stress on Productivity

As per Table 2 the correlation between components employee job stress and their productivity at 0.203 which is a very high negative relationship and the R^2 is 0.041 which indicates that the variance in the dependent variable i.e., Employee Productivity is explained by the Job Stress to the extent of 4.1%. The results of the regression coefficients reveal that the employee job stress found to be significantly influencing employee productivity, as the significance is less than 0.05 (5%). The results of this analysis are consistent with the theory that says that there is a negative relationship between employee job stress and productivity. The results indicate that increase in one unit in job stress, there will be a 0.279 unit decrease in employee productivity and vice versa. Variables are significant. The regression effect is 4.1%. Dependent variable: Productivity

Effect of Employment Strain on Organizational Commitment

The correlation between components employee job stress and organizational commitment at 0.639 which is a positive relationship and the R Square is 0.408 which indicates that the variance in the dependent variable i.e., organizational commitment is explained by the Job Stress to the extent of 40.8%. The results of the regression coefficients reveal that the employee job stress found to be significantly influencing the organizational commitment, as the significance is less than 0.05 (5%). The results indicate that increase in one unit in job stress, there will be a 0.694 unit increase in the organizational commitment and vice versa. The result can be in the form of the equation

The relation between Resource Constraints and Productivity

There is a positive correlation between resource constraints and productivity. The R square of the model is .004 which means that resource constraints have a 0.4% influence on employee productivity. The ANOVA table shows the significance .510 which is more than 0.05 indicating that there is no significant impact on productivity.

The relation between Work-life balance and Productivity

It depicts exists a positive correlation between work-life balance and productivity. The R^2 is .001 which means that work-life balance has a 0.1% influence on employee productivity. The ANOVA table shows the significance .697 which is more than 0.05 indicating that there is a significant impact on productivity.

The relation between Job security and Productivity

The result shows that there exists a positive correlation between work-life balance and productivity. The R square of the model is .001 which means that work-life balance has a 0.1% influence on employee productivity. The ANOVA table shows the significance .000 which is less than 0.05 indicating that there is a significant impact on productivity

The relation between Job involvement and Productivity

The model summary shows that there exists a positive correlation between Job involvement and productivity. The R square of the model is .008 which means that work-life balance has a

0.8% influence on employee productivity. The ANOVA table shows the significance .359 which is more than 0.05 indicating that there is no significant impact on productivity.

ANOVA Results for Differences in Age Group as per Table 3

Job Security: From the Anova test, the F value at 2.565, and the p-value at 0.018. Since the significance value is less than 5%, there exists mean differences in the opinions of selected employees on job security across their age groups at a 5% level of significance.

Resources Constraints: Anova test reveals that the F value at 1.374 and p-value at 0.225. Since the significance value is more than 5%, there does not exist any meaningful differences in the opinions of selected employees on resource constraints across their age groups at a 5% level of significance.

Work-Life Balance: Anova analysis shows the F value at 3.493 and p-value at 0.002. Since the significance value is less than 5%, there exists mean differences in the opinions of selected employees on work-life balance across their age groups at a 5% level of significance.

Job Involvement: Anova shows the F value at 2.777 and p-value at .011. Since the significance value is less than 5%, there exists mean differences in the opinions of selected employees on job involvement across their age groups at a 5% level of significance. Hence, the null hypothesis is rejected.

Interpersonal Relationship: Anova reveals that the F value at 3.593 and p-value at .002. Since the significance value is more than 5%, there does not exist mean differences in the opinions of selected employees on Interpersonal relationships across their age groups at a 5% level of significance. Hence, the null hypothesis is not rejected.

6. Suggestions

Employees working in shifts are seen to be more stressed out therefore suggestion to this is that if there are elderly or aged employees they need to give a general shift rather than night shifts. Even though there are measures taken by the organizations to reduce the stress they have implemented the Harmony principle where it is an activity that is used to reduce stress but employees feel that they should extend the days for the program conducted. It also implies that lower stress leads to higher productivity and higher commitment. Productivity and commitment are important outcomes for any organization. For new joiners, there should be a program so

that their mind should be molded to get adjusted to the organization and environment. Organizations should take corrective measures to reduce the stress of the employees which also helps them to maintain their work-life balance.

7. References

1. Anderzén, I. and Arnetz, B.B., 2005. The impact of a prospective survey-based workplace intervention program on employee health, biologic stress markers, and organizational productivity. *Journal of occupational and environmental medicine*, 47(7), pp.671-682.
2. Bar-On, R., Brown, J.M., Kirkcaldy, B.D., and Thome, E.P., 2000. Emotional expression and implications for occupational stress; an application of the Emotional Quotient Inventory (EQ-i). *Personality and individual differences*, 28(6), pp.1107-1118.
3. Bhavani Shree “A Study on Compensation and Benefits its Influence on Employee’s Performance in Milk Industry” **International Journal of Engineering Science and Computing**, 6.6 (2016): 2321-3361
4. Dwamena, M.A., 2012. Stress and its Effects on Employees Productivity—A Case Study of Ghana Ports and Harbours Authority, Takoradi (Doctoral dissertation).
5. Ekienabor E.E.; (2016) ‘Impact of Job Stress on Employees Productivity and Commitment International Journal for Research in Business Management and Accounting ISSN: 2455-6114, pp.124-133
6. Jex, S.M., and Bliese, P.D., 1999. Efficacy beliefs as a moderator of the impact of work-related stressors: a multilevel study. *Journal of applied psychology*, 84(3), p.349.
7. Khatibi, A., Asad, H., and Hamidi, M. (2009). The Relationship Between Job Stress and Organisational Commitment to National Olympic and Paralympic Academy. *World Journal of Sports Science*, Vol. 2, pp. 272-278
8. Karasek, R. A. (1979). Job Demands, Job Decision Latitude, and Mental Strain: Implications for Job Redesign. *Administrative Science Quarterly*, Vol 24, no. 2: 285-307. Karasek, R. A., and Theorell, T. (1990). *Healthy Work: Stress, Productivity, and The Reconstruction of Working Life*. Basic Books. New York.
9. Imtiaz, S., and Ahmad, S., 2009. Impact of stress on employee productivity, performance, and turnover; an important managerial issue. *International Review of Business Research Papers*, 5(4), pp.468-477.
10. Riaz, M., Ahmad, N., Riaz, M., Murtaza, G., Khan, T. and Firdous, H., 2016. Impact of Job Stress on Employee Job Satisfaction. *International Review of Management and Business Research*, 5(4), p.1370.

11. Shahid, M.N., Latif, K., Sohail, N., and Ashraf, M.A., 2012. Work stress and employee performance in the banking sector evidence from district Faisalabad, Pakistan. *Asian Journal of Business and Management Sciences*, 1(7), pp.38-47.
12. Nikolaou, I. and Tsaousis, I., 2002. Emotional intelligence in the workplace: Exploring its effects on occupational stress and organizational commitment. *The International Journal of Organizational Analysis*, 10(4), pp.327-342.
13. Slaski, M., and Cartwright, S., 2002. Health, performance, and emotional intelligence: An exploratory study of retail managers. *Stress and Health: Journal of the International Society for the Investigation of Stress*, 18(2), pp.63-68.
14. Lundberg, U., 1996. Influence of paid and unpaid work on psychophysiological stress responses of men and women. *Journal of Occupational Health Psychology*, 1(2), p.117.
15. Hafner, M., Van Stolk, C., Saunders, C.L., Krapels, J., and Baruch, B., 2015. *Health, wellbeing, and productivity in the workplace: A Britain's Healthiest Company summary report*. Rand Corporation.
16. Olusegun, A.J., Oluwasayo, A.J., and Olawoyim, O., 2014. An Overview Of The Effects Of Job Stress On Employees Performance In Nigeria Tertiary Hospitals. *Ekonomika*, 60(4).

Annexures

Table 1 Correlation

Correlations

		JS	PR	OC
JS	Pearson Correlation	1		
PR	Pearson Correlation	-0.203	1	
OC	Pearson Correlation	0.639		1
**. Correlation is significant at the 0.01 level (2-tailed).				

Table 2: Regression

Variables	R	R ²	Adjust R ²	F change	Sig
JS-PR	0.203	0.041	0.032	4.441	0.000
JS-OC	0.639	0.408	0.403	71.113	0.000
RC-PR	0.065	0.004	0.005	0.436	0.000
WLB-PR	0.038	0.001	0.008	0.152	0.697
JOS-PR	0.364	0.132	0.124	15.703	0.000
Jl-PR	0.09	0.008	0.001	0.848	0.000

Table :3 ANOVA Results for Differences in Age Group

Variable	Sum of Squares	Df	Mean Square	F	Sig.
Job Security	10.908	7	1.558	2.565	0.018
	58.939	243	0.608		
	69.848	250			
Resource Constraints	6.300	7	.900	1.374	.225
	63.547	243	.655		
	69.848	250			
Work-Life Balance	14.382	7	2.055	3.493	.002
	55.466	243	0.572		
	69.848	250			
Job Involvement	11.660	7	1.666	2.777	.011
	58.188	243	.600		
	69.848	250			
Interpersonal Relationship	11.705	7	2.055	3.593	.002
	58.143	243	0.572		
	69.848	250			

Work Environment	14.551	7	1.617	2.778	.006
	55.296	243	.582		
	69.848	250			
Employment Opportunities	20.981	7	2.997	5.950	.000
	48.866	243	.504		
	69.848	250			
Job Satisfaction	10.225	7	1.704	2.801	.015
	59.623	243	.608		
	69.848	250			
Compensation	10.888	7	1.361	2.216	.033
	58.960	243	.614		
	69.848	250			
Group Dynamics	2.566	7	.428	.623	.712
	67.282	243	.687		
	69.848	250			
Presentism	11.546	7	.962	1.518	.132
	58.302	243	.634		
	69.848	250			
Absenteeism	10.216	7	.929	1.448	.165
	59.631	243	.641		
	69.848	250			

Study of metallurgical changes and mechanical properties of dissimilar weldments developed by interpulse current TIG welding technique

September 2020 · *ARCHIVE Proceedings of the Institution of Mechanical Engineers Part C Journal of Mechanical Engineering Science 1989-1996 (vols 203-210)* 235(16):1-13

DOI:10.1177/0954406220960780

Authors:



Balram Yelamasetti

MLR Institute of Technology Hyderabad I...



T. Vishnu Vardhan

CMR Institute of Technology, Hyderabad

[Download citation](#)

[Copy link](#)

[Citations \(16\)](#)

[References \(25\)](#)

Abstract

This research manuscript compares the metallurgical changes and mechanical behavior of AISI 316 and Monel 400 dissimilar weldments developed by Interpulse TIG welding process with ERNiCrMo-3 and ER316 filler wires. Metallurgical aspects are envisioned by using optical and scanning electron microscopes. Mechanical behavior of welded joints were studied by conducting tensile and microhardness tests. Metallurgical study has shown that the ERNiCrMo-3 filler weldment divulged completely with austenitic phase structure at the weld zone. Also, at the HAZ of Monel 400 clear grain boundaries with fine grains were observed. The mechanical properties corroborated



[Request full-text PDF](#)

To read the full-text of this research, you can request a copy directly from the authors.

ResearchGate

Discover the world's research

- 25+ million members
- 160+ million publication pages
- 2.3+ billion citations

Improving the energy-absorbing properties of hybrid aluminum-composite tubes using nanofillers for crashworthiness applications

July 2020 · ARCHIVE Proceedings of the Institution of Mechanical Engineers Part C Journal of Mechanical Engineering Science 1989-1996 (vols 203-210) 235(8):095440622094226
DOI:10.1177/0954406220942267

Authors:

 **A Praveen Kumar**

 **Dr Maneiah**
CMR Technical Campus


 **L Ponraj Sankar**

[Download citation](#) [Copy link](#)

[Citations \(14\)](#) [References \(40\)](#) [Figures \(7\)](#)

Abstract and Figures

Thin-walled tubular configurations with hybridization concept have been gained special consideration in recent years owing to their substantial balance between light-weight characteristics and crashworthiness performance. In this context, some research studies have been concentrated on the feasibility of a thin-walled metal-composite hybrid tube. It is also eminent that the impact energy absorption capability of such hybrid tubes can further be enhanced through modification of the epoxy matrix by adding nanofillers. In this research article, aluminum-based multiwalled carbon nanotubes reinforced epoxy composite cylindrical tubes are introduced, and their

 [Download full-text PDF](#)

[Read full-text](#)

Advertisement

ResearchGate

Build the best teams in science and research.

[FIND OUT MORE →](#)

Find your next great hire on ResearchGate

We simplify hiring by helping you to target scientists based on their profiles, publications, and expertise.

[Find out more](#)


ResearchGate

Discover the world's research

- 25+ million members
- 160+ million publication pages
- 2.3+ billion citations

Hybrid electro search with genetic algorithm for task scheduling in cloud computing

August 2020 · Ain Shams Engineering Journal 12(1)
DOI:10.1016/j.asej.2020.07.003
License · CC BY-NC-ND 4.0



[Download full-text PDF](#)

[Read full-text](#)

Authors:



Velliangiri Sarveshwaran
SRM Institute of Science and Technology



Karthikeyan .P
Jain University



Arul Xavier
Karunya University



D. Baswaraj

[Download citation](#) [Copy link](#)

[Citations \(74\)](#) [References \(27\)](#) [Figures \(5\)](#)

Abstract and Figures

Cloud computing is on-demand Internet-based computing, which is a highly scalable service adopted by different working and non-working classes of people around the globe. Task scheduling one of the critical applications used by end-users and cloud service providers. The significant challenging in the task scheduler is to find an optimal resource for the given input task. In this paper, we proposed Hybrid Electro Search with a genetic algorithm (HESGA) to improve the behavior of task scheduling by considering

ResearchGate

Discover the world's research

- 25+ million members
- 160+ million publication pages
- 2.2+ billion citations

144 Views
5 CrossRef citations to date
1 Altmetric

A parametric study on the design factors influencing the thermal performance of nickel alloy C263 sandwich panels

T. Mahender, I. Balasundar & T. Raghu
Pages 526-540 | Received 14 Jul 2020, Accepted 12 Jan 2021, Published online: 24 Feb 2021

Cite this article <https://doi.org/10.1080/14484846.2021.1876601> [Check for updates](#)

[Full Article](#) [Figures & data](#) [References](#) [Citations](#) [Metrics](#) [Reprints & Permissions](#) [Read this article](#) [X](#) [f](#) [in](#) [e](#) [+](#)

Sample our Engineering & Technology Journals
>> [Sign in here](#) to start your access to the latest two volumes for 14 days

ABSTRACT

To protect the airframe and the payload of hypersonic cruise vehicles from aerothermal heating and aerodynamic loading, metallic thermal protection systems (MTPS) are intended to be used. MTPS are composite structures containing a combination of insulating material and two sandwich panels placed on top and bottom of it. There are numerous design factors influencing the (a) thermal performance and (b) density of these sandwich panels (SP). In the current study, the effect of six important geometric design parameters of nickel alloy C263 sandwich panel viz., (A) core cell shape, (B) core cell size, (C) core cell height (D) core sheet thickness, (E) top and (F) bottom face sheet thickness were evaluated and analysed using Taguchi-based design of experiments (DOE) approach. The results obtained were analysed using standard statistical analysis techniques in order to identify the optimum combination of design parameters and to ascertain the influence of each aforementioned design parameters on the performance of C263 sandwich panels. Further, the optimum combination of sandwich-panel design parameters that provides the best thermal

Related research

People also read	Recommended articles	Cited by 5
Metamodels to describe the high temperature deformation behaviour of Al 2014+2wt%TiB2 composite >		
T. Mahender et al. Advances in Materials and Processing Technologies Published online: 15 Feb 2022		